CHALMERS

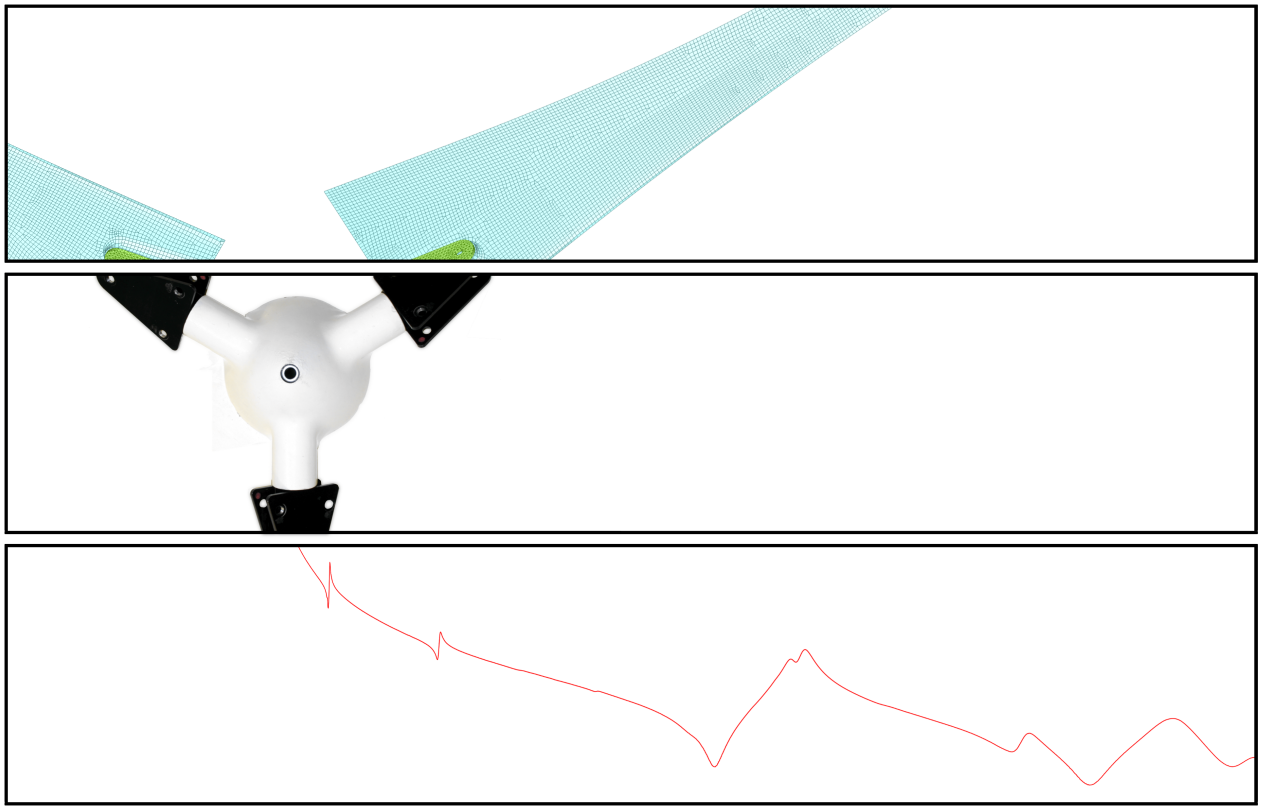

Experimental-Analytical Dynamic Substructuring

A State-Space Approach

Master's thesis in Applied Mechanics

MLADEN GIBANICA

Department of Applied Mechanics
Division of Dynamics
CHALMERS UNIVERSITY OF TECHNOLOGY
Göteborg, Sweden 2013
Master's thesis 2013:39

MASTER'S THESIS IN APPLIED MECHANICS

Experimental-Analytical Dynamic Substructuring

A State-Space Approach

MLADEN GIBANICA

Department of Applied Mechanics
Division of Dynamics
CHALMERS UNIVERSITY OF TECHNOLOGY
Göteborg, Sweden 2013

Experimental-Analytical Dynamic Substructuring
A State-Space Approach
MLADEN GIBANICA

Master's thesis 2013:39
ISSN 1652-8557
Department of Applied Mechanics
Division of Dynamics
Chalmers University of Technology
SE-412 96 Göteborg
Sweden
Telephone: +46 (0)31-772 1000

Cover:
In the upper upper part of the figure two finite element models of the blades are shown. The middle part shows a real component of the tested structure and the lower part visualises a frequency response function of a real blade.

Chalmers Reproservice
Göteborg, Sweden 2013

Experimental-Analytical Dynamic Substructuring
A State-Space Approach
Master's thesis in Applied Mechanics
MLADEN GIBANICA
Department of Applied Mechanics
Division of Dynamics
Chalmers University of Technology

Abstract

Substructuring is the process of decomposing a structure into parts, modelling these parts separately and assembling them again. In analytical dynamic substructuring the component mode synthesis (CMS) methods such as the Craig-Bampton method have been successfully used since the 1960s, usually employed to couple analytical models, but also as reduction methods. In this content, analytical models denote models from first principles, e.g. FE models, and experimental models denote models derived from measured data, e.g. from vibration tests where models are identified by system identification. With the recently renewed interest in experimental-analytical dynamic substructuring, methods requiring less information become competitive. Frequency-based substructuring (FBS) methods have usually been used to overcome the CMS shortcomings; these suffer from numerical ill-conditioning due to noisy data and introduce difficulties in the system identification of the coupled systems, however. A state-space based synthesis method developed by Sjövall and Abrahamsson has been proposed to circumvent difficulties which exist with both CMS and FBS methods.

For researchers to have a common testbed and be able to share data, the Society for Experimental Mechanics (SEM) Substructuring Focus Group have initiated a research project in experimental dynamic substructuring using the Ampair 600 wind turbine as a testbed. Previously, the blade-to-blade spread of said testbed has been quantified and a Finite Element (FE) model of the blades has been calibrated.

The next step in the research project is to couple the wind turbine parts by dynamic substructuring. The blades are coupled to analytical models of their mounting brackets using both experimental and analytical models of the blades. The coupled systems are validated by vibration measurements of the blade and bracket systems. Further, three blades are coupled to the wind turbine hub, where both experimental and analytical models of the blades are used with FE models of the hub and brackets. These couplings are also validated with respect to measurements of the assembled structure.

The state-space based substructuring method is focused on in this work where a quantitative and qualitative comparison with the widely used CMS and FBS methods is performed. It has been found that the state-space method is numerically unstable for higher order models, and an evaluation of these problems is performed. The state-space synthesis (SSS) method has been theoretically compared to the CMS method and the synthesis procedure translated to the general framework.

From this study it can be concluded that further work with the state-space method is necessary, especially with the numerical problems encountered, but also with the relatively high demand on pre-processing of data in order to couple systems in a valid manner. For experimental-analytical coupling where experimental models satisfy Newton's second law the state-space method has been shown to produce the same results as the FBS method. Thus, the method is very promising due to its simplicity. It has also been found that the dynamics of the coupling is of very high importance as only the low frequency modes correlated well. The spread between the blades is considerable and it is found that the blade bracket coupling correlates better for experimental models of the blades relative validation data. Inconclusive results for the hub assembly are obtained.

Keywords: Substructuring, Experimental-Analytical Dynamic, Modal Analysis, Vibration Testing, State-Space, Component Mode Synthesis, Frequency Based Substructuring, Automatic System Identification, Wind Turbines

Preface

The work performed in this thesis, over the course of five months from January to June 2013, has been part of a research project initiated by the Society for Experimental Mechanics Substructuring Focus Group. The author has had the opportunity to work with this project previously as part of a course given at Chalmers University of Technology and present a paper at the International Modal Analysis Conference before the thesis was started. This has contributed with gained insight in the testbed, the problem at hand and the field of experimental mechanics.

Hopefully, this thesis will show the potentials of a state-space based approach in substructuring but also highlight the encountered problems and differences between other methods.

Acknowledgements

I would like to thank thank my supervisor, Assistant Professor Anders T. Johansson, for the opportunity to perform my thesis within the field of substructuring but also for his encouragement and help along the way. A special thanks is directed towards him for allowing me to use his calibrated FE model of the blade, without which this thesis would have taken infinitely longer to perform. I am also grateful for the many scripts that were provided.

I would also like to thank my examiner, Full Professor Thomas Abrahamsson, firstly for the opportunity to attend the International Modal Analysis Conference which lead me into the field of experimental mechanics but also for supporting me with the work performed in this thesis.

A special thanks to Anders Liljerehn, industrial PhD student at Chalmers University of Technology and Sandvik Coromant, who helped with the encountered numerical problems in the state-space algorithm and Jan Möller for filling the hub with epoxy, even though a vacuum chamber had to be created. Also, I am grateful to Björn Andersson and Patrik Gillberg, fellow MSc students, for helping me with the setup of the fully assembled system.

Finally, I would like to thank the people at TU Delft, active in the substructuring field, who provided the bracket and hub geometries and consequently made it possible to create the finite element models of said parts.

Nomenclature

The theory used in this thesis come from a lot of different sources which use different notations. In writing this thesis the more modern notations were favoured but as theory from both structural dynamics and control theory were considered there was a conflict in notation which was solved by introducing new notations where necessary.

Abbreviations

CMS	Component mode synthesis
DOF	Degree of freedom
EOM	Equation of motion
FBS	FRF-based substructuring
FE	Finite element
FEMAP	Siemens FEMAP version 10.3.1 was used
FRD	Frequency response data
FRF	Frequency response function
LTI	Linear time invariant
MAC	Modal assurance criterion
MATLAB	Mathworks MATLAB versions 2011b, 2012b and 2013a were used
MD Nastran	MD Nastran version 2011.1 was used
MDOF	Multiple degrees of freedom
NX Nastran	NX Nastran version 8.1 was used
SEM	Society for Experimental Mechanics
SSS	State-space synthesis
SVD	Singular value decomposition

Subscripts

ω	Denotes the frequency domain
a	Denotes acceleration
b	Denotes body DOFs
c	Denotes interface DOFs
d	Denotes displacement
e	If placed before a symbol it denotes the eigenfrequency
$left$	Represents the left side of something, e.g. eigenvalues
$right$	Represents the right side of something, e.g. eigenvalues
v	Denotes velocity

Operators

$\mathcal{L}$	Laplace transform

Symbols

$\boldsymbol{\eta}$	Modal coordinate vector
$\boldsymbol{\Phi}$	Modal matrix
$\boldsymbol{\phi}_i$	Eigenvector i, $i = 1, \ldots, m$
$\boldsymbol{\xi}$	Represents the global set of modal coordinates
λ_i	Eigenvalue i, $i = 1, \ldots, m$
$\mathbf{A}$	State matrix

$\mathbf{B}$	Input matrix	
$\mathbf{C}$	Output matrix	
$\mathbf{D}$	Feedthrough matrix	
$\mathbf{E}$	Matrix describing the coupling DOFs	
$\mathbf{f}$	Load vector	N
$\mathbf{g}$	Interface forces	N
$\mathbf{H}$	Frequency response function matrix	
$\mathbf{K}$	Stiffness matrix	N/m
$\mathbf{L}$	Interface DOFs localisation matrix	
$\mathbf{M}$	Mass matrix	kg
$\mathbf{P}_a$	Rectangular matrix relating the output to the general accelerations	
$\mathbf{P}_d$	Rectangular matrix relating the output to the general displacement	
$\mathbf{P}_u$	Rectangular matrix relating the input forces to the load vector	
$\mathbf{P}_v$	Rectangular matrix relating the output to the general velocities	
$\mathbf{q}$	Generalised displacement vector	
$\mathbf{R}$	Reduction matrix	
$\mathbf{T}$	A transformation matrix	
$\mathbf{u}$	Input vector, usually force	N
$\mathbf{V}$	Damping matrix	Ns/m
$\mathbf{w}$	Vector with unique DOFs for a coupled system from all substructures	
$\mathbf{x}$	State vector	
$\mathbf{y}$	Output vector; usually displacement, velocity or acceleration	
$\mathbf{Z}$	Inverse frequency response matrix	
ρ	Density	kg/m^3
E	Elastic stiffness (Young's modulus)	N/m
h	Denotes the number of substructures	
j	Imaginary number	
m	Number of degrees of freedom	
n	Number of states	
r	Number of outputs	
s	Number of inputs	
${}_e\mathbf{\Omega}$	Eigenfrequency matrix	rad/sec
Superscripts		
(s)	Denotes substructure s	
$*$	Complex conjugate	

Symbols in boldface with capitalised letters represent matrices, e.g. the mass matrix $\mathbf{M}$. Symbols in boldface and lower case letters represent column vectors, e.g. the generalised displacement vector $\mathbf{q}$. All other symbols represent scalars.

Contents

Abstract i

Preface iii

Acknowledgements iii

Nomenclature v

Contents vii

1 Introduction 1
1.1 Background . . . 1
1.2 Purpose . . . 1
1.3 Limitations . . . 2
1.4 Outline . . . 2

2 Theory 3
2.1 Basic Properties . . . 3
2.1.1 Linear Time Invariant Systems . . . 3
2.1.2 Reciprocity . . . 3
2.1.3 Passivity . . . 3
2.1.4 Stability . . . 4
2.2 Second Order Form . . . 4
2.3 First Order Form . . . 5
2.4 Frequency Domain Formulation . . . 6
2.5 System Identification, Observability and Controllability . . . 7
2.6 Modal Assurance Criterion . . . 7
2.7 Reduction Techniques . . . 7
2.7.1 Modal Domain . . . 8
2.7.2 Craig Bampton Reduction . . . 8
2.8 Substructure Synthesis . . . 9
2.8.1 Different Modes . . . 9
2.8.2 Physical Domain Synthesis . . . 10
2.8.3 Component Mode Synthesis . . . 12
2.8.4 Frequency Response Function-based Synthesis . . . 14
2.8.5 State-Space Model Synthesis . . . 14
2.8.6 Experimental and Analytical Substructuring . . . 17
2.9 State-Space Synthesis . . . 18
2.9.1 General Framework . . . 18
2.9.2 Second Order Form Equivalent of Synthesised First Order Form . . . 20
2.10 Interface Excitation . . . 22
2.11 Physical Models . . . 24

3 Method 24
3.1 Analytical Models . . . 24
3.1.1 Blade . . . 24
3.1.2 Bracket . . . 25
3.1.3 Hub Bracket . . . 26
3.2 Experiments . . . 27
3.2.1 Test Setup . . . 28
3.2.2 Alterations . . . 30
3.3 Experimental Models . . . 30
3.3.1 General . . . 32
3.3.2 Blade . . . 32

3.3.3 Blade Bracket . . . 34
3.3.4 Blade Bracket Hub . . . 35
3.3.5 Physical Models . . . 35
3.4 Coupling . . . 37
3.4.1 Blade Bracket . . . 37
3.4.2 Bracket Hub . . . 37

4 Results **37**
4.1 Blade Models . . . 38
4.2 Blade Bracket Models . . . 41
4.3 Analytical Coupling . . . 43
4.3.1 Blade Bracket . . . 43
4.3.2 Blade Bracket Hub . . . 45
4.4 Experimental-Analytical Coupling . . . 45
4.4.1 Blade Bracket . . . 45
4.4.2 Blade Bracket Hub . . . 49
4.5 Numerical Problems . . . 49
4.6 Unstable Systems . . . 53
4.6.1 Violation of Newton's Second Law for Analytical Models . . . 53
4.6.2 Passivity . . . 57

5 Discussion **57**
5.1 Models . . . 58
5.2 Synthesis . . . 58
5.3 Numerical Instability . . . 59
5.4 Physical Laws . . . 59
5.5 Theoretical Development . . . 60

6 Conclusion **60**

References **61**

A Experiments **64**

B Reciprocity **65**

C Modeshapes **66**

D Frequency Response Functions **69**

1 Introduction

A short background of the topic studied is given, followed by the purpose, content, limitations and outline of this thesis.

1.1 Background

Substructuring builds on the idea that a complex problem, that might not be solvable directly, or would take a long time to solve, can be decomposed into subcomponents which can be solved quickly and then assembled back into the original structure. The basic principle of decomposing an object into subcomponents, solving them, and assembling them again is used in the finite element (FE) method, where the subcomponents are called elements. This decomposition brings with it not only simplicity but also speed as it allows for parallel computing which increases the speed of the analysis. For a more thorough historical background of the subject along with significant work in the field, see de Klerk et al. [KRV08].

In structural dynamics, and computational methods in mechanics in general, a way to increase the speed of the analysis even further is to reduce the set of degrees of freedom (DOFs) for each substructure. From this smaller set of DOFs, an approximate model is obtained for each substructure and finally the substructures are coupled to form a reduced model of the original structure. This is called dynamic substructuring.

The subcomponents do not have to be analytical models but can also be experimentally acquired models. A complex structure which consists of many parts, for instance a car or a wind turbine, can be disassembled into its components. For these parts, or substructures, it is possible to create models from various experiments. These experimental models can then be coupled to give the solution for the full structure which is denoted experimental substructuring.

Of particular interest in this thesis is to couple experimental models to analytical models, which is often called experimental-analytical dynamic substructuring. This makes it possible to build experimental models from substructures that are too complex or would be too expensive to model and couple them to simpler substructures which can easily be modelled analytically.

In de Klerk et al. [KRV08], three classifications of dynamic substructuring is introduced. The component mode synthesis (CMS) method, where the substructures are reduced to a modal domain and the coupling, or synthesis, is between these reduced systems, as explained in [CK06; Cra00; KRV08]. The second approach is a frequency based one where the frequency response functions (FRFs) of the substructures are coupled; this method is commonly denoted FRF-based substructuring (FBS), see [BJ60; JBF88; KRV08]. The third method is direct coupling, i.e. coupling in the physical domain, see [KRV08]. In this thesis a fourth method, not classified in [KRV08] is used. It is based on coupling of first order state-space models. For further details about state-space synthesis see Sjövall [SA07]. Methods based on state-space synthesis are fairly new compared to the three classified methods.

The subject of substructuring has been an open research area ever since its advent in the 1960s, [KRV08], and with the advances made in computing and experimental equipment there has been a renewed interest in the subject. There is hope that coupling between experimental and analytical models will decrease the cost of complex mechanical systems such as cars, air planes, rocket launchers and wind turbines, if some parts can be modelled by, e.g. FEs whilst other parts can be experimentally acquired models. Thus, more reliable structures can be built which last longer and in turn become more environmentally friendly. Substructuring also offers the possibility for companies to share confidential data in the form of reduced models.

The structure used for investigation of substructuring in this thesis was proposed by the Society for Experimental Mechanics (SEM) Substructuring Focus Group to serve as a testbed in the effort to advance research in substructuring. The structure is the Ampair 600 wind turbine which is further detailed by Mayes [May12a]. The purpose of this structure is to serve as a reference for researchers around the world. Because it is open to the public, the results can be shared between researchers which is otherwise a frequent problem with industrial components. The data is shared online through a wiki [Onl].

1.2 Purpose

Generally, experimental substructuring techniques in use today work on simple academic examples but their use on real world problems have been restrained by poor results and cumbersome procedures, e.g. it is hard to

measure rotational degrees of freedom and rigid body modes and it is especially hard to account for dynamics in joints [KRV08].

This work aims to increase the knowledge of the chosen test structure and couple the parts of the testbed. It is also the intent of this thesis to popularise the state-space synthesis method developed by Sjövall [SA07], used extensively by Liljerehn [Lil12], and compare this method to the more popular CMS and FBS methods, with the testbed as a case study. Also of interest in this context is to compare the state-space method with the well known CMS method in a theoretical manner. Further, it is known that the dynamic properties of the blades differ [Gib+13] and thus it is of interest to find the difference between the blade bracket system as well. The assumption that the blades are linear in a large frequency interval is also of interest to investigate as this is used for coupling in this thesis.

Herein, the blades, brackets and the hub of the Ampair 600 wind turbine are considered. These components are coupled using CMS, FBS and state-space synthesis method. The CMS is used between analytical models and the FBS and state-space synthesis methods are used for the experimental and experimental-analytical coupling. For reference, the whole structure is also experimentally measured.

The Ampair 600 wind turbine blades, consisting of a composite hull around a solid core, have been thoroughly tested in dynamic and static measurements as well as destructive tests to quantify the material parameters [HA12; NM12; Gib+13; Joh+13; Lin13]. A calibrated FE model of the blades has also been developed by Johansson et al. [Joh+13] which is used in this thesis. New FE models of the hub and bracket are created from geometry, received from TU Delft, with standard material properties.

Recently, a number of researchers have been investigating the various parts of the the testbed where different coupling methods have been employed for substructuring but also quantifying the dynamics of the joints [Rah12; Roh12; RM13; NM13; MNM13; Bru+13; RKR13; Ste+13]. The results in this thesis will be quantitatively compared to these studies.

1.3 Limitations

As stated, this work uses a testbed which was proposed by the SEM Substructuring Focus Group, the Ampair 600 wind turbine, see Mayes [May12a]. The whole structure is fairly large and complex and all parts are not available at the university where this thesis is written. Thus, only parts of the testbed are studied in this thesis, namely the blades, the hub and the brackets connecting the blades to the hub. The dynamics of the mechanical parts inside the hub is eliminated according to SEM instructions, [Onl], by filling the assembled hub with epoxy to simplify the model of the hub. The dynamics of the joints will not be focused on but a few different coupling configurations will be considered.

Neither the bracket nor the hub FE models are experimentally validated. A brief verification of the analytical results is performed along with an analysis of the adequate reduction order. Also, errors in the measurements, such as the approximate direct accelerance transfer functions and shifted resonance frequencies, will not be discussed at length but mentioned briefly.

As data for the same structure is available from different sources a qualitative comparison of the results would be highly interesting. This will however not be considered here as it involves a high amount of work.

1.4 Outline

The theory necessary for this thesis is presented in chapter 2. It starts with an explanation of the basics of linear systems in section 2.1, including definitions of reciprocity, passivity and stability. In section 2.2 and 2.3, the second and first order formulations of mechanical systems are explained along with a method to transform a second order system to first order form. The frequency domain representation is explained in section 2.4. The concept of observability, controllability, system identification and modal correlation are explained briefly in sections 2.5 and 2.6, respectively. Two different reduction techniques are described in section 2.7. In section 2.8, the theory for the different dynamic substructuring methods are presented. In section 2.9, the state-space synthesis method is compared to the CMS method and in section 2.10 it is explained how reciprocity is enforced for experimental models. In section 2.11 it is explained how physical models can be enforced.

In chapter 3, the methodology used in the experiments, identification of models and coupling is presented. The different analytical models are shown and described in section 3.1. In section 3.2, a detailed description of how the experiments were performed is presented. The experimentally acquired models, and how they were

obtained, are described in section 3.3. The coupling procedures for the different considered cases are presented in section 3.4.

The results are presented in chapter 4. The experimental and analytical blade and blade bracket models are presented in sections 4.1 and 4.2, followed by the analytical and experimental-analytical coupling in sections 4.3 and 4.4. Then, in section 4.5 the numerical properties of the state-space algorithm are evaluated. In section 4.6 the impact that non-physicality in the systems have on the state-space model is evaluated.

In chapter 5 the results are discussed and compared to other work on the same testbed and to other work using the state-space method. In chapter 6 the conclusion for this thesis is given.

2 Theory

In this chapter the theory used in this thesis is explained. First, a brief overview of the basic properties of linear systems are summarised. Then, second order form models in the physical domain are explained followed by first order form models and a frequency domain representation of these models. Following is a brief section on observability, controllability and system identification. Sections 2.1 to 2.5 constitute a prelude to the substructuring theory. Then, the Modal Assurance Criterion (MAC) and reduction techniques used are explained. The three substructuring methods: Component Mode Synthesis (CMS), Frequency Response Function Based Synthesis (FBS) and State-Space Synthesis (SSS) are explained in section 2.8. The theoretical investigation between the state-space and the CMS method is shown in section 2.9. An outline of how to address non-measured interfaces and how to enforce physicality for measured systems is presented in sections 2.10 and 2.11.

2.1 Basic Properties

In this section, properties of linear system theory and assumption relevant to the systems studied are presented.

2.1.1 Linear Time Invariant Systems

All systems studied in this thesis are considered to be linear time invariant (LTI) systems. Mathematically, a system is said to be linear if it satisfies the additivity and homogeneity properties. A linear transformation from a vector space V to W is a function $T : V \to W$, where $\boldsymbol{\alpha}$ and $\boldsymbol{\beta}$ are vectors and c is a scalar, [HK71].

$$\mathbf{T}(\boldsymbol{\alpha} + \boldsymbol{\beta}) = \mathbf{T}\boldsymbol{\alpha} + \mathbf{T}\boldsymbol{\beta} \tag{2.1}$$

$$\mathbf{T}(c\boldsymbol{\alpha}) = c(\mathbf{T}\boldsymbol{\alpha}) \tag{2.2}$$

For a time invariant system the following property must be satisfied: If an input $u(t)$ into the system produces an output $y(t)$, then any time shift δ for the same input $u(t + \delta)$ will produce a equally time shifted output $y(t + \delta)$, [Kai80].

2.1.2 Reciprocity

For a linear system the Maxwell-Betti reciprocal theorem states that a force $\mathbf{f}_1$ applied at position 1, which causes a response $\mathbf{q}_2$ at position 2, is equal to the response $\mathbf{q}_1$ obtained at position 1, if a force $\mathbf{f}_2$ is applied at position 2 according to Figure 2.1. The mathematical relation is shown in eq (2.3) and is further explained by Reddy [Red08]. This is a crucial theorem that will be used to invoke reciprocity in the measured systems.

$$\mathbf{f}_1\mathbf{q}_1 = \mathbf{f}_2\mathbf{q}_2 \tag{2.3}$$

2.1.3 Passivity

The passivity criterion states that the power supplied to the system is non-negative and can be zero only for components without damping. Physical models satisfy the passivity criterion implicitly while experimentally identified models are not necessarily passive. For analytical models the passivity must be enforced with some form of damping that is added to the analytical system, [SA07].

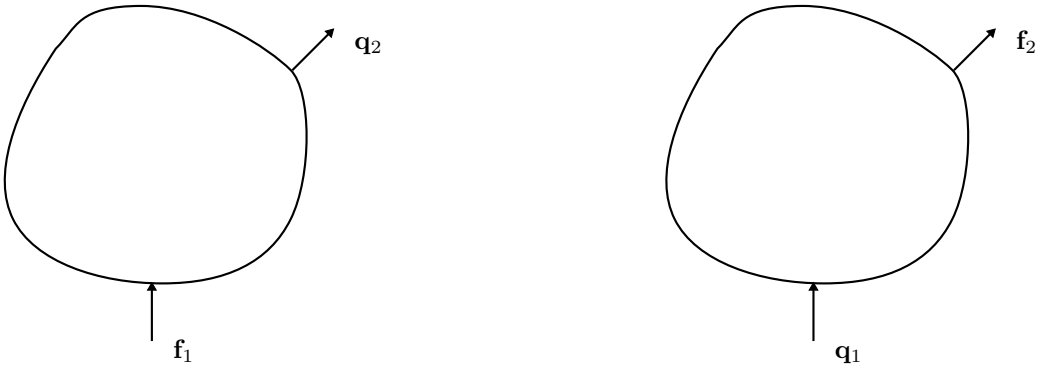

Figure 2.1: *Maxwell-Betti reciprocity.*

2.1.4 Stability

A system is considered asymptotically stable if the real part of its poles is negative, stable if the real part is zero and unstable if the real part is positive, see Meirovitch [Mei96]. An instability analysis is performed in section 4.6.

2.2 Second Order Form

Discrete, linearised, viscously damped, non-gyroscopic and non-circulatory equations of motion (EOMs) for mechanical systems in structural dynamics are usually written as second order ordinary differential equations, [CK06].

$$\mathbf{M}\ddot{\mathbf{q}}(t) + \mathbf{V}\dot{\mathbf{q}}(t) + \mathbf{K}\mathbf{q}(t) = \mathbf{f}(t) \tag{2.4}$$

On the left hand side of this equation, $\mathbf{q} \in \mathbb{R}^m$ represents the displacement vector and $\mathbf{M}$, $\mathbf{V}$ and $\mathbf{K}$ represent the square mass, damping and stiffness matrices, respectively. On the right hand side of this equation, $\mathbf{f}$ is the load vector. This equation describes a multiple degree of freedom (MDOF) physical system, e.g. derived through Newton's laws of motion, where m is the number of degrees of freedom (DOFs).

The load vector $\mathbf{f}$, which associates an applied load to each DOF of the model can be rewritten under the assumption that there is force input to the system only at a subset of the DOFs, e.g. at boundaries. The rectangular matrix $\mathbf{P}_u$ is then set up to relate the input $\mathbf{u} \in \mathbb{R}^s$ to the load vector $\mathbf{f}$, [Sjö04], according to eq (2.5). The index s denotes the number of inputs.

$$\mathbf{f}(t) = \mathbf{P}_u\mathbf{u}(t) \tag{2.5}$$

It is also possible to measure the output generated from this system. A selected set of output DOF is related to the displacement vector as follows.

$$\mathbf{y}_d(t) = \mathbf{P}_d\mathbf{q}(t) \tag{2.6}$$

Here, $\mathbf{y} \in \mathbb{R}^r$ is the output vector, subscript d denotes displacement output and the notation r denotes the number of outputs. The rectangular matrix $\mathbf{P}_d$ relates the output to the displacement. There is a similar relation for velocity outputs, $\mathbf{y}_v(t) = \mathbf{P}_v\dot{\mathbf{q}}(t)$. Then, $\mathbf{P}_v$, is the rectangular matrix relating the velocity output to the velocities and subscript v stands for velocity. Accelerations can also be outputs of the system and are denoted with a subscript a and $\mathbf{P}_a$ is the rectangular matrix that relates the output to the accelerations.

Experimentally acquired systems are damped implicitly while analytical systems must be explicitly damped in order to satisfy the passivity criterion. In this thesis the damping is modelled as a multiple of the the mass matrix. Thus the damping matrix is calculated as follows, where α is a scalar.

$$\mathbf{V} = \alpha\mathbf{M} \tag{2.7}$$

There are a few properties that the mass, damping and stiffness matrices must posses. This implies that the strain and kinetic energy produced from an arbitrary displacement and velocity vector are positive, respectively.

Firstly the matrices must be symmetric, i.e. $\mathbf{M} = \mathbf{M^T}$, $\mathbf{V} = \mathbf{V^T}$ and $\mathbf{K} = \mathbf{K^T}$. The second property is that the matrices must be positive semidefinite, i.e. $\mathbf{q^T M q} \geq 0$, $\mathbf{q^T V q} \geq 0$ and $\mathbf{q^T K q} \geq 0$, $\forall \mathbf{q} \in \mathbb{R}^m$. The stiffness matrix is positive definite except for systems allowing rigid-body displacement. The mass matrix is positive definite except when some DOF have no inertia (usually rotational DOF). For a thorough explanation see [CK06].

2.3 First Order Form

In control theory (and experimental mechanics) a system usually has multiple inputs and multiple outputs (MIMO) that measure the system's response. Such systems are usually modelled as a set of inputs and outputs related to internal states governed by first order differential equations. This is usually called a state-space formulation [Kai80] and is written as follows.

$$\begin{cases} \dot{\mathbf{x}}(t) = \mathbf{A}\mathbf{x}(t) + \mathbf{B}\mathbf{u}(t) \\ \mathbf{y}(t) = \mathbf{C}\mathbf{x}(t) + \mathbf{D}\mathbf{u}(t) \end{cases} \tag{2.8}$$

Here, $\mathbf{x} \in \mathbb{R}^n$ is the state vector with n states, $\mathbf{u} \in \mathbb{R}^s$ is the input vector and $\mathbf{y} \in \mathbb{R}^r$ is the output vector. In this thesis the input will always be a force unless stated otherwise. Matrices $\mathbf{A}$, $\mathbf{B}$, $\mathbf{C}$ and $\mathbf{D}$ are the state, input, output and feedthrough matrices, respectively. Here assumed constant. For a system with force inputs and where the output is either displacement or velocity the feedthrough matrix will be zero in accordance with Newton's second law; this will be shown below.

The state-space representation is often desired when acquiring experimental data, i.e. from system identification [Lju99], but a second order analytical system as described in eq (2.4) and (2.6) can also be written on first order form. In fact any integer order linear system can be written on first order form, [Abr00]. To transform the second order differential equation, eq (2.4), to a first order differential equation the state vector is defined as follows.

$$\mathbf{x}(t) = \begin{Bmatrix} \mathbf{q}(t) \\ \dot{\mathbf{q}}(t) \end{Bmatrix} \tag{2.9}$$

The number of states is then $n = 2m$. Now, in order to obtain a state-space formulation from the second order formulation the first step is to pre-multiply eq (2.4) by $\mathbf{M}^{-1}$ and using eq (2.5), the following is obtained.

$$\mathbf{I}\ddot{\mathbf{q}}(t) + \mathbf{M}^{-1}\mathbf{V}\dot{\mathbf{q}}(t) + \mathbf{M}^{-1}\mathbf{K}\mathbf{q}(t) = \mathbf{M}^{-1}\mathbf{P}_u\mathbf{u}(t) \tag{2.10}$$

This can further be rewritten using a block matrix formulation (note that the identity matrix does not perform any transformation and is omitted).

$$\ddot{\mathbf{q}}(t) = -\begin{bmatrix} \mathbf{M}^{-1}\mathbf{K} & \mathbf{M}^{-1}\mathbf{V} \end{bmatrix} \begin{Bmatrix} \mathbf{q}(t) \\ \dot{\mathbf{q}}(t) \end{Bmatrix} + \begin{bmatrix} \mathbf{M}^{-1}\mathbf{P}_u \end{bmatrix} \mathbf{u}(t) \tag{2.11}$$

For reasons which will soon be evident this equation can be regarded as the second of two equations. The first equation is obtained as a dummy equation for the velocities.

$$\dot{\mathbf{q}}(t) = \begin{bmatrix} \mathbf{0} & \mathbf{I} \end{bmatrix} \begin{Bmatrix} \mathbf{q}(t) \\ \dot{\mathbf{q}}(t) \end{Bmatrix} + \begin{bmatrix} \mathbf{0} \end{bmatrix} \mathbf{u}(t) \tag{2.12}$$

These two linear equations are then composed and written on matrix form.

$$\begin{bmatrix} \dot{\mathbf{q}}(t) \\ \ddot{\mathbf{q}}(t) \end{bmatrix} = \begin{bmatrix} \mathbf{0} & \mathbf{I} \\ -\mathbf{M}^{-1}\mathbf{K} & -\mathbf{M}^{-1}\mathbf{V} \end{bmatrix} \begin{Bmatrix} \mathbf{q}(t) \\ \dot{\mathbf{q}}(t) \end{Bmatrix} + \begin{bmatrix} \mathbf{0} \\ \mathbf{M}^{-1}\mathbf{P}_u \end{bmatrix} \mathbf{u}(t) \tag{2.13}$$

The output, as shown in eq (2.6) but here generalised for both displacement, velocities and accelerations, is defined as follows.

$$\mathbf{y}(t) = \begin{bmatrix} \mathbf{P}_d & \mathbf{P}_v \end{bmatrix} \begin{Bmatrix} \mathbf{q}(t) \\ \dot{\mathbf{q}}(t) \end{Bmatrix} + \begin{bmatrix} \mathbf{D} \end{bmatrix} \mathbf{u}(t) \tag{2.14}$$

Note that the feedthrough is zero, i.e. no direct term $\mathbf{D}$ is present when the output is displacement and/or velocity. This is because the state vector contains both displacements and velocities. The output for the

displacement can be identified as $\mathbf{y} = \mathbf{C}_d\mathbf{x}$, while for velocities, $\mathbf{y} = \mathbf{C}_v\mathbf{x}$ and for accelerations as $\mathbf{y} = \mathbf{D}\mathbf{u}$. Rewriting eq (2.13) and (2.14) with the state variable the following two equations are acquired.

$$\begin{cases} \dot{\mathbf{x}}(t) = \begin{bmatrix} \mathbf{0} & \mathbf{I} \\ -\mathbf{M}^{-1}\mathbf{K} & -\mathbf{M}^{-1}\mathbf{V} \end{bmatrix} \mathbf{x}(t) + \begin{bmatrix} \mathbf{0} \\ \mathbf{M}^{-1}\mathbf{P}_u \end{bmatrix} \mathbf{u}(t) \\ \mathbf{y}(t) = \begin{bmatrix} \mathbf{P}_d & \mathbf{P}_v \end{bmatrix} \mathbf{x}(t) \end{cases} \tag{2.15}$$

The general state-space formulation, with no feedthrough, is then written as follows.

$$\begin{cases} \dot{\mathbf{x}}(t) = \mathbf{A}\mathbf{x}(t) + \mathbf{B}\mathbf{u}(t) \\ \mathbf{y}(t) = \mathbf{C}\mathbf{x}(t) \end{cases} \tag{2.16}$$

The state, input and output matrices for this particular realisation are identified as shown below.

$$\mathbf{A} = \begin{bmatrix} \mathbf{0} & \mathbf{I} \\ -\mathbf{M}^{-1}\mathbf{K} & -\mathbf{M}^{-1}\mathbf{V} \end{bmatrix}, \quad \mathbf{B} = \begin{bmatrix} \mathbf{0} \\ \mathbf{M}^{-1}\mathbf{P}_u \end{bmatrix}, \quad \mathbf{C} = \begin{bmatrix} \mathbf{P}_d & \mathbf{P}_v \end{bmatrix} \tag{2.17}$$

For a newtonian mechanical system, as is considered in this thesis, where Newton's second law applies such that $\mathbf{f} = m\mathbf{a}$, where f is a force, m is mass and a is acceleration, it is implied that if the input to the system is a force there is no direct relation between the displacement and velocity, meaning that $\mathbf{CB} = \mathbf{0}$. The derivation of the first order form from an analytical second order form presented here is found in Appendix A in [Sjö04].

It should be noted that there exist many ways of rewriting the first order system that will be used in this thesis, this will be shown when needed.

2.4 Frequency Domain Formulation

The second and first order approaches presented so far are both time based. In experimental structural dynamics it is also interesting to study systems in the frequency domain. For the transformation from a time domain representation to a frequency domain representation the Laplace transform is used, see Folland [Fol09].

$$f_\omega(s) = \mathcal{L}\{f(t)\}(s) = \int_0^\infty \mathrm{e}^{-st} f(t)\mathrm{d}t \tag{2.18}$$

Capital letters are usually used to represent functions which are in the frequency domain but here the subscript ω will be used, i.e. $\mathcal{L}\{f(t)\}(s) = f_\omega$, as capital letters are reserved for matrices.

The two properties of the Laplace transform that will be used here are the following, [Fol09].

$$\mathcal{L}\{f'(t)\}(s) = sf_\omega(s) - f(0) \tag{2.19}$$

$$\mathcal{L}\{f''(t)\}(s) = s^2 f_\omega(s) - sf(0) - f'(0) \tag{2.20}$$

With these two properties, assuming that the two initial conditions are $f(0) = 0$ and $f'(0) = 0$, and rewriting the variable s as $s = j\omega$, where, j, is the imaginary number and ω is the frequency, the second order eq (2.4) can be transformed to the frequency domain.

$$(\mathbf{K} + j\omega\mathbf{V} - \omega^2\mathbf{M})\mathbf{q}_\omega(\omega) = \mathbf{f}_\omega(\omega) \tag{2.21}$$

This is the second order equation in the frequency domain, usually written in the following way.

$$\mathbf{Z}(\omega)\mathbf{q}_\omega(\omega) = \mathbf{f}_\omega(\omega) \quad \rightarrow \quad \mathbf{q}_\omega(\omega) = \mathbf{H}(\omega)\mathbf{f}_\omega(\omega) \tag{2.22}$$

Assuming that the responses are displacements the FRF matrix $\mathbf{H}$ is then denoted the receptance matrix and the inverse FRF matrix $\mathbf{Z}$ is denoted the dynamic stiffness matrix. If the responses are velocities then the FRFs are called mobility and the inverse is called mechanical impedance. Accelerance FRFs are acquired when the responses are accelerations and the inverse is called apparent mass, see Ewins [Ewi00]. There exists simple relations between these three FRFs. The Laplace transform of the displacements $\mathbf{q}(t)$ is $\mathbf{q}(\omega)_\omega$, for velocities $\dot{\mathbf{q}}(t)$ the Laplace transform, with $s = j\omega$, is $j\omega\mathbf{q}(\omega)_\omega$ and for accelerations $\ddot{\mathbf{q}}(t)$ the Laplace transform, again with $s = j\omega$, is $-\omega^2\mathbf{q}(\omega)_\omega$. Thus, it is easy to convert between the three different FRFs, see Ewins [Ewi00].

The first order differential equation shown in eq (2.8) can also be transformed to the frequency domain in a similar fashion.

$$j\omega \mathbf{x}_\omega(\omega) = \mathbf{A}\mathbf{x}_\omega(\omega) + \mathbf{B}\mathbf{u}_\omega(\omega) \tag{2.23}$$

$$\mathbf{y}_\omega(\omega) = \mathbf{C}\mathbf{x}_\omega(\omega) + \mathbf{D}\mathbf{u}_\omega(\omega) \tag{2.24}$$

Rewriting eq (2.23) and inserting it into eq (2.24) gives the following.

$$\mathbf{y}_\omega(\omega) = \mathbf{C}((j\omega\mathbf{I} - \mathbf{A})^{-1}\mathbf{B} + \mathbf{D})\mathbf{u}_\omega(\omega) = \mathbf{H}(\omega)\mathbf{u}_\omega(\omega) \tag{2.25}$$

Here, $\mathbf{H}$ is the same receptance matrix as before if the outputs are displacements.

2.5 System Identification, Observability and Controllability

System identification is performed on experimentally obtained frequency domain data with a method called N4SID from MATLAB's System Identification Toolbox [Lju99] to estimate a state-space model, i.e. to obtain a first order form, or rather the quadruple set $\{\mathbf{A}, \mathbf{B}, \mathbf{C}, \mathbf{D}\}$.

The theory behind system identification is out of the scope of this thesis. It is further described by Ljung [Lju99], McKelvey et al. [MAL96] and Van Overschee and DeMoor [OM94]. In order to automate the system identification process a method for automatic model order estimation developed at Chalmers University of Technology by Vahid Yaghoubi and Thomas Abrahamsson [YA12] was used along with the N4SID method. This newly developed method starts with a high order model and removes states that give a small contribution to the output in a multi-step procedure. Models of the same order are also compared against each other under different criteria further explained in [YA12]. Thus, the method only asks the user for a high model order to start with, everything else is automated.

In experimental mechanics and control theory in general, it is of importance to be able to measure and excite all the system states. The observability condition describes the ability of the outputs to describe all states of the system. The controllability condition on the other hand describes the ability of the input to excite all the system states. These two conditions were not used explicitly but rather had to be thought of during the experiments and analysis. Thus, for a theoretical explanation see [Kai80]

2.6 Modal Assurance Criterion

The Modal Assurance Criterion (MAC) is used to compare the collinearity of two vectors. It should also be noted that there exist different techniques for evaluating modal correlation, e.g. the MOC (Modal Observability Correlation) which also includes the information of the eigenfrequencies, see [YA12]. The MAC is further described by Allemang [All02] and Ewins [Ewi00]. It is calculated as follows.

$$MAC_{kl} = \frac{|\boldsymbol{\phi}_l^T \boldsymbol{\phi}_k^*|^2}{(\boldsymbol{\phi}_l^T \boldsymbol{\phi}_l^*)(\boldsymbol{\phi}_k^T \boldsymbol{\phi}_k^*)} \tag{2.26}$$

Here, *, represents complex conjugate and subscripts k and l represent the two sets of eigenvectors to be compared.

2.7 Reduction Techniques

In order to be able to handle industrial sized FE models, with hundreds of thousands of DOFs, in MATLAB the number of DOFs must be reduced. This is achieved by model reduction. In this thesis, modal reduction and Craig-Bampton reduction will be employed but there are other reduction methods that are useful for different purposes, e.g. Guyan-Irons, see [CK06]. Note that modal reduction in general consists of a transformation to the modal domain, where modal truncation can be performed, see section 2.7.1.

2.7.1 Modal Domain

To go from the physical domain to the modal domain the mode-superposition method is used, see Craig[CK06], where the physical DOFs are transformed to modal DOFs as follows.

$$\mathbf{q}(t) = \mathbf{\Phi}\boldsymbol{\eta}(t) \tag{2.27}$$

The transformation from physical coordinates $\mathbf{q}$ to modal coordinates (or principal coordinates) $\boldsymbol{\eta}$ is achieved by a transformation matrix $\mathbf{\Phi}$. This particular transformation matrix is the modal matrix which contain the undamped free-vibration modes.

$$\mathbf{\Phi} = \begin{bmatrix} \boldsymbol{\phi}_1 & \boldsymbol{\phi}_2 & \dots & \boldsymbol{\phi}_{m-1} & \boldsymbol{\phi}_m \end{bmatrix} \tag{2.28}$$

Every eigenvector $\boldsymbol{\phi}_i$ corresponds to an eigenvalue λ_i and the modes are usually sorted such that $\lambda_1 < \lambda_2 < \dots < \lambda_m$.

The free-vibration modes are attained from the generalised eigenvalue problem for the homogeneous undamped equation of motion.

$$\mathbf{M}\ddot{\mathbf{q}}(t) + \mathbf{K}\mathbf{q}(t) = \mathbf{0} \tag{2.29}$$

The corresponding eigenvalue problem is defined as shown in eq (2.30), [HK71].

$$\left[\mathbf{K} - \mathbf{\Lambda}\mathbf{M}\right]\mathbf{\Phi} = \mathbf{0} \tag{2.30}$$

The eigenvalue matrix $\mathbf{\Lambda}$ is related to the eigenfrequency matrix of the considered mechanical systems such that $\mathbf{\Lambda} = {}_e\mathbf{\Omega^2}$, where ${}_e\mathbf{\Omega}$ is the eigenfrequency matrix.

A very important feature of the modal matrix is orthogonality, i.e. $\boldsymbol{\phi}_r^T\mathbf{M}\boldsymbol{\phi}_s = 0$, $\boldsymbol{\phi}_r^T\mathbf{V}\boldsymbol{\phi}_s = 0$ and $\boldsymbol{\phi}_r^T\mathbf{K}\boldsymbol{\phi}_s = 0$ if ${}_e\omega_r \neq {}_e\omega_s$. This means that the transformed mass, stiffness and damping matrices to modal coordinates are diagonal matrices which means that the equation of motion in modal coordinates are uncoupled.

To transform the physical second order differential equation to modal coordinates eq (2.27) is used in (2.4), which is also pre-multiplied by the transpose of the modal matrix.

$$\mathbf{\Phi}^T\mathbf{M}\mathbf{\Phi}\ddot{\boldsymbol{\eta}}(t) + \mathbf{\Phi}^T\mathbf{V}\mathbf{\Phi}\dot{\boldsymbol{\eta}}(t) + \mathbf{\Phi}^T\mathbf{K}\mathbf{\Phi}\boldsymbol{\eta}(t) = \mathbf{\Phi}^T\mathbf{f}(t) \tag{2.31}$$

Thus, the transformed differential equation can be written as follows.

$$\mathbf{M}_m\ddot{\boldsymbol{\eta}}(t) + \mathbf{V}_m\dot{\boldsymbol{\eta}}(t) + \mathbf{V}_m\boldsymbol{\eta}(t) = \mathbf{f}_m(t) \tag{2.32}$$

Where the modal mass, stiffness, damping, and force vector are identified as follows.

$$\mathbf{M}_m = \mathbf{\Phi}^T\mathbf{M}\mathbf{\Phi}, \quad \mathbf{V}_m = \mathbf{\Phi}^T\mathbf{V}\mathbf{\Phi}, \quad \mathbf{K}_m = \mathbf{\Phi}^T\mathbf{K}\mathbf{\Phi}, \quad \mathbf{f}_m(t) = \mathbf{\Phi}^T\mathbf{f}(t) \tag{2.33}$$

In eq (2.32) the second order differential equation is written as m uncoupled differential equations. In order to reduce the model order some modes from the modal matrix (transformation matrix) are removed, usually higher modes, i.e. a process denoted modal truncation.

2.7.2 Craig Bampton Reduction

Like the modal transformation, the Craig-Bampton reduction transforms the physical coordinates to modal coordinates, but additionally allows for defining a set of physical DOFs that are retained. This is particularly useful in dynamic substructuring as the coordinates describing the internal dynamics, $\mathbf{q}_b$, can be reduced to a very small order of generalised coordinates (in this case modal coordinates), $\boldsymbol{\eta}_b$, and the coupling DOFs kept in physical coordinates, $\mathbf{q}_c$.

To perform a Craig-Bampton reduction on the MDOF equation of motion, in eq (2.4); a particular transformation matrix $\mathbf{T}$ is used.

$$\mathbf{q}(t) = \begin{Bmatrix} \mathbf{q}_c(t) \\ \mathbf{q}_b(t) \end{Bmatrix} = \begin{bmatrix} \mathbf{I} & \mathbf{0} \\ \mathbf{\Psi}_{FM} & \mathbf{\Psi}_{CM} \end{bmatrix} \begin{Bmatrix} \mathbf{q}_c(t) \\ \boldsymbol{\eta}_b(t) \end{Bmatrix} = \mathbf{T} \begin{Bmatrix} \mathbf{q}_c(t) \\ \boldsymbol{\eta}_b(t) \end{Bmatrix} \tag{2.34}$$

The body (or interior) part of the fixed-interface modes is here denoted by $\mathbf{\Psi}_{FM}$ while $\mathbf{\Psi}_{CM}$ denotes the body part of the constraint-mode matrix [CK06]. The different modes are further described in section 2.8.1. The subscript c denotes the interface DOFs and thematrix de subscript b denotes the body DOFs.

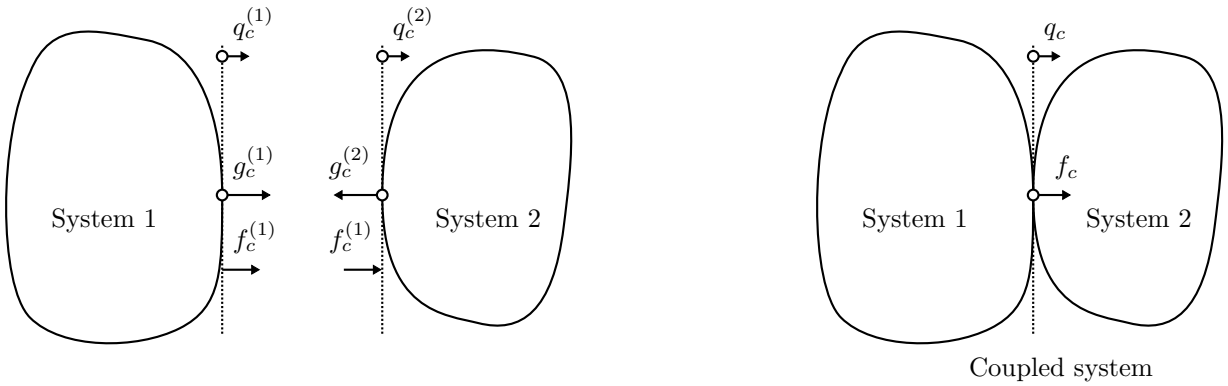

Figure 2.2: *Two separate systems and the coupled system.*

Thus, eq (2.34) is inserted into the second order system (2.4) and pre-multiplied by the transposed transformation matrix and the following is obtained.

$$\mathbf{T}^T\mathbf{M}\mathbf{T}\begin{Bmatrix}\ddot{\mathbf{q}}_c(t)\\ \ddot{\boldsymbol{\eta}}_b(t)\end{Bmatrix} + \mathbf{T}^T\mathbf{V}\mathbf{T}\begin{Bmatrix}\dot{\mathbf{q}}_c(t)\\ \dot{\boldsymbol{\eta}}_b(t)\end{Bmatrix} + \mathbf{T}^T\mathbf{K}\mathbf{T}\begin{Bmatrix}\mathbf{q}_c(t)\\ \boldsymbol{\eta}_b(t)\end{Bmatrix} = \mathbf{T}^T\mathbf{f}(t) \tag{2.35}$$

The new mass, damping and stiffness matrices can then be identified along with the transformed force vector.

$$\mathbf{M}_{cb}\begin{Bmatrix}\ddot{\mathbf{q}}_c(t)\\ \ddot{\boldsymbol{\eta}}_b(t)\end{Bmatrix} + \mathbf{V}_{cb}\begin{Bmatrix}\dot{\mathbf{q}}_c(t)\\ \dot{\boldsymbol{\eta}}_b(t)\end{Bmatrix} + \mathbf{K}_{cb}\begin{Bmatrix}\mathbf{q}_c(t)\\ \boldsymbol{\eta}_b(t)\end{Bmatrix} = \mathbf{f}_{cb}(t) \tag{2.36}$$

$$\mathbf{M}_{cb} = \mathbf{T}^T\mathbf{M}\mathbf{T}, \quad \mathbf{V}_{cb} = \mathbf{T}^T\mathbf{V}\mathbf{T}, \quad \mathbf{K}_{cb} = \mathbf{T}^T\mathbf{K}\mathbf{T}, \quad \mathbf{f}_{cb}(t) = \mathbf{T}^T\mathbf{f}(t) \tag{2.37}$$

For a thorough explanation see Craig [CK06]. It is worth to mention that the Craig-Bampton reduction was performed in MD Nastran, see the MSC Nastran Support for more information [Manb].

2.8 Substructure Synthesis

In this section the different substructuring methods will be presented. Coupling in the physical domain, coupling between reduced components, coupling between FRFs and finally the state-space coupling procedure will be presented. Further, a brief explanation between experimental and analytical substructuring is given. The notations are adopted as close as possible to the notations used by de Klerk et al. [KRV08]. Also, a brief introduction is given to the different kinds of modes that are of relevance in dynamic substructuring.

In general, when components are to be coupled, two conditions must be fulfilled; compatibility and force equilibrium. This thesis will only treat what de Klerk et al. [KRV08] refers to as the primal formulation, which implies that the displacements are defined and interface forces are eliminated. The primal formulation in the physical domain is assembled in the same manner as FE elements, see de Klerk et al. [KRV08]. In Figure 2.2 two bodies to be coupled are illustrated with their related forces and displacements outlined. This figure will be referred to when describing the different synthesis techniques below.

When coupling two structures, which are described by m_1 and m_2 DOFs, the assembled structure will consist of $m_1 + m_2 - m_c$ coordinates, where m_c is the number of couplings. This holds for direct coupling, CMS and FBS. Notice that for state-space coupling there exist twice as many states as DOFs and thus if $n = 2m$, for two structures with n_1 and n_2 states and m_c coupling coordinates the coupled system will contain $n_1 + n_2 - 2m_c$ states, [SA07].

The reader should also note that the explicit time dependency is dropped for the derivations of the coupling methods for brevity.

2.8.1 Different Modes

In section 2.7.2 the notion of fixed-interface and constraint modes was introduced. In the CMS method there exist different kinds of modes that can be used to describe the components; these are called component modes.

Normal modes can be divided into fixed-interface normal modes which have the boundary DOFs fixed while the internal DOFs are free and free-interface normal modes which have all the DOFs free. The free-interface modes are what will be referred to as the modeshapes, i.e. the free-free normal modes of the FE model will be compared to an approximation of the free-free experimental modes in the MAC correlations. There are also so-called loaded-interface normal modes which can be useful in experimental substructuring; the interface used for coupling is then loaded with some additional mass. The transmission simulator method is based on this premiss.

Constraint modes are modes obtained as the static deformation of a structure subject to a unit displacement at one DOF in a specific set, call it set $\mathcal{A}$, and where the other DOFs in that set are restrained and all other DOFs not in this particular set are free. The set of interface constraint modes are very useful in CMS methods as it is easy to enforce compatibility between components. Further, rigid body modes are undeformed modes which describe the rotation and translation of the object. For free-free structures there exist six rigid body modes.

Attachment and inertia-relief modes are the last form of modes presented here; the reader can read more about different types of modes in Craig [CK06]. Attachment modes are defined as the structure displacement vector subject to a force at one DOF from a particular set, again denoted by $\mathcal{A}$. Thus, they describe deformation of a structure that is subject to a loading, i.e. in the vibration tests the obtained modeshapes are these kind of modes. It should be noted that these attachment modes are affected by rigid body modes, if the structure was tested in a free-free like condition.

2.8.2 Physical Domain Synthesis

The EOMs as shown in eq (2.4) can be rewritten to separate interface and other forces, here denoted $\mathbf{f}$ and $\mathbf{g}$, respectively. Superscript (s) denote substructure number s.

$$\mathbf{M}^{(s)}\ddot{\mathbf{q}}^{(s)}(t) + \mathbf{V}^{(s)}\dot{\mathbf{q}}^{(s)}(t) + \mathbf{K}^{(s)}\mathbf{q}^{(s)}(t) = \mathbf{f}^{(s)}(t) + \mathbf{g}^{(s)}(t) \tag{2.38}$$

All of these substructures can be cast into a block diagonal matrix formulation shown below.

$$\mathbf{M}\ddot{\mathbf{q}} + \mathbf{V}\dot{\mathbf{q}} + \mathbf{K}\mathbf{q} = \mathbf{f} + \mathbf{g} \tag{2.39}$$

If the number of substructures is h, the diagonal matrices and corresponding force and displacement vectors are identified as follows.

$$\mathbf{M} = diag(\mathbf{M}^{(1)}, \ldots, \mathbf{M}^{(h)}), \quad \mathbf{V} = diag(\mathbf{V}^{(1)}, \ldots, \mathbf{V}^{(h)}), \quad \mathbf{K} = diag(\mathbf{K}^{(1)}, \ldots, \mathbf{K}^{(h)}) \tag{2.40}$$

$$\mathbf{q} = [\mathbf{q}^{(1)}, \ldots, \mathbf{q}^{(h)}]^T, \quad \mathbf{f} = [\mathbf{f}^{(1)}, \ldots, \mathbf{f}^{(h)}]^T, \quad \mathbf{g} = [\mathbf{g}^{(1)}, \ldots, \mathbf{g}^{(h)}]^T \tag{2.41}$$

Note that the matrices and vectors above are assembled into matrices and vectors containing h subsystems. Thus, these symbols will be used interchangeably when describing only one system or h systems; there is no difference in the general theory as long as everything is ordered.

In Figure 2.2, both the external and the interface forces at the coupling point are shown as well as the displacements. To couple the two structures, i.e. system 1 and system 2, the following must be true: $q_c^{(1)} = q_c^{(2)}$. In other words, the displacement at the coupling point for system 1 and 2 must be equal. This is known as compatibility. The forces acting at the coupling point must satisfy the following requirement, $f_c = f_c^{(1)} + g_c^{(1)} + f_c^{(2)} - g_c^{(2)} = f_c^{(1)} + f_c^{(2)}$, or formulated in another way, $g^{(1)} - g_c^{(2)} = 0$, meaning that the resultant of the interface forces must be zero, known as equilibrium.

The compatibility condition can be written on matrix form as follows.

$$\mathbf{E}\mathbf{q} = \mathbf{0} \tag{2.42}$$

The matrix $\mathbf{E}$ describes the coupling DOFs. If the DOFs are matching, as will be assumed, the matrix is a signed Boolean matrix which means that it contains only $1, -1$ and 0. This means that the number of columns of $\mathbf{E}$ is m times h and the number of rows is the number of coupling DOFs. Note that in de Klerk et al. [KRV08], this matrix is denoted $\mathbf{B}$ but to avoid confusion with the input matrix in the state-space formulation the notation is changed.

Let $\mathbf{L}$ be a Boolean matrix, i.e. consisting of only 1 and 0, which localises the interface DOFs of the substructures from the whole set with m times h DOF. Then the matrix formulation of the equilibrium condition can then be formulated as shown below.

$$\mathbf{L}^T\mathbf{g} = \mathbf{0} \tag{2.43}$$

Both the compatibility and equilibrium conditions stated above hold in a theoretical sense. When modelling a joint or a sliding problem, these requirements must be relaxed. This is however not considered in this thesis.

The total system with compatibility and equilibrium conditions is given below.

$$\begin{cases} \mathbf{M}\ddot{\mathbf{q}} + \mathbf{V}\dot{\mathbf{q}} + \mathbf{K}\mathbf{q} = \mathbf{f} + \mathbf{g} \\ \mathbf{E}\mathbf{q} = \mathbf{0} \\ \mathbf{L}^T\mathbf{g} = \mathbf{0} \end{cases} \tag{2.44}$$

A unique set of DOFs of the coupled system is defined and the interface forces are eliminated using the interface equilibrium as in FE assembly.

$$\mathbf{q} = \mathbf{L}\mathbf{w} \tag{2.45}$$

In the above equation the unique set of DOFs is defined as $\mathbf{w}$. Note again that the notation used in de Klerk et al. [KRV08] for the unique set of DOFs is $\mathbf{q}$ but this notation is changed as the generalised coordinates are already defined with this symbol. Further in de Klerk et al. [KRV08], the DOFs are defined as $\mathbf{u}$ whereas in this thesis they are defined as $\mathbf{q}$ and $\mathbf{u}$ in this thesis represents the system input.

The relation between $\mathbf{E}$ and $\mathbf{L}$ is shown below.

$$\mathbf{E}\mathbf{q} = \mathbf{E}\mathbf{L}\mathbf{w} = \mathbf{0} \tag{2.46}$$

It is noted in the above equation that $\mathbf{L}$ is the nullspace of $\mathbf{E}$.

$$\mathbf{L} = null(\mathbf{E}) \tag{2.47}$$

The EOM, of all the substructures, eq (2.39), can be expressed in terms of the unique set of DOFs $\mathbf{w}$, defined in eq 2.46. The compatibility condition is satisfied from the choice of $\mathbf{w}$ and hence the total system can be written as follows.

$$\begin{cases} \mathbf{M}\mathbf{L}\ddot{\mathbf{w}} + \mathbf{V}\mathbf{L}\dot{\mathbf{w}} + \mathbf{K}\mathbf{L}\mathbf{w} = \mathbf{f} + \mathbf{g} \\ \mathbf{L}^T\mathbf{g} = \mathbf{0} \end{cases} \tag{2.48}$$

Further, if the system is pre-multiplied by $\mathbf{L}^T$ and it is realised that $\mathbf{g}$ is zero, the total system is reduced to the following.

$$\tilde{\mathbf{M}}\ddot{\mathbf{w}} + \tilde{\mathbf{V}}\dot{\mathbf{w}} + \tilde{\mathbf{K}}\mathbf{w} = \tilde{\mathbf{f}} \tag{2.49}$$

The stiffness, damping and mass matrices and the force vector are identified as below.

$$\tilde{\mathbf{M}} = \mathbf{L}^T\mathbf{M}\mathbf{L}, \quad \tilde{\mathbf{V}} = \mathbf{L}^T\mathbf{V}\mathbf{L}, \quad \tilde{\mathbf{K}} = \mathbf{L}^T\mathbf{K}\mathbf{L}, \quad \tilde{\mathbf{f}} = \mathbf{L}^T\mathbf{f} \tag{2.50}$$

The reader is referred to the paper by de Klerk et al. [KRV08] for a thorough explanation of the above derivations.

Primal direct coupling is used by the FE method assembly process and is frequently used for coupling non-reduced analytical models. In an experimental setting it is usually more common to describe the model in the modal or frequency domain and thus the used coupling method is either component mode synthesis or frequency based substructuring.

2.8.3 Component Mode Synthesis

CMS methods are based on coupling of components that are in a reduced space, for example in the modal domain. This is a very usual coupling method for analytical models, for which the coupling conditions can be tracked exactly which is shown below.

The procedure to coupled reduced structures is analogous to direct coupling but with an additional transformation. First the generalised coordinates are transformed to a set of reduced coordinates, usually modal (where many different modes can be used, free modes, fixed interface modes etc.). Here the symbol $\boldsymbol{\eta}$ will be used to represent the reduced set, which also represents the modal DOF.

$$\mathbf{q} \approx \mathbf{R}\boldsymbol{\eta} \tag{2.51}$$

Thus, the generalised displacements are approximately the same as the product of the reduction matrix $\mathbf{R}$ and the modal coordinates, or in other words, the reduction matrix maps the modal coordinates to generalised physical coordinates. The reduction matrix is block diagonal, one block for each substructure.

$$\mathbf{R} = diag(\mathbf{R}^{(1)}, \ldots, \mathbf{R}^{(\mathbf{h})}) \tag{2.52}$$

Thus, with this transformation matrix eq (2.38) can be transformed to eq (2.53). Note that the transformed equations will in fact resemble the modal transformation given in eq 2.32. The same notations will be used but the reader should be aware that they do not necessarily describe the same system.

$$\mathbf{M}\ddot{\boldsymbol{\eta}}(t) + \mathbf{V}\dot{\boldsymbol{\eta}}(t) + \mathbf{K}\boldsymbol{\eta}(t) = \mathbf{f}(t) + \mathbf{g}(t) + \mathbf{r}(t) \tag{2.53}$$

Notice that a vector $\mathbf{r}$ is introduced which is used to describe the residual forces introduced by the approximation. The reduced equilibrium forces are obtained such that $\mathbf{Rr} = \mathbf{0}$. Thus, the system matrices and the internal and external forces can be identified as follows.

$$\bar{\mathbf{M}}_m = \mathbf{R}^T\mathbf{M}\mathbf{R}, \quad \bar{\mathbf{V}}_m = \mathbf{R}^T\mathbf{V}\mathbf{R}, \quad \bar{\mathbf{K}}_m = \mathbf{R}^T\mathbf{K}\mathbf{R}, \quad \bar{\mathbf{f}}_m = \mathbf{R}^T\mathbf{f}, \quad \bar{\mathbf{g}}_m = \mathbf{R}^T\mathbf{g} \tag{2.54}$$

The compatibility condition for the reduced equation system can then be formulated as follows.

$$\mathbf{E}_m\boldsymbol{\eta} = \mathbf{0} \tag{2.55}$$

$$\mathbf{E}_m = \mathbf{E}\mathbf{R} \tag{2.56}$$

The global set of modal coordinates that satisfy the compatibility condition can also be found.

$$\boldsymbol{\eta} = \mathbf{L}_m\boldsymbol{\xi} \tag{2.57}$$

Here $\boldsymbol{\xi}$ represents the global set of modal coordinates and $\mathbf{L}_m$ is the primal assembly matrix. Again it can be shown that $\mathbf{L}_m$ is the nullspace of $\mathbf{E}_m$.

$$\mathbf{E}_m\boldsymbol{\eta} = \mathbf{E}_m\mathbf{L}_m\boldsymbol{\xi} = \mathbf{0} \tag{2.58}$$

$$\mathbf{L}_m = null(\mathbf{E}_m) = null(\mathbf{E}\mathbf{R}) \tag{2.59}$$

Thus the following final equation is found for the substructures.

$$\begin{cases} \mathbf{M}_m\ddot{\boldsymbol{\eta}} + \mathbf{V}_m\dot{\boldsymbol{\eta}} + \mathbf{K}_m\boldsymbol{\eta} = \mathbf{f}_m + \mathbf{g}_m \\ \mathbf{E}_m\boldsymbol{\eta} = \mathbf{0} \\ \mathbf{L}_m^T\mathbf{g}_m = \mathbf{0} \end{cases} \tag{2.60}$$

The same procedure as in the direct coupling is used with $\boldsymbol{\eta} = \mathbf{L}_m\boldsymbol{\xi}$.

$$\begin{cases} \mathbf{M}_m\mathbf{L}_m\ddot{\boldsymbol{\xi}} + \mathbf{V}_m\mathbf{L}_m\dot{\boldsymbol{\xi}} + \mathbf{K}_m\mathbf{L}_m\boldsymbol{\xi} = \mathbf{f}_m + \mathbf{g}_m \\ \mathbf{E}_m\mathbf{L}_m\boldsymbol{\xi} = \mathbf{0} \\ \mathbf{L}_m^T\mathbf{g}_m = \mathbf{0} \end{cases} \tag{2.61}$$

Lastly, the equation system above is pre-multiplied by transpose of the primal assembly matrix $\mathbf{L}_m^T$ and it is noted that $\mathbf{E}_m\mathbf{L}_m$ is zero as $\mathbf{L}_m = null(\mathbf{E}_m)$. The coupled system is then obtained.

$$\bar{\mathbf{M}}_m\ddot{\boldsymbol{\xi}} + \bar{\mathbf{V}}_m\dot{\boldsymbol{\xi}} + \bar{\mathbf{K}}_m\boldsymbol{\xi} = \bar{\mathbf{f}}_m \tag{2.62}$$

The assembled system matrices and the force vector can be identified as shown below.

$$\bar{\mathbf{M}}_m = \mathbf{L}_m^T\mathbf{M}_m\mathbf{L}_m, \quad \bar{\mathbf{V}}_m = \mathbf{L}_m^T\mathbf{V}_m\mathbf{L}_m, \quad \bar{\mathbf{K}}_m = \mathbf{L}_m^T\mathbf{K}_m\mathbf{L}_m, \quad \bar{\mathbf{f}}_m = \mathbf{L}_m^T\mathbf{f}_m \tag{2.63}$$

It should be noted that this coupling method, for analytical models, yields very accurate approximations as the coupling is made in the physical domain even though the substructures are in a reduced domain. This is because the transformation matrix is known and every transformation can be tracked. In experimental substructuring this method is problematic as the reduction matrix is not explicitly known, making the user lost in a space of modal coordinates. That is, it is no longer possible to define the coupling conditions in the physical domain but rather modal coordinates must be chosen for coupling. It can be difficult to chose the right modal coordinates as the coupling condition between two substructures must still have a physical meaning. Usually the higher modes are chosen as coupling coordinates. Allen and Mayes [AM07] have studied the best set of generalised modal coordinates to be used for coupling. They have formed a method dubbed the Maximum Rank Coordinate Choice (MRCC) which ensures that the coupling constraint matrix will not be singular. The coupling constraint matrix is formulated by selecting a set of constraint coordinates and a set of internal, or body, coordinates (the term modal and reduced will be dropped here and the meaning of coordinates is to imply modal coordinates in the following) and expressing the constraint coordinates with respect to the internal, as follows.

$$\begin{Bmatrix}\boldsymbol{\eta}_1\\ \boldsymbol{\eta}_2\end{Bmatrix} = \mathbf{T}_{dummy}\begin{Bmatrix}\boldsymbol{\eta}_c\\ \boldsymbol{\eta}_b\end{Bmatrix} \tag{2.64}$$

Here $\boldsymbol{\eta}_{1,2}$ represent two substructures and $\mathbf{T}_{dummy}$ is a sorting matrix to achieve this mapping. The problem can now be reformulated as the question of which DOFs to select as interface coordinates. If the reduced kinematic constraint equation, equation (2.55), is multiplied by the sorting matrix and split into a constraint part and an internal part the following is obtained.

$$\mathbf{E}_m\mathbf{T}_{dummy}\begin{Bmatrix}\boldsymbol{\eta}_c\\ \boldsymbol{\eta}_b\end{Bmatrix} = \hat{\mathbf{E}}_m\begin{Bmatrix}\boldsymbol{\eta}_c\\ \boldsymbol{\eta}_b\end{Bmatrix} = \begin{bmatrix}\mathbf{E}_{m,c} & \mathbf{E}_{m,b}\end{bmatrix}\begin{Bmatrix}\boldsymbol{\eta}_c\\ \boldsymbol{\eta}_b\end{Bmatrix} = \mathbf{0} \tag{2.65}$$

Here, $\hat{\mathbf{E}}_\mathbf{m}$ is the transformed constraint matrix for reduced systems. Thus the constraint coordinates can be written in terms of the body coordinates.

$$\boldsymbol{\eta}_c = -\mathbf{E}_{m,c}^{-1}\mathbf{E}_{m,b}\boldsymbol{\eta}_b \tag{2.66}$$

Thus, implying that an incorrect choice of the constraint coordinates can result in a singular matrix $\mathbf{E}_{m,c}$. The solution is to decompose the kinematic constraint matrix with the Singular Value Decomposition (SVD) [GL96].

$$\mathbf{E}_m = \mathbf{U}_a\mathbf{S}_a\mathbf{V}_a^T \tag{2.67}$$

By the definition of the SVD, the matrices $\mathbf{U}_a$ and $\mathbf{V}_a$ (not to be confused with the damping matrix, also known as $\mathbf{V}$) are orthogonal matrices and $\mathbf{S}_a$ is a diagonal matrix with singular values in decreasing order. If $\mathbf{V}_a = \mathbf{T}_{dummy}$ is inserted into equation (2.65), the following is obtained, due to the orthogonality property of the SVD.

$$\hat{\mathbf{E}}_m = \mathbf{U}_a\mathbf{S}_a \tag{2.68}$$

Thus, the columns of $\hat{\mathbf{E}}_m$ are linearly independent and consequently the matrix can be inverted. If the coordinates corresponding to the lowest singular values are chosen as coupling coordinates no physical information should be lost from the system either. For a thorough explanation and study of this approach, see Allen and Mayes [AM07].

2.8.4 Frequency Response Function-based Synthesis

The frequency domain substructuring method will be derived according to de Klerk et al. [KRV08]. The FBS method can be traced back to Bishop and Johnson [BJ60]. In this thesis the formulation presented by Jetmundsen et al. [JBF88] is used in the calculations because of its superior numerical properties, i.e. only one matrix inversion is required which is important since the FRF matrices can very easily be ill-conditioned at the antiresonances. It should also be noted that this method has been extended to allow for flexible joints to be modelled as well, by Liu and Ewins [LE02].

When experimental measurements are performed the dynamics of a mechanical system are usually obtained in the form of frequency response functions. Thus the mass, damping and stiffness matrices are not explicitly known. Also, accelerance data is usually obtained since the sensors most frequently measure accelerations. This data must be converted to receptance in order to enforce compatibility conditions. To couple structures in the frequency domain the primal formulation will be used. First, the physical second order form must be transformed into the frequency domain, which was performed in section 2.4. In short, eq (2.44) is transformed to the frequency domain where $\mathbf{Z}$ is the dynamic stiffness matrix.

$$\begin{cases} \mathbf{Z}(\omega)\mathbf{q}_\omega(\omega) = \mathbf{f}_\omega(\omega) + \mathbf{g}_\omega(\omega) \\ \mathbf{E}\mathbf{u}_\omega(\omega) = \mathbf{0} \\ \mathbf{L}^T\mathbf{g}_\omega(\omega) = \mathbf{0} \end{cases} \tag{2.69}$$

Interface kinematic constraints are established in the same manner as for the primal coupling in the physical domain, a unique set of interface DOFs denoted $\mathbf{w}_\omega$ are chosen and $\mathbf{E}$ and $\mathbf{L}$ are found as before, thus yielding the coupled equation as shown below.

$$\tilde{\mathbf{Z}}(\omega)\mathbf{w}_\omega(\omega) = \tilde{\mathbf{f}}_\omega(\omega) \tag{2.70}$$

The coupled dynamic stiffness matrix and the force vector are identified as follows.

$$\tilde{\mathbf{Z}} = \mathbf{L}^T\mathbf{Z}_\omega\mathbf{L}, \quad \tilde{\mathbf{f}}_\omega = \mathbf{L}^T\mathbf{f}_\omega \tag{2.71}$$

Note that the formulation derived by Jetmundsen et al. [JBF88] is used in the calculations and it is given here without derivation.

$$\begin{bmatrix} \mathbf{H}_{bb} & \mathbf{H}_{bc} & \mathbf{H}_{bb} \\ \mathbf{H}_{cb} & \mathbf{H}_{cc} & \mathbf{H}_{cb} \\ \mathbf{H}_{bb} & \mathbf{H}_{bc} & \mathbf{H}_{bb} \end{bmatrix} = \begin{bmatrix} \mathbf{H}^1_{bb} & \mathbf{H}^1_{bc} & \mathbf{0} \\ \mathbf{H}^1_{cb} & \mathbf{H}^1_{cc} & \mathbf{0} \\ \mathbf{0} & \mathbf{0} & \mathbf{H}^2_{bb} \end{bmatrix} - \begin{bmatrix} \mathbf{H}^1_{bc} \\ \mathbf{H}^1_{cc} \\ -\mathbf{H}^2_{bc} \end{bmatrix} \left[\mathbf{H}^1_{cc} + \mathbf{H}^2_{cc}\right]^{-1} \begin{bmatrix} \mathbf{H}^1_{bc} \\ \mathbf{H}^1_{cc} \\ -\mathbf{H}^2_{bc} \end{bmatrix}^T \tag{2.72}$$

Here, $\mathbf{H}$, stands for the FRFs while the superscript, $\{1, 2\}$, denotes substructure one and two, respectively. The subscript, $\{b, c\}$, denotes the internal (or body) and constraint (or coupling) DOFs, respectively.

Notice that the FBS method does not have the same problems as the CMS method, that is the selection of coupling DOFs as the FBS method is based on an input/output relation only and coupling is performed directly on the outputs describing the physical constraints.

2.8.5 State-Space Model Synthesis

Sjövall and Abrahamsson have developed a method for coupling based on first order state-space form [SA07; Sjö04]. It should be noted that there exist other state-space coupling methods, e.g. by Su and Juang [SJ94] which is similar to the method proposed by Sjövall and Abrahamsson. The state-space method is most useful for experimental models but also works for analytical models as a second order analytical model can easily be transformed to first order form, as shown in section 2.3. The method will be derived from a analytical second order system, i.e. from eq (2.4) to relate it to the previously derived coupling techniques.

$$\mathbf{M}\ddot{\mathbf{q}} + \mathbf{V}\dot{\mathbf{q}} + \mathbf{K}\mathbf{q} = \mathbf{P}_u\mathbf{u} \tag{2.73}$$

Here, $\mathbf{q}$, represents the generalised displacement vector and $\mathbf{M}$, $\mathbf{V}$ and $\mathbf{K}$ represent the mass, damping and stiffness matrices, respectively. This system can be rewritten to first order form by introducing a state vector as follows.

$$\mathbf{x} = \begin{Bmatrix} \mathbf{q} \\ \dot{\mathbf{q}} \end{Bmatrix}, \quad \dot{\mathbf{x}} = \begin{Bmatrix} \dot{\mathbf{q}} \\ \ddot{\mathbf{q}} \end{Bmatrix} \tag{2.74}$$

The state-space formulation for structure i is then the following.

$$\begin{cases} \dot{\mathbf{x}}^i = \mathbf{A}^i\mathbf{x}^i + \mathbf{B}^i\mathbf{u}^i \\ \mathbf{y}^i = \mathbf{C}^i\mathbf{x}^i \end{cases} \tag{2.75}$$

Without losing generality the input and output vectors $\mathbf{y}$ and $\mathbf{u}$ for structure i are ordered such that the input and output at the coupling DOFs are placed on top of the vectors, as shown below.

$$\mathbf{u}^i = \begin{Bmatrix} \mathbf{u}_c^i \\ \mathbf{u}_b^i \end{Bmatrix}, \quad \mathbf{y}^i = \begin{Bmatrix} \mathbf{y}_c^i \\ \mathbf{y}_b^i \end{Bmatrix} \tag{2.76}$$

In order to transform the state-space equation to a coupling form, a similarity transformation is used to get the following state vector.

$$\tilde{\mathbf{x}}^i = \mathbf{T}^i\mathbf{x}^i = \begin{Bmatrix} \dot{\mathbf{y}}_c^i \\ \mathbf{y}_c^i \\ \mathbf{x}_b^i \end{Bmatrix} \tag{2.77}$$

This transformation matrix is formed in two steps, where the first is shown below.

$$\mathbf{T}_0 = \begin{bmatrix} \mathbf{C}_{c,v} \\ \mathbf{C}_{c,d} \\ \mathbf{N} \end{bmatrix} = \begin{bmatrix} \mathbf{C}_{c,d}\mathbf{A} \\ \mathbf{C}_{c,d} \\ \mathbf{T}_{0,3} \end{bmatrix} \tag{2.78}$$

It is known that if the systems outputs are displacements then these outputs can be written as velocity outputs by $\mathbf{y}_v = \dot{\mathbf{y}}_d = \mathbf{C}_d\dot{\mathbf{x}} = \mathbf{C}_d\mathbf{A}\mathbf{x} + \mathbf{C}_d\mathbf{B}\mathbf{u}$, where $\mathbf{C}_d\mathbf{B} = 0$, to satisfy Newton's second law. If the output matrix $\mathbf{C}$ is given without a subscript, displacements are implied. The last row in the transformation matrix, $\mathbf{T}_{0,3}$, is an arbitrary subspace of the nullspace of $\mathbf{B}_c$ so that $\mathbf{N}\mathbf{B}_c = \mathbf{0}$ and $\mathbf{T}_0$ is non-singular. The matrices $\mathbf{B}_c$ and $\mathbf{C}_c$ are the first n_c columns and rows of $\mathbf{B}$ and $\mathbf{C}$, respectively. Further, the final transformation matrix is obtained as follows.

$$\mathbf{T} = \begin{bmatrix} \mathbf{C}_{c,v} \\ \mathbf{C}_{c,d} \\ \mathbf{N}(\mathbf{I} - \mathbf{A}\mathbf{Z}_{0,1}\mathbf{C}_c) \end{bmatrix} = \begin{bmatrix} \mathbf{T}_1 \\ \mathbf{T}_2 \\ \mathbf{T}_3 \end{bmatrix} \tag{2.79}$$

There will be special interest devoted to the choice of the arbitrary subspace matrix in section 4.5. The inverse of the transformation matrix is obtained as below.

$$\mathbf{Z} = \mathbf{T}^{-1} \equiv \begin{bmatrix} \mathbf{Z}_1 & \mathbf{Z}_2 & \mathbf{Z}_3 \end{bmatrix} \tag{2.80}$$

No further derivation of the transformation matrix is given but the interested user can find it in [SA07;

Sjö04]. The obtained coupling form is shown below.

$$\begin{cases} \tilde{\mathbf{A}}^i = \mathbf{T}^i \mathbf{A}^i \mathbf{T}^{i^{-1}} = \begin{bmatrix} \mathbf{A}^i_{vv} & \mathbf{A}^i_{vd} & \mathbf{A}^i_{vb} \\ \mathbf{I} & \mathbf{0} & \mathbf{0} \\ \mathbf{0} & \mathbf{A}^i_{bd} & \mathbf{A}^i_{bb} \end{bmatrix} \\ \tilde{\mathbf{B}}^i = \mathbf{T}^i \mathbf{B}^i = \begin{bmatrix} \mathbf{B}^i_{vv} & \mathbf{B}^i_{vb} \\ \mathbf{0} & \mathbf{0} \\ \mathbf{0} & \mathbf{B}^i_{bb} \end{bmatrix} \\ \tilde{\mathbf{C}}^i = \mathbf{C}^i \mathbf{T}^{i^{-1}} = \begin{bmatrix} \mathbf{0} & \mathbf{I} & \mathbf{0} \\ \mathbf{C}^i_{bv} & \mathbf{C}^i_{bd} & \mathbf{C}^i_{bb} \end{bmatrix} \end{cases} \tag{2.81}$$

This coupling form can then be reduced into the synthesised state-space model by using the compatibility and set equilibrium at the interface as before. This is achieved in almost the same way as for the direct coupling method as it is in fact time dependant quantities in the spatial domain that are to be coupled, i.e. $\mathbf{y}_c$ and $\mathbf{u}_c$. From Figure 2.2 the following relations must hold.

$$\begin{cases} \ddot{\mathbf{y}}^1_c = \ddot{\mathbf{y}}^2_c = \ddot{\bar{\mathbf{y}}}_c \\ \dot{\mathbf{y}}^1_c = \dot{\mathbf{y}}^2_c = \dot{\bar{\mathbf{y}}}_c \\ \mathbf{y}^1_c = \mathbf{y}^2_c = \bar{\mathbf{y}}_c \\ \mathbf{u}^1_c = \mathbf{u}^{1,2}_{c,g} + \mathbf{u}^1_{c,f} \\ \mathbf{u}^2_c = -\mathbf{u}^{1,2}_{c,g} + \mathbf{u}^2_{c,f} \\ \mathbf{u}_c = \mathbf{u}^1_c + \mathbf{u}^2_c \end{cases} \tag{2.82}$$

In short, it can be realised that the first block equation on the coupling state-space form is on second order form. If two substructures to be coupled, then the two first second order form equations are summed and rearranged to assemble the synthesised second order form equation $\bar{\mathbf{y}}_c$ and the rest is assembled manually. This procedure is further explained in section 2.9.1, where the state-space synthesis is rewritten to the general framework presented by de Klerk et al. [KRV08].

$$\begin{aligned} \begin{Bmatrix} \ddot{\bar{\mathbf{y}}}_c \\ \dot{\bar{\mathbf{y}}}_c \\ \dot{\mathbf{x}}^1_b \\ \dot{\mathbf{x}}^2_b \end{Bmatrix} &= \begin{bmatrix} \bar{\mathbf{A}}_{vv} & \bar{\mathbf{A}}_{vd} & \bar{\mathbf{A}}^1_{vb} & \bar{\mathbf{A}}^2_{vb} \\ \mathbf{I} & \mathbf{0} & \mathbf{0} & \mathbf{0} \\ \mathbf{0} & \mathbf{A}^1_{bd} & \mathbf{A}^1_{bb} & \mathbf{0} \\ \mathbf{0} & \mathbf{A}^2_{bd} & \mathbf{0} & \mathbf{A}^2_{bb} \end{bmatrix} \begin{Bmatrix} \dot{\bar{\mathbf{y}}}_c \\ \bar{\mathbf{y}}_c \\ \mathbf{x}^1_b \\ \mathbf{x}^2_b \end{Bmatrix} + \begin{bmatrix} \bar{\mathbf{B}}_{vv} & \bar{\mathbf{B}}^1_{vb} & \bar{\mathbf{B}}^2_{vb} \\ \mathbf{0} & \mathbf{0} & \mathbf{0} \\ \mathbf{0} & \mathbf{B}^1_{bb} & \mathbf{0} \\ \mathbf{0} & \mathbf{0} & \mathbf{B}^2_{bb} \end{bmatrix} \begin{Bmatrix} \bar{\mathbf{u}}_c \\ \mathbf{u}^1_b \\ \mathbf{u}^2_b \end{Bmatrix} \\ \begin{Bmatrix} \bar{\mathbf{y}}_c \\ \mathbf{y}^1_b \\ \mathbf{y}^2_b \end{Bmatrix} &= \begin{bmatrix} \mathbf{0} & \mathbf{I} & \mathbf{0} & \mathbf{0} \\ \mathbf{C}^1_{bv} & \mathbf{C}^1_{bd} & \mathbf{C}^1_{bb} & \mathbf{0} \\ \mathbf{C}^2_{bv} & \mathbf{C}^2_{bd} & \mathbf{0} & \mathbf{C}^2_{bb} \end{bmatrix} \begin{Bmatrix} \dot{\bar{\mathbf{y}}}_c \\ \bar{\mathbf{y}}_c \\ \mathbf{x}^1_b \\ \mathbf{x}^2_b \end{Bmatrix} \end{aligned} \tag{2.83}$$

The synthesised **A** and **B** parts of the second order equation can be identified as follows.

$$\begin{cases} \mathbf{K} = (\mathbf{B}^1_{vv} + \mathbf{B}^2_{vv})^{-1} \\ \bar{\mathbf{A}}_{vv} = \mathbf{B}^1_{vv}\mathbf{K}\mathbf{A}^2_{vv} + \mathbf{B}^2_{vv}\mathbf{K}\mathbf{A}^1_{vv} \\ \bar{\mathbf{A}}_{vd} = \mathbf{B}^1_{vv}\mathbf{K}\mathbf{A}^2_{vd} + \mathbf{B}^2_{vv}\mathbf{K}\mathbf{A}^1_{vd} \\ \bar{\mathbf{A}}^1_{vb} = \mathbf{B}^2_{vv}\mathbf{K}\mathbf{A}^1_{vb} \\ \bar{\mathbf{A}}^2_{vb} = \mathbf{B}^1_{vv}\mathbf{K}\mathbf{A}^2_{vb} \\ \bar{\mathbf{B}}_{vv} = \mathbf{B}^1_{vv}\mathbf{K}\mathbf{B}^2_{vv} \\ \bar{\mathbf{B}}^1_{vb} = \mathbf{B}^2_{vv}\mathbf{K}\mathbf{B}^1_{vb} \\ \bar{\mathbf{B}}^2_{vb} = \mathbf{B}^1_{vv}\mathbf{K}\mathbf{B}^2_{vb} \end{cases} \tag{2.84}$$

For a thorough derivation of this method the reader is strongly advised to read Sjövall's Licentiate thesis [Sjö04] but also the article [SA07].

Sjövall argues that this method is closely related to the FBS method derived earlier as the same compatibility and equilibrium conditions are used for coupling. The advantage, compared to the FBS method, outlined by Su and Juang in [SJ94], who basically state that it is easier to obtain correct models of substructures than of complex objects. It is then implied that it would be beneficial to obtain a first order model from the coupled systems with the FBS method. Also, the system identification process will filter the data and remove noise which is easily amplified in the FBS method, even with the method proposed by Jetmundsen. This is generally no problem in the state-space method but instead there is a possibility of having system identification errors propagate and amplify in the coupled procedure. A numerical investigation between the state-space method and the FBS method is performed in section 4.4.1.

Compared to the direct coupling, the state-space method could also be argued to couple substructures directly. Further, it could be argued to be a CMS coupling as the internal part of the model is described by a first order form and its states. Also, specifically it resembles the Craig-Bampton coupling in that the coupling DOFs are retained. It should be noted that compared to the CMS method, where modal coordinates are coupled and the user does not have a sense of the physical coordinates, the state-space method presents a powerful alternative where the user is fully aware of what DOFs are used in the coupling in an experimental setting.

In [SA07], Sjövall argues that some criteria must be fulfilled for the state-space coupling to be valid. As discussed before the systems must be passive, see section 2.1.3, thus damping must be introduced in the analytical systems. It is argued that the model order is of importance [Sjö07] and different methods are proposed in order to determine the order correctly, which is here solved by using the algorithm developed by Yaghoubi [YA12]. It is also important, in substructuring in general, to include low frequency residual modes, meaning modes under the measured frequency range. This is a consequence of Rayleigh's theorem, see Meirovitch [Mei96]. The theorem states that the synthesised system is highly affected by the subcomponents low frequency residual modes. If only rigid body modes are missing it is valid to use the rigid body modes extracted from FE models. Finally, the subsystems must also be physically consistent which have been discussed throughout this chapter. Further discussed in section 3.3.5.

2.8.6 Experimental and Analytical Substructuring

In experimental substructuring many problems must be overcome that do not exist when coupling analytically derived models but there are also problems which exist in both cases. Some of these problem will be outlined here.

One of the most important problems are how the rotational DOF should be measured as outlined by de Klerk et al. [KRV08]. Different approaches to remedy this exist where one is to assume that the interface only has rigid motion which implies that if six DOFs are measured at three positions, which is the assumption in isostatic coupling, then the rotational DOFs can be reconstructed from the measured DOFs. This will only give good results up to frequencies which the modeshapes starts to deform at the interface area.

How the coupling should be modelled is another problem that exists in both analytical and experimental substructuring. In this thesis six DOFs will be coupled to each other but the real coupling is much more complex with three bolts holding the two parts together. The dynamics of the joints may also be nonlinear which is another research topic in substructuring, not considered in this thesis.

In experimental substructuring with the CMS method there is also problems with modal truncation, where all the modes describing the system are not considered. This is circumvented with the FBS and state-space methods.

Also in experimental substructuring, the rigid body modes can be hard to obtain but are essential in the CMS method for successful coupling. The FBS method does not depend on this as the modes are implicitly included in the measured data, shown in section 3.3.2. The state-space method is also dependant on the rigid body modes and these must be estimated, by measuring them or, as in this thesis, inserting the FE rigid body modes.

It should be pointed out that de Klerk et al. [KRV08] argues that all reduced models that are to be coupled can be referred to as CMS methods. For example, Craig-Bampton coupling would fall under this category even though the actual coupling is done with physical coordinates. Direct coupling is considered for unreduced models only, which means that all experimental models fall under either CMS or FBS coupling methods. It is of interest to categorise the state-space coupling method developed by Sjövall and Abrahamsson [SA07]. It is also, like the Craig-Bampton method, coupled with physical coordinates while the internal coordinates are described by the system states.

As a final note it has been shown that the choice of coupling DOFs in experimental substructuring with the CMS method can be chosen with certainty of not losing any physical information by Allen and Mayes [AM07]. The state-space method circumvents this problem by obtaining a model on first order form where the interface states are the actual outputs of the system.

2.9 State-Space Synthesis

It is of interest to translate the state-space form into the general framework presented by de Klerk et al. in [KRV08] and also compare it to the CMS method.

2.9.1 General Framework

In order to rewrite the coupling procedure derived in [SA07] into the general framework established by de Klerk et al. [KRV08] and hence use the $\mathbf{E}$ and $\mathbf{L}$ matrices defined in section 2.8, the coupling form must be augmented from its original form. It is known from [Sjö04] that $\mathbf{B}_{vv}$ is the inertia at the interface DOFs. It is also seen that the first block row of the coupling form represents a second order equation for the interface DOFs as shown in eq (2.85). The system i on coupling form can be explicitly written as follows.

$$\begin{aligned}
\begin{Bmatrix} \ddot{\mathbf{y}}_c^i \\ \dot{\mathbf{y}}_c^i \\ \dot{\mathbf{x}}_b^i \end{Bmatrix} &= \begin{bmatrix} \mathbf{A}_{vv}^i & \mathbf{A}_{vd}^i & \mathbf{A}_{vb}^i \\ \mathbf{I} & \mathbf{0} & \mathbf{0} \\ \mathbf{0} & \mathbf{A}_{bd}^i & \mathbf{A}_{bb}^i \end{bmatrix} \begin{Bmatrix} \dot{\mathbf{y}}_c^i \\ \mathbf{y}_c^i \\ \mathbf{x}_b^i \end{Bmatrix} + \begin{bmatrix} \mathbf{B}_{vv}^i & \mathbf{B}_{vb}^i \\ \mathbf{0} & \mathbf{0} \\ \mathbf{0} & \mathbf{B}_{bb}^i \end{bmatrix} \begin{Bmatrix} \mathbf{u}_c^i \\ \mathbf{u}_b^i \end{Bmatrix} \\
\begin{Bmatrix} \mathbf{y}_c^i \\ \mathbf{y}_b^i \end{Bmatrix} &= \begin{bmatrix} \mathbf{0} & \mathbf{I} & \mathbf{0} \\ \mathbf{C}_{bv}^i & \mathbf{C}_{bd}^i & \mathbf{C}_{bb}^i \end{bmatrix} \begin{Bmatrix} \dot{\mathbf{y}}_c^i \\ \mathbf{y}_c^i \\ \mathbf{x}_b^i \end{Bmatrix}
\end{aligned} \tag{2.85}$$

In order to use the de Klerk formulation, the second order equation from eq (2.85) must be pre-multiplied by the inverse of $\mathbf{B}_{vv}^i$, shown below.

$$\mathbf{B}_{vv}^{i^{-1}} \ddot{\mathbf{y}}_c^i = \mathbf{B}_{vv}^{i^{-1}} \mathbf{A}_{vv}^i \dot{\mathbf{y}}_c^i + \mathbf{B}_{vv}^{i^{-1}} \mathbf{A}_{vd}^i \mathbf{y}_c^i + \mathbf{B}_{vv}^{i^{-1}} \mathbf{A}_{vb}^i \mathbf{x}_b^i + \mathbf{u}_c^i + \mathbf{B}_{vv}^{i^{-1}} \mathbf{B}_{vb}^i \mathbf{u}_b^i \tag{2.86}$$

Further, the coupling conditions for the state-space system on coupling form which are outlined in section 2.8.5 are here generalised for coupling of h systems with the formulation given by de Klerk et al. [KRV08] with the $\mathbf{E}$ and $\mathbf{L}$ matrices.

The $\mathbf{u}_f$ and $\mathbf{u}_c$ parts correspond to the external and interface loading, respectively. The interface forces must be eliminated and the displacement, velocity and acceleration at the interface DOFs must be equal for the coupled components. The de Klerk general framework introduces a matrix $\mathbf{E}$ to satisfy the compatibility condition and the localising matrix $\mathbf{L}$ can be formed from the nullspace of the $\mathbf{E}$ matrix such that equilibrium is satisfied.

The derivations can be started from a general state-space formulation where the coupling form transformation matrix $\mathbf{T}$ is introduced, see section 2.8.5. Here, the matrices and vectors will be assembled on block diagonal form with h system blocks, as outlined in the direct coupling approach in section 2.8.2. The general state-space formulation is written as follows, where the states, inputs and outputs must be formulated such that the interface inputs and outputs are placed on top, shown in section 2.8.5.

$$\begin{cases} \dot{\mathbf{x}} = \mathbf{A}\mathbf{x} + \mathbf{B}\mathbf{u} \\ \mathbf{y} = \mathbf{C}\mathbf{x} \end{cases} \tag{2.87}$$

Transformed to the coupled form with the transformation matrix $\mathbf{T}$, where $\tilde{\mathbf{A}} = \mathbf{T}^{-1}\mathbf{A}\mathbf{T}$, $\tilde{\mathbf{B}} = \mathbf{T}\mathbf{B}$, $\tilde{\mathbf{C}} = \mathbf{C}\mathbf{T}^{-1}$ and $\tilde{\mathbf{x}} = \mathbf{T}\mathbf{x}$. The coupling form is then obtained as shown below.

$$\begin{cases} \dot{\tilde{\mathbf{x}}} = \tilde{\mathbf{A}}\tilde{\mathbf{x}} + \tilde{\mathbf{B}}\mathbf{u} \\ \mathbf{y} = \tilde{\mathbf{C}}\tilde{\mathbf{x}} \end{cases} \tag{2.88}$$

Rewriting the system by pre-multiplying by $\mathbf{B}_{vv}^{-1}$ as outlined in eq (2.86) requires the forming of a new matrix denoted $\mathbf{M}_B$, built as shown below.

$$\mathbf{M}_B = diag(diag(\mathbf{B}_{vv}^{1^{-1}}, \mathbf{I}, \mathbf{I}), \ldots, diag(\mathbf{B}_{vv}^{h^{-1}}, \mathbf{I}, \mathbf{I})) \tag{2.89}$$

It should be noted that $\mathbf{B}_{vv} = \mathbf{T}_1\mathbf{B}_c$ where $\mathbf{T}_1 = \mathbf{C}_c\mathbf{A}$ and $\mathbf{B}_c$ is a part of $\mathbf{B} = \begin{bmatrix}\mathbf{B}_c & \mathbf{B}_b\end{bmatrix}$, as shown in section 2.8.5. Thus, the new state-space system is formed as follows.

$$\begin{cases} \mathbf{M}_B\dot{\tilde{\mathbf{x}}} = \mathbf{M}_B\tilde{\mathbf{A}}\tilde{\mathbf{x}} + \mathbf{M}_B\tilde{\mathbf{B}}\mathbf{u} \\ \mathbf{y} = \tilde{\mathbf{C}}\tilde{\mathbf{x}} \end{cases} \tag{2.90}$$

Now the $\mathbf{E}$ and $\mathbf{L}$ matrices are introduced, where compatibility is described with $\mathbf{E}\tilde{\mathbf{x}} = \mathbf{0}$ and the equilibrium with $\mathbf{L}^T\mathbf{u}_{c,g} = \mathbf{0}$. The matrix $\mathbf{L}$ is formed as $\mathbf{L} = null(\mathbf{E})$ such that the following is satisfied: $\mathbf{E}\tilde{\mathbf{x}} = \mathbf{E}\mathbf{L}\tilde{\mathbf{z}} = \mathbf{0}$ and $\tilde{\mathbf{x}} = \mathbf{L}\tilde{\mathbf{z}}$. The new state vector $\tilde{\mathbf{z}}$ represents the new states after coupling. The synthesised state-space model is then formed as follows.

$$\begin{cases} \mathbf{L}^T\mathbf{M}_B\mathbf{L}\dot{\tilde{\mathbf{z}}} = \mathbf{L}^T\mathbf{M}_B\tilde{\mathbf{A}}\mathbf{L}\tilde{\mathbf{z}} + \mathbf{L}^T\mathbf{M}_B\tilde{\mathbf{B}}\mathbf{u} \\ \mathbf{y} = \tilde{\mathbf{C}}\mathbf{L}\tilde{\mathbf{z}} \end{cases} \tag{2.91}$$

As a final step, $(\mathbf{L}^T\mathbf{M}_B\mathbf{L})^{-1}$, is pre-multiplied to the first equation in eq (2.91) and a new transformation matrix must be introduced to reduce the excess inputs and outputs. The new matrix is denoted $\mathbf{L}_u$ and is formed from a matrix $\mathbf{E}_u$ as before, $\mathbf{L}_u = null(\mathbf{E}_u)$. In other words, for a system with two synthesised components the new reduction matrix is $\mathbf{E}_u = [\mathbf{I} \quad \mathbf{0} \quad \mathbf{0} \quad \mathbf{0}]$. This is easily generalised for multiple components in a straight forward manner. The implication of this transformation is that in the synthesised model, to which this new matrix is applied, the first component of the considered vector will be removed. This new matrix is introduced in the equations by $\mathbf{u} = \mathbf{L}_u\bar{\mathbf{u}}$ and $\bar{\mathbf{y}} = \mathbf{L}_u^T\mathbf{y}$ as shown in eq (2.93). The last step is only true for systems with equal number of inputs and outputs but is easily generalised, i.e. two matrices must be formed separately. The final system can be written as follows.

$$\begin{cases} \dot{\tilde{\mathbf{z}}} = \hat{\mathbf{A}}\tilde{\mathbf{z}} + \hat{\mathbf{B}}\bar{\mathbf{u}} \\ \bar{\mathbf{y}} = \hat{\mathbf{C}}\tilde{\mathbf{z}} \end{cases} \tag{2.92}$$

Each part in the equation above is then identified as shown below.

$$\begin{cases} \hat{\mathbf{A}} = (\mathbf{L}^T\mathbf{M}_B\mathbf{L})^{-1}(\mathbf{L}^T\mathbf{M}_B\tilde{\mathbf{A}}\mathbf{L}) \\ \hat{\mathbf{B}} = (\mathbf{L}^T\mathbf{M}_B\mathbf{L})^{-1}(\mathbf{L}^T\mathbf{M}_B\tilde{\mathbf{B}})\mathbf{L}_u \\ \hat{\mathbf{C}} = \mathbf{L}_u^T(\tilde{\mathbf{C}}\mathbf{L}) \end{cases} \tag{2.93}$$

The described method will produce exactly the same results as shown in section 2.8.5 but the states will be in another order compared to the original formulation.

As a final note, the formulation described above might increase the severity of the encountered numerical problems, described in section 4.5, as there are two matrix inverses involved in the synthesis procedure, while there is only one in the formulation shown by Sjövall [SA07]. On the other hand, it is easier to couple multiple components with the presented method. This procedure is used in the hub assembly coupling in chapter 4.

2.9.2 Second Order Form Equivalent of Synthesised First Order Form

There is interest in comparing the state-space method to the more common CMS method in a theoretical setting to verify that the two methods produce the same systems.

An analytical model written on second order form can easily be rewritten on first order form by doubling the number of states, shown in section 2.3. The transformation from a first order form to a second order form with half the number of states is not as trivial, even when possible. Assume that the second order system shown in eq (2.10) is had. This system can be rewritten on the form shown in eq (2.15), where it is assumed, for simplicity, that the velocity output is zero and the displacement output matrix is the identity matrix: $\mathbf{P}_u = \mathbf{I}$, such that all DOFs are considered as outputs. The system output is shown below.

$$\mathbf{y} = \mathbf{C}\mathbf{x} = \begin{bmatrix}\mathbf{I} & \mathbf{0}\end{bmatrix}\mathbf{x} \tag{2.94}$$

A new transformation matrix is introduced in eq (2.95) which transforms a general state-space system to coupling form under the assumption that the original system is analytically derived with state vector $\mathbf{x}^T = \begin{bmatrix}\mathbf{x} & \dot{\mathbf{x}}\end{bmatrix}^T$ and output matrix $\mathbf{C}$ defined as above.

$$\mathbf{T}^i = \begin{bmatrix}\mathbf{C}_c^i\mathbf{A}^i \\ \mathbf{C}_c^i \\ \mathbf{C}_b^i\mathbf{A}^i \\ \mathbf{C}_b^i\end{bmatrix} \tag{2.95}$$

This transformation will produce a new state vector, $\tilde{\mathbf{x}} = \begin{bmatrix}\dot{\mathbf{y}}_c^i & \mathbf{y}_c^i & \dot{\mathbf{y}}_b^i & \mathbf{y}_b\end{bmatrix}^T$, where the superscript i represents the subcomponent system. Again, the subscript c denotes the coupling partition of the input and output matrices, i.e. the block row and column of the $\mathbf{B}$ and $\mathbf{C}$ matrices, respectively. The difference between this transformation and the transformation given by Sjövall, presented in section 2.8.5, is that the internal states are represented by physical coordinates here. In a theoretical representation this is valid, but in an experimental representation it would imply a significant constraint on the model to allow only twice as many states as there are sensors. Another condition is that $rank(\mathbf{C}) = n/2$ where n is the number of states, otherwise the transformed system will be reduced by this transformation. It should also be stated that for analytical models, where all the transformations are known and it is possible to trace every step, the new transformation is in fact preferred as the creation of the subspace of the nullspace is avoided. It is assumed that the system is physical, i.e. $\mathbf{CB} = \mathbf{0}$, a property which is satisfied for FE models. The newly obtained coupling form is shown below. The coupling form obtained through the transformation in eq (2.95) is shown below.

$$\begin{cases} \tilde{\mathbf{A}}^i = \mathbf{T}^i\mathbf{A}^i{\mathbf{T}^i}^{-1} = \begin{bmatrix}\mathbf{A}_{cvc}^i & \mathbf{A}_{cdc}^i & \mathbf{A}_{cvb}^i & \mathbf{A}_{cdb}^i \\ \mathbf{I} & \mathbf{0} & \mathbf{0} & \mathbf{0} \\ \mathbf{A}_{bvc}^i & \mathbf{A}_{bdc}^i & \mathbf{A}_{bvb}^i & \mathbf{A}_{bdb}^i \\ \mathbf{0} & \mathbf{0} & \mathbf{I} & \mathbf{0}\end{bmatrix} \\ \tilde{\mathbf{B}}^i = \mathbf{T}^i\mathbf{B}^i = \begin{bmatrix}\mathbf{C}_c^i\mathbf{A}^i\mathbf{B}^i \\ \mathbf{C}_c^i\mathbf{B}^i \\ \mathbf{C}_b^i\mathbf{A}^i\mathbf{B}^i \\ \mathbf{C}_b^i\mathbf{B}^i\end{bmatrix} = \begin{bmatrix}\mathbf{C}_c^i\mathbf{A}^i\mathbf{B}^i \\ \mathbf{0} \\ \mathbf{C}_b^i\mathbf{A}^i\mathbf{B}^i \\ \mathbf{0}\end{bmatrix} = \begin{bmatrix}\mathbf{B}_{c,c}^i & \mathbf{B}_{c,b}^i \\ \mathbf{0} & \mathbf{0} \\ \mathbf{B}_{bc}^i & \mathbf{B}_{bb}^i \\ \mathbf{0} & \mathbf{0}\end{bmatrix} \\ \tilde{\mathbf{C}}^i = \mathbf{C}^i{\mathbf{T}^i}^{-1} = \begin{bmatrix}\mathbf{I} & \mathbf{0} & \mathbf{0} & \mathbf{0} \\ \mathbf{0} & \mathbf{0} & \mathbf{I} & \mathbf{0}\end{bmatrix} \end{cases} \tag{2.96}$$

It can be shown that the transformation of the input matrix $\mathbf{CAB}$, with the assumptions introduced above, can be simplified to the inverse mass matrix.

$$\mathbf{CAB} = \begin{bmatrix}\mathbf{I} & \mathbf{0}\end{bmatrix}\begin{bmatrix}\mathbf{0} & \mathbf{I} \\ -\mathbf{M}^{-1}\mathbf{K} & -\mathbf{M}^{-1}\mathbf{V}\end{bmatrix}\begin{bmatrix}\mathbf{0} \\ \mathbf{M}^{-1}\end{bmatrix} = \mathbf{M}^{-1} \tag{2.97}$$

With this knowledge, it is possible to simplify the $\tilde{\mathbf{B}}$ matrix as follows.

$$\begin{cases} \mathbf{B}^i_{cc} = \mathbf{M}^{i^{-1}}_{cc} \\ \mathbf{B}^i_{cb} = \mathbf{M}^{i^{-1}}_{cb} = \mathbf{0} \\ \mathbf{B}^i_{bc} = \mathbf{M}^{i^{-1}}_{bc} = \mathbf{0} \\ \mathbf{B}^i_{bb} = \mathbf{M}^{i^{-1}}_{bb} \end{cases} \tag{2.98}$$

The second and third equations are realised because the mass matrix is diagonal and the entries in the n_c first rows and n_b last columns of this matrix are zero.

To synthesise two (or more) systems, the procedure described in section 2.9.1 is used, which produces a synthesised system, here reorganised, such that it is recognisable as the usual state-space formulation of a second order system.

$$\begin{Bmatrix} \dot{\bar{\mathbf{y}}}_c \\ \dot{\mathbf{y}}^1_b \\ \dot{\mathbf{y}}^2_b \\ \ddot{\bar{\mathbf{y}}}_c \\ \ddot{\mathbf{y}}^1_b \\ \ddot{\mathbf{y}}^2_b \end{Bmatrix} = \begin{bmatrix} \mathbf{0} & \mathbf{0} & \mathbf{0} & \mathbf{I} & \mathbf{0} & \mathbf{0} \\ \mathbf{0} & \mathbf{0} & \mathbf{0} & \mathbf{0} & \mathbf{I} & \mathbf{0} \\ \mathbf{0} & \mathbf{0} & \mathbf{0} & \mathbf{0} & \mathbf{0} & \mathbf{I} \\ \bar{\mathbf{A}}_{cdc} & \bar{\mathbf{A}}^1_{cdb} & \bar{\mathbf{A}}^2_{cdb} & \bar{\mathbf{A}}_{cvc} & \bar{\mathbf{A}}^1_{cvb} & \bar{\mathbf{A}}^2_{cvb} \\ \mathbf{A}^1_{bdc} & \mathbf{A}^1_{bdb} & \mathbf{0} & \mathbf{A}^1_{bvc} & \mathbf{A}^1_{bvb} & \mathbf{0} \\ \mathbf{A}^2_{bdc} & \mathbf{0} & \mathbf{A}^2_{bdb} & \mathbf{A}^2_{bvc} & \mathbf{0} & \mathbf{A}^2_{bvb} \end{bmatrix} \begin{Bmatrix} \bar{\mathbf{y}}_c \\ \mathbf{y}^1_b \\ \mathbf{y}^2_b \\ \dot{\bar{\mathbf{y}}}_c \\ \dot{\mathbf{y}}^1_b \\ \dot{\mathbf{y}}^2_b \end{Bmatrix} + \begin{bmatrix} \mathbf{0} & \mathbf{0} & \mathbf{0} \\ \mathbf{0} & \mathbf{0} & \mathbf{0} \\ \mathbf{0} & \mathbf{0} & \mathbf{0} \\ \bar{\mathbf{B}}_{cc} & \mathbf{0} & \mathbf{0} \\ \mathbf{0} & \mathbf{B}^1_{bb} & \mathbf{0} \\ \mathbf{0} & \mathbf{0} & \mathbf{B}^2_{bb} \end{bmatrix} \begin{Bmatrix} \bar{\mathbf{u}}_c \\ \mathbf{u}^1_b \\ \mathbf{u}^2_b \end{Bmatrix}$$
$$\begin{Bmatrix} \bar{\mathbf{y}}_c \\ \mathbf{y}^1_b \\ \mathbf{y}^2_b \end{Bmatrix} = \begin{bmatrix} \mathbf{I} & \mathbf{0} & \mathbf{0} & \mathbf{0} & \mathbf{0} & \mathbf{0} \\ \mathbf{0} & \mathbf{I} & \mathbf{0} & \mathbf{0} & \mathbf{0} & \mathbf{0} \\ \mathbf{0} & \mathbf{0} & \mathbf{I} & \mathbf{0} & \mathbf{0} & \mathbf{0} \end{bmatrix} \begin{Bmatrix} \bar{\mathbf{y}}_c \\ \mathbf{y}^1_b \\ \mathbf{y}^2_b \\ \dot{\bar{\mathbf{y}}}_c \\ \dot{\mathbf{y}}^1_b \\ \dot{\mathbf{y}}^2_b \end{Bmatrix} \tag{2.99}$$

The lower part can be identified as a second order system which is directly comparable to the direct coupling procedure.

Thus, the new system can be identified with the general state-space formulation given in eq (2.15) but here the interface coordinates differ and thus it should be compared to a synthesised second order system which is here only shown and not derived, cf. [CK06]. The two second order systems can be written with an interface part (c) and a body part (b) for two components, $i = 1, 2$.

$$\begin{cases} \mathbf{M}^i = \begin{bmatrix} \mathbf{M}^i_{cc} & \mathbf{0} \\ \mathbf{0} & \mathbf{M}^i_{bb} \end{bmatrix} \\ \mathbf{K}^i = \begin{bmatrix} \mathbf{K}^i_{cc} & \mathbf{K}^i_{cb} \\ \mathbf{K}^i_{bc} & \mathbf{K}^i_{bb} \end{bmatrix} \\ \mathbf{V}^i = \begin{bmatrix} \mathbf{V}^i_{cc} & \mathbf{V}^i_{cb} \\ \mathbf{V}^i_{bc} & \mathbf{V}^i_{cc} \end{bmatrix} \end{cases} \tag{2.100}$$

The synthesised system then becomes.

$$\begin{cases} \mathbf{M}_{as} = \begin{bmatrix} \mathbf{M}_{cc}^1 + \mathbf{M}_{cc}^2 & \mathbf{0} & \mathbf{0} \\ \mathbf{0} & \mathbf{M}_{bb}^1 & \mathbf{0} \\ \mathbf{0} & \mathbf{0} & \mathbf{M}_{bb}^2 \end{bmatrix} \\ \mathbf{K}_{as} = \begin{bmatrix} \mathbf{K}_{cc}^1 + \mathbf{K}_{cc}^2 & \mathbf{K}_{cb}^1 & \mathbf{K}_{cb}^2 \\ \mathbf{K}_{bc}^1 & \mathbf{K}_{bb}^1 & \mathbf{0} \\ \mathbf{K}_{bc}^2 & \mathbf{0} & \mathbf{K}_{bb}^2 \end{bmatrix} \\ \mathbf{V}_{as} = \begin{bmatrix} \mathbf{V}_{cc}^1 + \mathbf{V}_{cc}^2 & \mathbf{V}_{cb}^1 & \mathbf{V}_{cb}^2 \\ \mathbf{V}_{bc}^1 & \mathbf{V}_{bb}^1 & \mathbf{0} \\ \mathbf{V}_{bc}^2 & \mathbf{0} & \mathbf{V}_{bb}^2 \end{bmatrix} \end{cases} \tag{2.101}$$

For comparison, the second order system from eq (2.99) is pre-multiplied by the inverse of its input matrix which is diagonal and the new matrix is split in two, one part representing the stiffness and the other the damping. The following is then obtained.

$$\begin{cases} \mathbf{M}_{as} \equiv \mathbf{M}_{sss} = \begin{bmatrix} \bar{\mathbf{B}}_{cc}^{-1} & \mathbf{0} & \mathbf{0} \\ \mathbf{0} & \bar{\mathbf{B}}_{bb}^{1^{-1}} & \mathbf{0} \\ \mathbf{0} & \mathbf{0} & \bar{\mathbf{B}}_{bb}^{2^{-1}} \end{bmatrix} = \begin{bmatrix} \mathbf{M}_{cc}^1 + \mathbf{M}_{cc}^2 & \mathbf{0} & \mathbf{0} \\ \mathbf{0} & \mathbf{M}_{bb}^1 & \mathbf{0} \\ \mathbf{0} & \mathbf{0} & \mathbf{M}_{bb}^2 \end{bmatrix} \\ \mathbf{K}_{as} \equiv \mathbf{K}_{sss} = \begin{bmatrix} \bar{\mathbf{B}}_{cc}^{-1}\bar{\mathbf{A}}_{cdc} & \bar{\mathbf{B}}_{cc}^{-1}\bar{\mathbf{A}}_{cdb}^1 & \bar{\mathbf{B}}_{cc}^{-1}\bar{\mathbf{A}}_{cdb}^2 \\ \bar{\mathbf{B}}_{bb}^{1^{-1}}\mathbf{A}_{bdc}^1 & \bar{\mathbf{B}}_{bb}^{1^{-1}}\mathbf{A}_{bdb}^1 & \mathbf{0} \\ \bar{\mathbf{B}}_{bb}^{2^{-1}}\mathbf{A}_{bdc}^2 & \mathbf{0} & \bar{\mathbf{B}}_{bb}^{2^{-1}}\mathbf{A}_{bdb}^2 \end{bmatrix} = \begin{bmatrix} \mathbf{K}_{cc}^1 + \mathbf{K}_{cc}^2 & \mathbf{K}_{cb}^1 & \mathbf{K}_{cb}^2 \\ \mathbf{K}_{bc}^1 & \mathbf{K}_{bb}^1 & \mathbf{0} \\ \mathbf{K}_{bc}^2 & \mathbf{0} & \mathbf{K}_{bb}^2 \end{bmatrix} \\ \mathbf{V}_{as} \equiv \mathbf{V}_{sss} = \begin{bmatrix} \bar{\mathbf{B}}_{cc}^{-1}\bar{\mathbf{A}}_{cvc} & \bar{\mathbf{B}}_{cc}^{-1}\bar{\mathbf{A}}_{cvb}^1 & \bar{\mathbf{B}}_{cc}^{-1}\bar{\mathbf{A}}_{cvb}^2 \\ \bar{\mathbf{B}}_{bb}^{1^{-1}}\mathbf{A}_{bvc}^1 & \bar{\mathbf{B}}_{bb}^{1^{-1}}\mathbf{A}_{bvb}^1 & \mathbf{0} \\ \bar{\mathbf{B}}_{bb}^{2^{-1}}\mathbf{A}_{bvc}^2 & \mathbf{0} & \bar{\mathbf{B}}_{bb}^{2^{-1}}\mathbf{A}_{bvb}^2 \end{bmatrix} = \begin{bmatrix} \mathbf{V}_{cc}^1 + \mathbf{V}_{cc}^2 & \mathbf{V}_{cb}^1 & \mathbf{V}_{cb}^2 \\ \mathbf{V}_{bc}^1 & \mathbf{V}_{bb}^1 & \mathbf{0} \\ \mathbf{V}_{bc}^2 & \mathbf{0} & \mathbf{V}_{bb}^2 \end{bmatrix} \end{cases} \tag{2.102}$$

It is now obvious that both methods produce exactly the same systems. The theoretical development is further discussed in section 5.5.

2.10 Interface Excitation

In order to couple two substructures the interface displacements and forces must be known. For analytical models this is very easy to achieve as the displacement and input at every location is known from the analysis. In experimental models this condition is harder to satisfy. One must have sensors measuring the output at the interface locations but one must also have inputs at all the interface locations. This can be cumbersome as it might be very hard to attach a shaker at the interface locations. To circumvent this problem the basic property of reciprocity can be used if the experimental system can be assumed linear. One must have at least one co-located sensor actuator-pair as shown in Figure 2.3. The figure shows the input at location u^1 and also an output at this location y^1. There are also two other outputs measured, y^2 and y^3. The structure is to be coupled at locations 2 and 3 and thus the inputs at these locations must be known. Measuring this system will give an FRF matrix with dimensions 3×1, where rows correspond to outputs and columns to inputs.

$$\begin{Bmatrix} y_\omega^1(\omega) \\ y_\omega^2(\omega) \\ y_\omega^3(\omega) \end{Bmatrix} = \begin{bmatrix} H^{1,1}(\omega) \\ H^{2,1}(\omega) \\ H^{3,1}(\omega) \end{bmatrix} u_\omega^1(\omega) \tag{2.103}$$

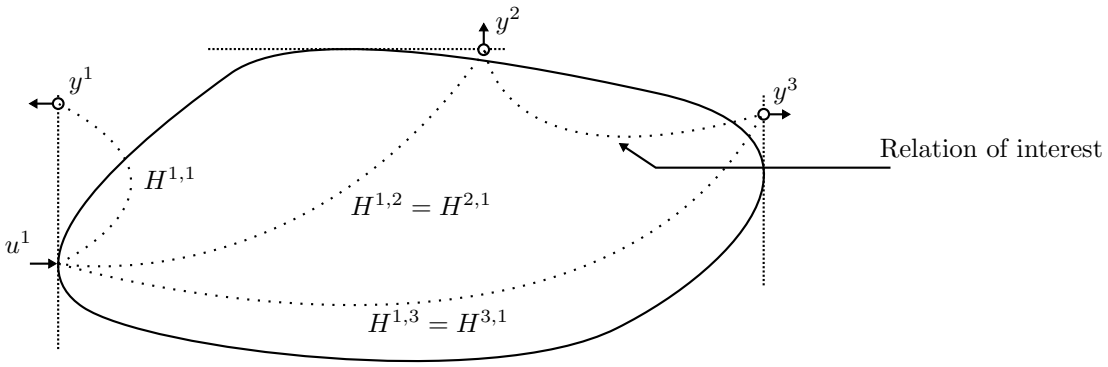

Figure 2.3: *Body with one input and three outputs, to be connected at two points.*

It is easy to see, directly from the reciprocity principle shown in section 2.1.2, that the receptance matrices $H^{1,3}$ and $H^{1,3}$ can be formed as $H^{i,j} = H^{j,i}$. It is not as easy to realise how the relation between $H^{2,2}$, $H^{2,3}$, $H^{3,2}$ and $H^{3,3}$ can be constructed.

For a second order system, as shown in eq (2.4), with proportional damping $\mathbf{V} = \alpha\mathbf{M}$, the FRF matrix in terms of eigenvectors (in the modal domain) can be written as follows.

$$H^{i,j}(\omega) = \sum_{r=1}^{N} \frac{\mathbf{\Phi}_{i,r}\mathbf{\Phi}_{j,r}}{(k_r - \omega^2 m_r) + j\omega c_r} \tag{2.104}$$

Where k_r is the modal stiffness, c_r is the modal damping, m_r is the modal mass and j is the imaginary unit. It can be seen from this equation that a transfer function with any combination can be built.

For a state-space model there exist a similar relation where the first order system is taken to modal form and then transformed back to first order from but with the same number of inputs as outputs. In the example given by Figure 2.3 the information in the input matrix $\mathbf{B}$ that is missing is the coupling part $\mathbf{B}_c$. Modal analysis is then used to obtain this part. First, it should be noted that a first order system can be transformed into a block-diagonal form in a manner similar to a second order system. The following can be obtained if $\mathbf{\Phi}_{left}$ and $\mathbf{\Phi}_{right}$ represent the left and right eigenvectors of $\mathbf{A}$, respectively.

$$\mathbf{A}^d = \mathbf{\Phi}_{left}\mathbf{A}\mathbf{\Phi}_{right}, \quad \begin{bmatrix}\mathbf{B}_c^d & \mathbf{B}_b^d\end{bmatrix} = \mathbf{\Phi}_{left}\begin{bmatrix}\mathbf{B}_c & \mathbf{B}_b\end{bmatrix}, \quad \begin{bmatrix}\mathbf{C}_c^d \\ \mathbf{C}_b^d\end{bmatrix} = \begin{bmatrix}\mathbf{C}_c \\ \mathbf{C}_b\end{bmatrix}\mathbf{\Phi}_{right} \tag{2.105}$$

From the reciprocity theorem the following is known.

$$\begin{cases} \mathbf{C}_b^d(j\omega\mathbf{I} - \mathbf{A}^d)^{-1}\mathbf{B}_c^d = \mathbf{C}_c^d(j\omega\mathbf{I} - \mathbf{A}^d)^{-1}\mathbf{B}_b^d \\ (j\omega\mathbf{I} - \mathbf{A}^d)^{-1} = diag(\dfrac{1}{j\omega - \lambda_1}, \dfrac{1}{j\omega - \lambda_2}, \dots) \end{cases} \tag{2.106}$$

It is known that the contribution from mode r is equal to both $H^{i,j}$ and $H^{j,i}$ and the following is then true.

$$\begin{cases} \dfrac{c_{b,r}^d b_{c,r}^d}{j\omega - \lambda_r} = \dfrac{c_{c,r}^d b_{b,r}^d}{j\omega - \lambda_r} \\ c_{b,r}^d b_{c,r}^d = c_{c,r}^d b_{b,r}^d \\ b_{c,r}^d = \dfrac{c_{c,r}^d b_{b,r}^d}{c_{b,r}^d} \end{cases} \tag{2.107}$$

From the equation above it is realised that from the transformed $\mathbf{B}$ and $\mathbf{C}$ matrices a full $\mathbf{B}$ matrix can be built. To transform the input matrix back, the right eigenvectors are used.

$$\mathbf{B}_c = \mathbf{\Phi}_{right}\mathbf{B}_c^d \tag{2.108}$$

There are a few restrictions that the data must fulfil in order to get correct results from this procedure. First, all modes must be controllable from the co-located excitation. If they are not and a force input at the interface locations would have excited these modes, a model without these states is obtained. Secondly, this

procedure puts high demand on the testing and the vibration amplitudes must not become too large or too small. This derivation is found in Sjövall [Sjö04] and the the topic is further described by Ewins, Kailath and Abrahamsson [Ewi00; Kai80; Abr90].

2.11 Physical Models

In order to satisfy the passivity criterion outlined in section 2.1.3. The obtained first order form from system identification is rewritten on second order form where the passivity criterion and Newton's second law are fulfilled. An optimisation routine proposed by by Sjövall [Sjö07] is employed which minimises the transfer function error ϵ, defined as.

$$\epsilon = \sum_k \mathbf{e}_k^* \mathbf{W}_k \mathbf{e}_k \tag{2.109}$$

The term $\mathbf{e}_k = (\mathbf{C}(j\omega_k \mathbf{I} - \mathbf{A})^{-1} - \mathbf{H}_{X,k})$ is the residual vector, $\mathbf{W}_k$ is the weighting matrix and $\mathbf{H}_{X,k}$ is the measured FRF matrix, at frequency k. The damping is assumed to be of Caughey type, [Sjö07]. A modal second order form is obtained, which is described in section 2.7.1, that is cast into first order form and used in the coupling procedures. Non-passive and passive systems are compared in section 4.6.2.

3 Method

In this chapter, a description of the FE models used in this thesis is given along with a detailed description of how experiments were performed, experimental models acquired and substructuring performed.

Three different blades from the same Ampair 600 wind turbine were considered in this thesis, i.e. when bought, the blades came in a group intended to constitute one wind turbine. There were also three brackets that were chosen so that each blade was mounted to the same bracket. One hub was used to mount the blades with mounted brackets. Lastly, the integral parts that went into the hub, screws, springs, etc. were not considered in the analytical models.

The three experimental blades will be denoted by their serial number; 841, 722 and 819. The brackets were also marked with numbers, 01, 02 and 03. Coupling took place between blade 841 and bracket 01, blade 722 and bracket 02 and blade 819 and bracket 03. The bracket numbers will usually be omitted when the blade bracket configuration is discussed but occasionally they will be abbreviated as blade/bracket, e.g. 841/01/H would represent a hub mounted to bracket 01 which in turn is mounted to blade 841.

3.1 Analytical Models

The meaning of an analytical model in this thesis is a FE model. The three FE models that were used were created in FEMAP and solved with MD Nastran. NX Nastran was used for verification where non-reduced models were solved.

3.1.1 Blade

A variant of the blade FE model described in [Joh+13] (Nastran model can be found online at [Onl]) was used and is visualised in Figure 3.1. The model consisted of 20523 nodes and 96416 elements. The model has a solid core, for which solid elements were used and a laminate skin model, for which laminate plate elements were used. For a thorough explanation of the composite material model and how it was calibrated, see Johansson et al. [Joh+13].

The accelerometer positions used in the vibrations test and for the FE blade model are shown in Figure 3.1. These were chosen as close to the physical locations of the accelerometers as possible for the MAC correlations to yield correct results. Note that the numbering starts at the coupling positions. For isostatic coupling, six DOFs had to be fixed, at three locations, for all rigid body modes to be locked. These DOFs are aligned with the global coordinate system as the surface is considered perfectly flat and aligned with the experimentally measured directions at these points. At position 3, with numbering from Figure 3.1, 3 DOFs (x, y and z) were fixed, at position 5, 2 DOFs (y and z) were fixed and at position 6, 1 DOF (z) was fixed as seen in Figure 3.2a.

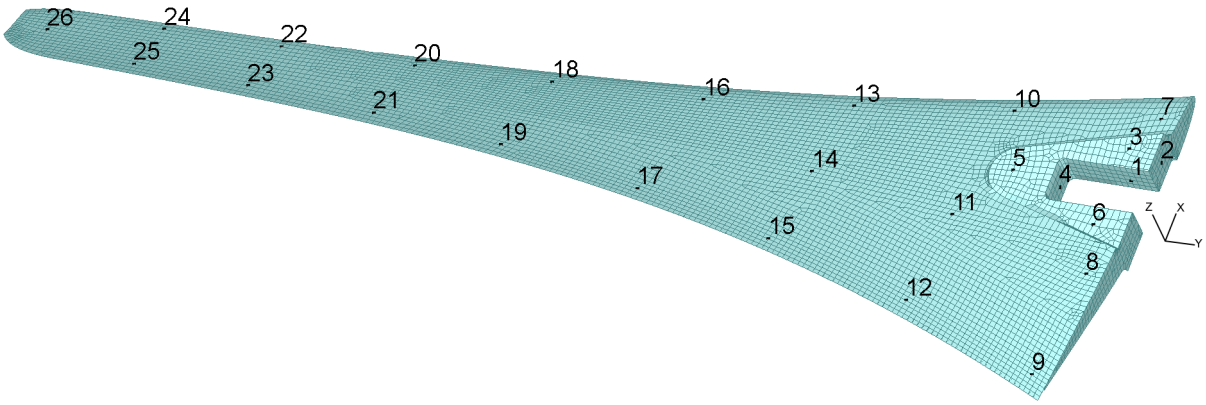

Figure 3.1: *FE model of the blade with numbering used in the FE model but also during the vibration tests.*

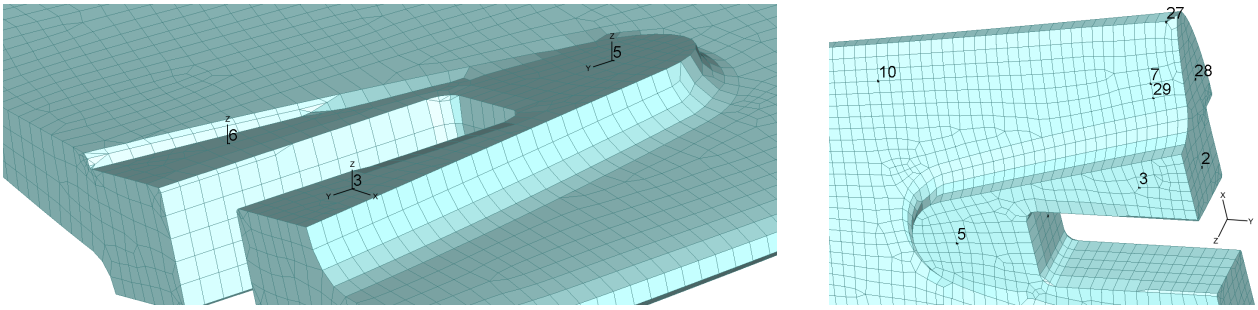

(a) *Blade coupling positions and numbering.*

(b) *Close-up view of the three inputs of the blade.*

Figure 3.2: *Blade coupling and input positions. (a) The isostatic coupling positions and their DOFs. (b) A view of the input in the x (27), y (28) and z (29) directions for the blade.*

It should be noted that the coordinate alignment seen in Figure 3.2a is an ideal case, in reality, e.g. the three translation DOFs at position 3 were not perfectly aligned with the coordinate system, further described in section 3.3.2. All other positions shown in Figure 3.1 had only one DOF, measuring in the normal direction (outwards from the blade surface) and were aligned with a local coordinate system. In Figure 3.2b, inputs in the x, y and z directions are marked with numbers 27, 28 and 29, respectively. Note that for the input positions the local z coordinates, directed inwards, are retained.

Different coupling configurations were tested for the analytical case. These are shown in Figure 3.3. A coupling denoted *high*, because of its increase in stiffness of the system, can be seen in Figure 3.3a, where the part of the blade that was in contact with the bracket had all the DOFs constrained with rigid links that were attached to a node with six DOFs located in the centre of the three bolt holes. Consequently, a coupling denoted *low*, because it gave a lower system stiffness relative the *high* configuration but higher than for the unaltered component, can be seen in Figure 3.3b, where the area around the holes on the blade have been constrained with rigid links to make the blade and thus the coupling stiffer. The same coupling DOFs as for the isostatic case were used for the *low* configuration. Note that all constraints for the *low* configuration are on the same side of the blade which creates asymmetric modeshapes.

3.1.2 Bracket

The bracket geometry was received from TU Delft. It was modelled by 24707 solid parabolic elements and an isotropic material model with stiffness $E = 2 \cdot 10^{11}\ N/m^2$ and density $\rho = 5000\ kg/m^3$. The shaft which is inserted into the bracket was modelled as an integrated part of the bracket. Parabolic elements were used so that the shaft curvature would be described better. The bracket model is shown in Figure 3.4. The numbers 1, 2 and 3 are the coupling positions coupled to the blade at positions 3, 4 and 5 (for the isostatic and *low* case),

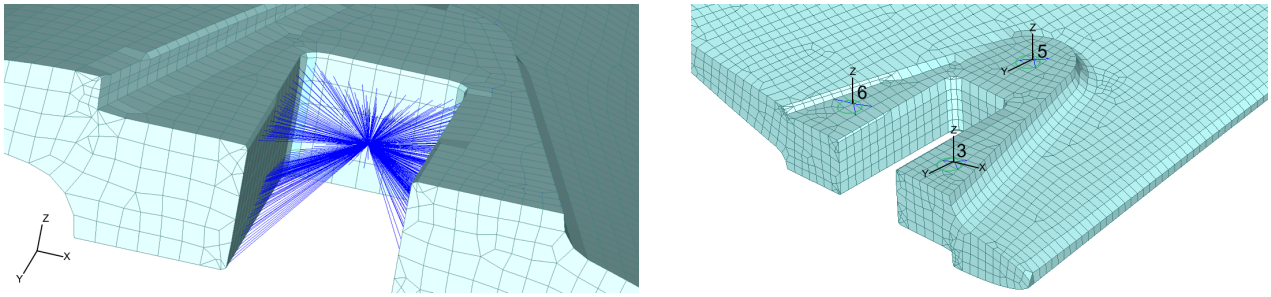

(a) *High coupling configuration.* (b) *Low coupling configuration.*

Figure 3.3: *The two alternative coupling configurations relative the isostatic for the FE blade. (a) The high coupling configuration with rigid links attached to a six DOFs coupling node. (b) The low coupling configuration with rigid links around the bolt holes on one side of the blade.*

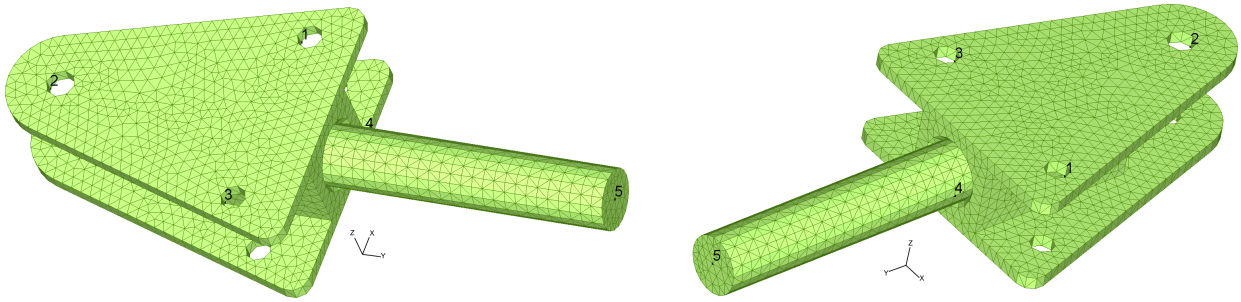

(a) *FE model of the bracket, viewed from same angle as the FE blade.* (b) *FE model of the bracket with the used numbering.*

Figure 3.4: *Two vies of the FE bracket with numbering. (a) Same view as for the blade FE model. (b) The numberings used, where positions 1, 2 and 3 are coupling positions and 4 and 5 correspond to where the accelerometers were attached in the measurements.*

thus matching DOFs were used at each of the components coupling locations.

The bracket, like the blade, was tested using different coupling configurations. The same arrangement for the coupling type *high* was made as for the blade, as seen in Figure 3.5a. All the DOFs on the bracket in contact with the blade when mounted were constrained with rigid links to a six DOFs node located at the centre of the three holes. The *low* coupling type was constrained at the holes of the bracket, see Figure 3.5b. Note that all constraints are on one side of the bracket. It should be noted that the *high* coupling configuration could not be used with experimental models of the blade without altering the coupling DOFs for the experimental system. The isostatic and *low* configurations were used in the experimental-analytical coupling. All three configurations were used in coupling of the analytical models .

3.1.3 Hub Bracket

The goal of this thesis is to couple experimental and analytical models of the blades to analytical models of the hub and brackets and because of this no model of the hub alone was created. The configuration of the hub relative to the blades was unimportant as the hub was modelled as a symmetric structure and thus no record of which blade was coupled where was kept. Two models were used, one which used the isostatic coupling configuration and one which used the *high* coupling configuration, explained in section 3.1.2. No model of the *low* configuration was used.

As for the bracket model, the geometry for the hub was received from TU Delft. It was modelled together with three brackets in a single mesh with 116876 solid parabolic elements with the same material strength as the bracket, this model is shown in Figure 3.6. Although the hub model has the same stiffness as the bracket, a higher density was used such that the total mass of the model corresponded to the real mass of the assembled hub with brackets and filled with epoxy, thus the density used was $\rho = 3530\ kg/m^3$. In order to mitigate the

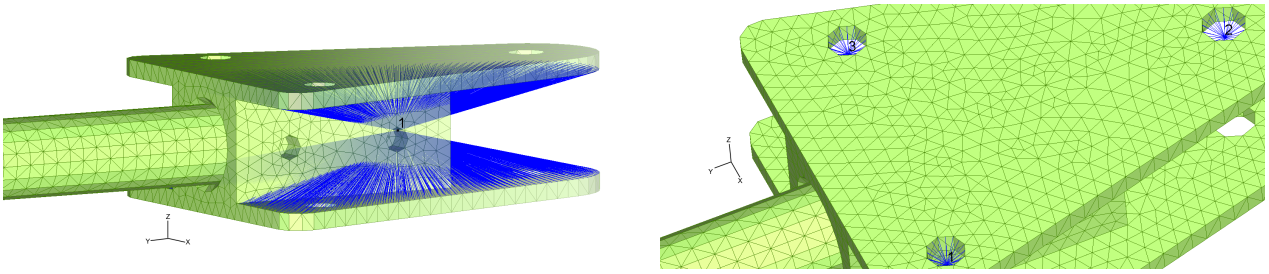

(a) *High coupling configuration.* (b) *Low coupling configuration.*

Figure 3.5: *The two alternative coupling configurations relative the isostatic for the FE bracket. (a) The high coupling configuration with rigid links attached to a six DOFs coupling node, only used in analytical coupling. (b) The low coupling configuration with rigid links around the bolt holes on one side of the bracket.*

dynamics of the hub internal parts the hub was filled with epoxy according to instructions found here [Onl].

The pitch angle configuration of the bracket was found to be of importance and the experimental accelerometer measurement directions had to be matched. The angle was chosen as an approximation and is shown in Figure 3.7.

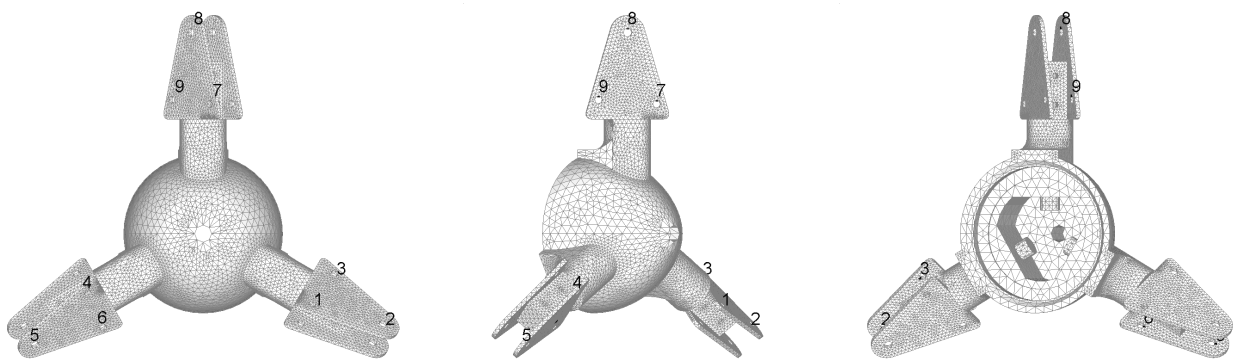

(a) *Front view of the hub.* (b) *Side view of the hub.* (c) *The hub seen from behind.*

Figure 3.6: *Different views of the hub FE model.*

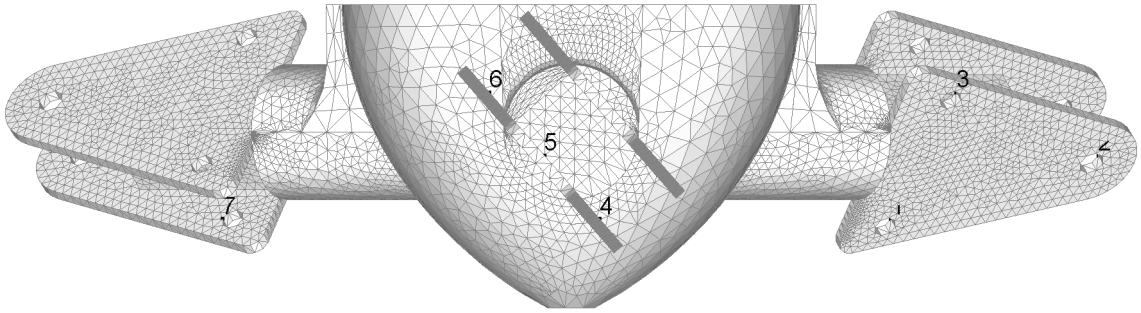

Figure 3.7: *FE model of the hub showing the angle of the attached bracket.*

3.2 Experiments

The experiments were performed at Chalmers Vibration and Smart Structures Lab. The measurements were performed with a stepped sine input with 0.25 Hz step size from 20 to 800 Hz for the blade and blade bracket measurements. For the fully assembled system the measurements were performed from 10 to 300 Hz with a

step size of 0.1 Hz and 0.01 Hz at some particular frequency intervals. A total of three measurements for the blade and blade bracket models were made, respectively. Only one measurement was performed for the fully assembled system. The configurations considered were: the three blades alone, the three blades with brackets mounted, the hub with brackets and blades mounted. Thus in total 19 individual measurement setups were required for the components used. Note that measurements made in a specific direction (x, y or z) means that the input was aligned with that axis. See Figure 3.1 for an orientation of an generic blade and Figure 3.2b for the different input locations.

All the parts used in this thesis, the blades, the brackets, the hub and the internal parts, and how they were assembled are shown in Appendix A.

3.2.1 Test Setup

The three different input directions are shown in Figure 3.8. This coordinate system is consistent with the FE analysis coordinate system.

The general test setup is shown in Figure 3.9a. It was exactly the same, both for the measurement of blades alone and for the blade measurements with a bracket attached. It can be seen, from Figure 3.8, that the measured blades (and bracket mounted blades) were hung at three locations when measured in the x and y directions, which made it easier to position the components relative to the load cell. Measurements in the z direction for the blade and blade with attached bracket were only hung at two positions. Further, it should be noted that the components were hung in fasteners which were glued to the components, the same fastener was used for the load cell attachment and can be seen in Figure 3.11c. All the fasteners were mounted on the blades during all measurements for consistency.

The interface locations of the blade are shown in Figure 3.2a for the analytical model and are visible for the real blade in Figure 3.10c but with the interface accelerometer from position 6 located under the stinger and used as a direct accelerance for a comparison with the accelerometer at position 1.

For a view of a bracket and blade assembled see Figure 3.9b. A detailed view of the interface accelerometers can also be seen. Different input directions to the bracket coupled with a blade had the same accelerometer locations and the same input locations were used as shown in Figure 3.8.

The setup for the measurements of the fully assembled hub with brackets and blades is shown in Figure 3.10a and 3.10b. The accelerometer placements can be seen in Figure 3.25, which shows an FE representation of the structure. Only one measurement was performed with input at position 19.

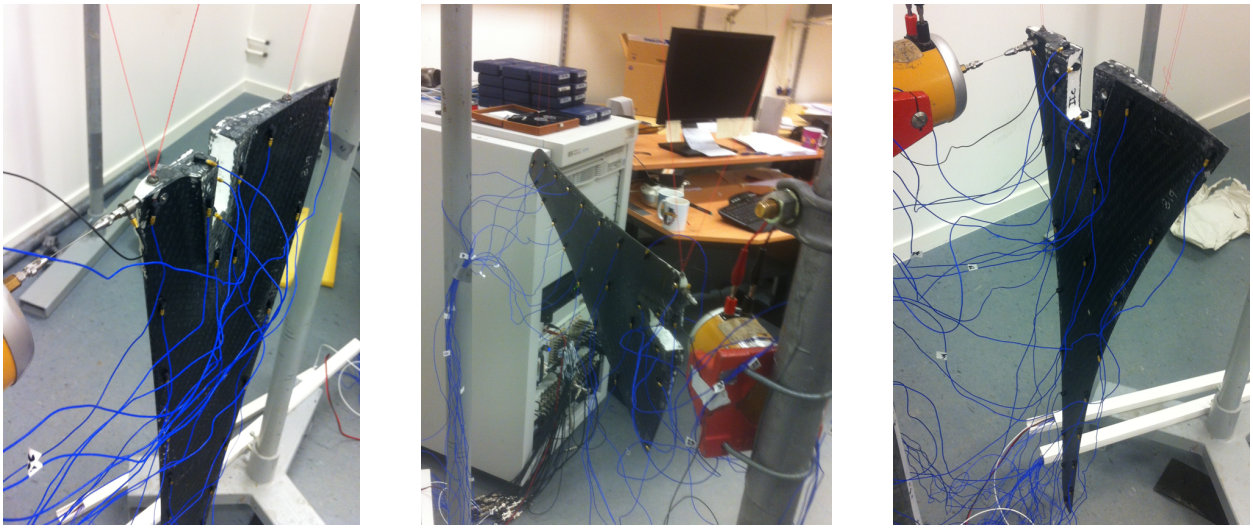

(a) *Input in the x direction.* (b) *Input in the y direction.* (c) *Input in the z direction.*

Figure 3.8: *The input directions and test setup for the blades.*

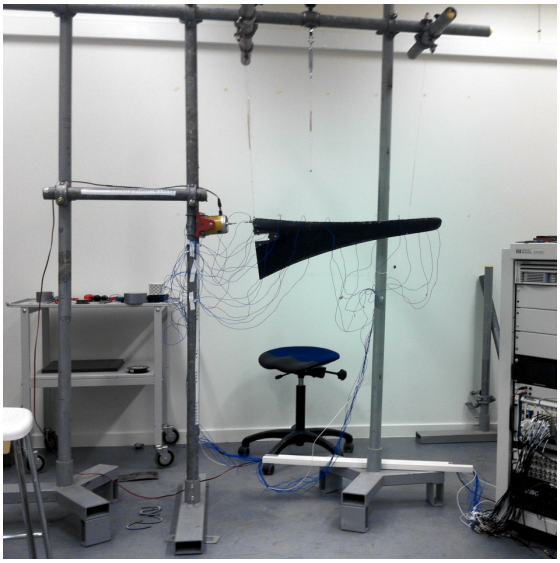

(a) *Overview.*

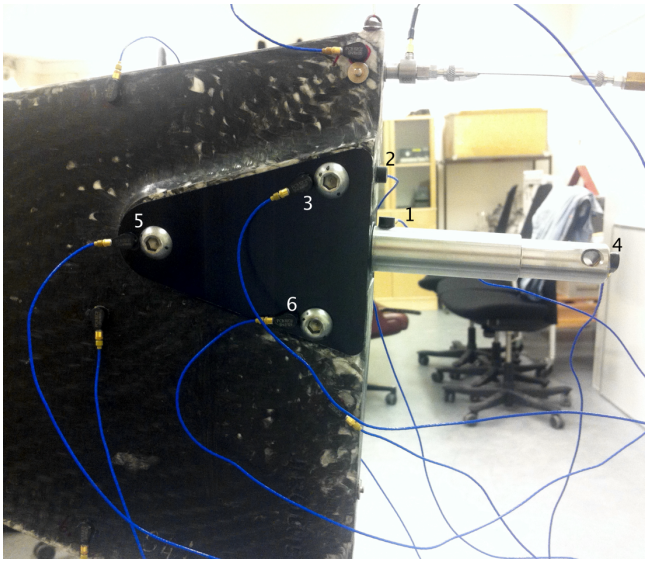

(b) *Detailed view of blade bracket assembly.*

Figure 3.9: *The overview of the test setup is shown in figure (a) for a blade measurement but was the same for all measurements. In figure (b) a detailed view of the blade bracket assembly is shown with the accelerometer placements.*

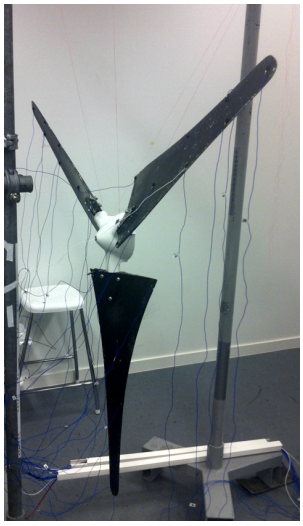

(a) *Fully assembled structure.*

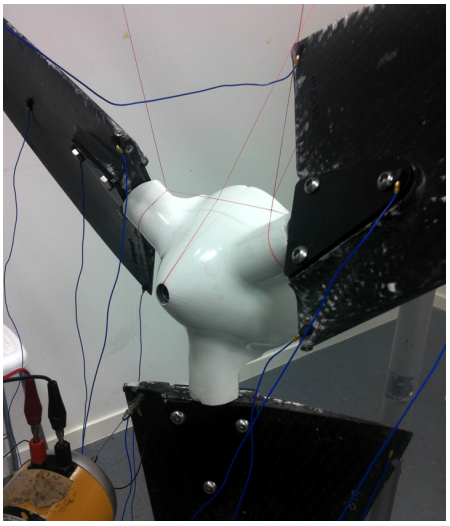

(b) *Detailed view of hub input.*

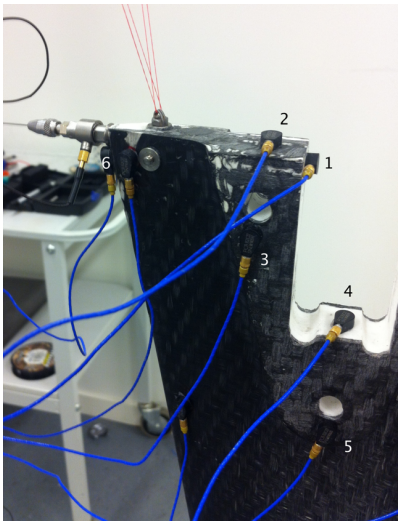

(c) *Detailed view of reference interface.*

Figure 3.10: *(a) An overview of the fully assembled test object and how it is hung on the surrounding structure. (b) The input location for the fully assembled structure. (c) A detailed view of the coupling accelerometer locations of a blade measured in the x direction with accelerometer six acting as a direct accelerance.*

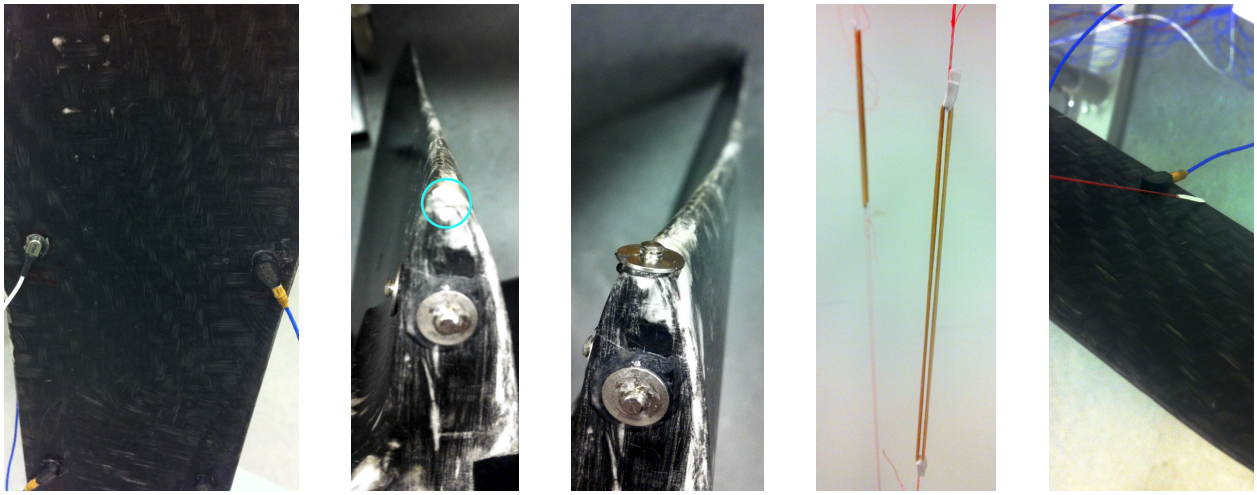

(a) *Accelerometers.* (b) *Flattening.* (c) *Mounts.* (d) *Rubber bands.* (e) *Tape.*

Figure 3.11: *Alterations to the blade and test equipment. (a) The difference between the Dytran and PCB accelerometers. (b) The corner that had to be flattened. (c) The mount fastened at the flattened corner. (d) The rubber bands that were inserted between the stiff cords to lower the bouncing rigid body mode. (e) When the blade was measured in the y direction it had to be supported at the tip as well.*

3.2.2 Alterations

There were a few alterations made to the measurement system and measured objects along the way which should be pointed out as they could potentially constitute sources of errors. All the alterations are shown in Figure 3.11.

All measurements were performed with 25 PCB 352C22 (0.5 gramme) accelerometers and 1 Dytran 3224A1 (0.2 gramme) accelerometer except for blade 819, with and without bracket, which was measured with 26 PCB accelerometers. The accelerometers were single axis and had a transverse sensitivity of ≤ 5 %. There was a significant difference in the output produced by the two accelerometer types, seen in Figure 3.11a. Only 1 channel out of 26 was affected, which is why the difference was neglected although it is shown to impact the first modes, see section 4.1 and Appendix C.

Because the blade was very flat it was particularly hard to perform measurements with an input in the x direction. Thus, the blade had to be altered by flattening a corner, i.e. changing the geometry and removing some mass. This alteration was neglected as well as the same alteration was performed for all blades and the modification was considered small. See Figures 3.11b and 3.11c for the alteration and fixture mounting.

Measurements in the y direction activated rigid body modes that had a very high frequency relative to the first flexible mode and contaminated the first resonance. To overcome this problem the test object was supported in a more flexible way; by rubber bands inserted between stiff cords, see Figure 3.11d. This changed the system characteristic to some extent but also gave much cleaner FRFs, see Figure 3.13. All experiments were performed with these rubber bands to avoid any variations in the eigenfrequencies between the three measurements of the same object. The measurement in the y direction meant that the blade had to be supported at the tip as shown in Figure 3.11e. In order for the blade, which was sharp at the edge, not to cut through the cord, a soft and light material was inserted between the contact surface.

3.3 Experimental Models

To obtain experimental models, system identification was performed on the obtained frequency response data (FRD). MATLAB's System Identification Toolbox was used with the method N4SID, which is a state-space subspace method, see McKelvey [MAL96]. Further, a method developed by Yaghoubi and Abrahamsson for automatic model order selection and system identification was used, see [YA12; YA13].

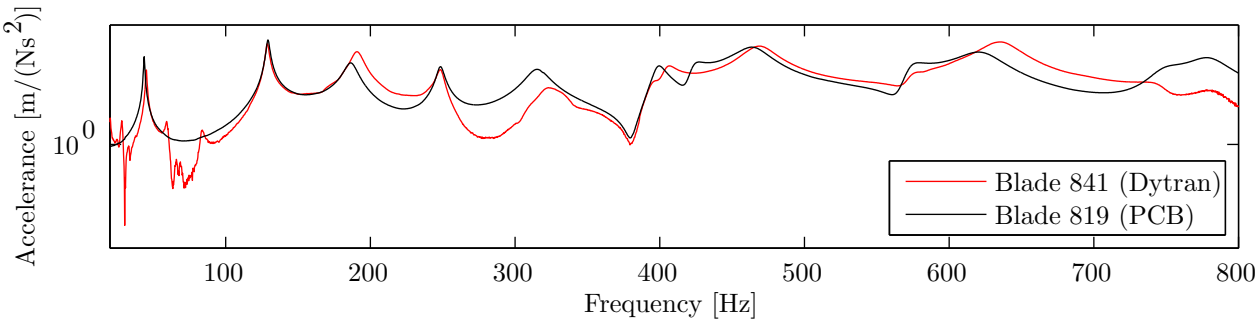

(a) *Whole FRF.*

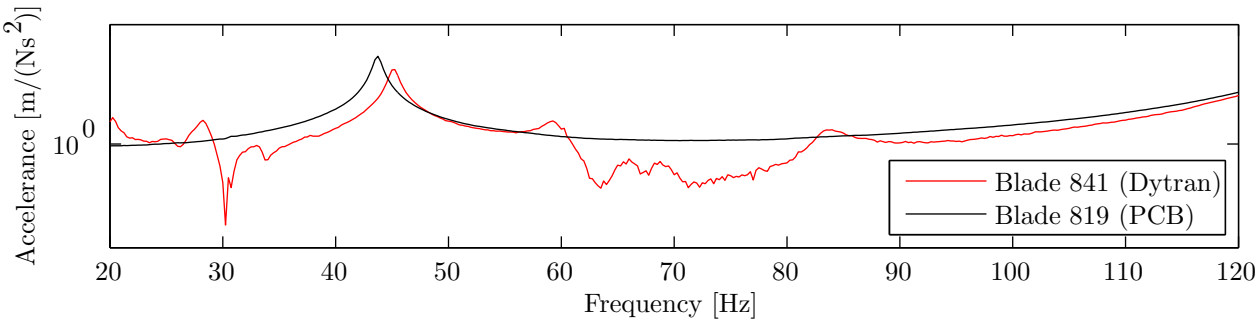

(b) *Detailed view of the low frequency area.*

Figure 3.12: *The difference between the two accelerometers for input in z and output from channel 20. (a) The measured frequency range. (b) A detailed view of the first resonance.*

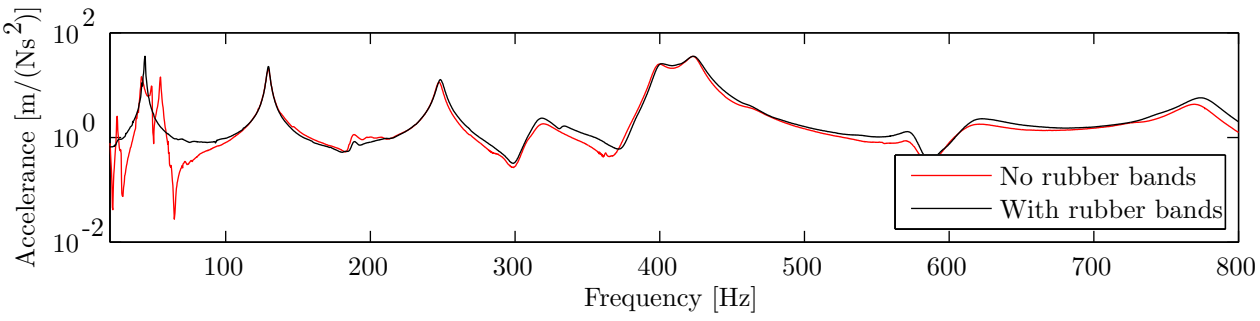

(a) *Whole FRF.*

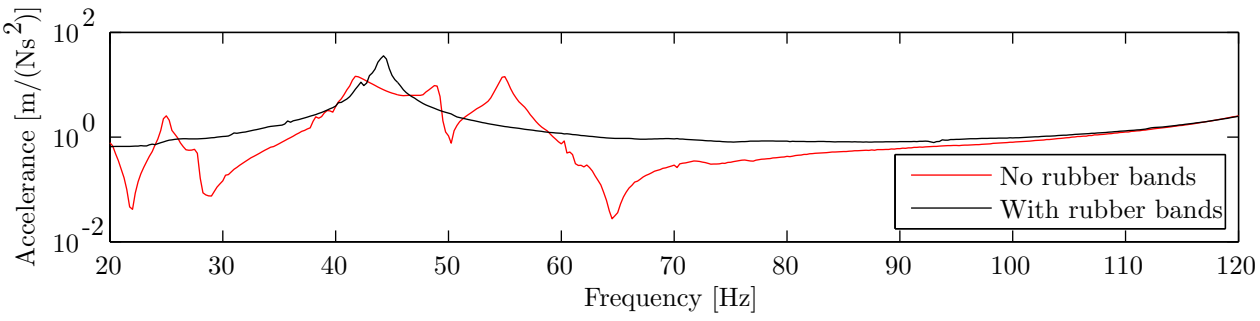

(b) *Detailed view of the low frequency area.*

Figure 3.13: *The impact of the rubber bands on the measurements for blade 819 with input in y and output from channel 26. (a) The whole FRF is shown for two measurements, with and without rubber bands. (b) A detailed view of the first resonance.*

3.3.1 General

A first attempt at system identification was made with MATLAB's System Identification Toolbox. The order of the system was partly guessed, from the number of visible resonances in the measured data, and in part used the toolbox's built in order estimation. This identification attempt resulted in poor models, especially for the blade with mounted bracket model. The second attempt was based on estimating a very big model, with many states, around 100. These states were then manually removed. This attempt was very tedious as a lot of states were put in the low frequency area which was fairly noisy for identification on receptance data. This meant that even a model order of 100 states missed some eigenfrequencies in the higher frequency area. Attempting the same procedure on mobility data gave better result but still gave three states where only one should exist. Thus, an automated method for order selection and identification developed by Yaghoubi and Abrahamsson was used, see [YA12; YA13]. This method is based on obtaining a few realisations of the same data and performing statistical evaluations, using the MOC, to discard non-physical modes. The only input required by the user is a high model order to start from.

In general, the method worked very well for the experimental data of the blade. Only occasionally did it give non-physical modes that could be removed manually by transforming the state-space system to diagonal form by the same technique that a second order system was transformed to modal form. Thus, the transformed $\mathbf{A}$ matrix was a diagonal matrix with the system's eigenvalues. In order to remove states corresponding to some particular eigenvalues, the specific row and column were removed from the $\mathbf{A}$ matrix, the same row from the $\mathbf{B}$ matrix and the same column from the $\mathbf{C}$ matrix. After the reduction, the $\mathbf{B}$ and $\mathbf{C}$ matrices were re-estimated and rigid body modes added to the system. It was also found that the method worked best with accelerance data because it accounted less for the noisy low frequency area where only a few modes were located and which were easy to identify, see Figure 3.14. It was of interest to obtain state-space models without a feedthrough matrix $\mathbf{D}$, thus the identification had to be on either mobility or receptance data. Identification of mobility data was found to be satisfactory. The difference between accelerance, mobility and receptance can be seen in Figure 3.14.

The experimental models were constructed from constructed data stemming from multiple measurements and the dynamic properties were not identical in each test. Thus, one model essentially had three different eigenfrequencies for each real eigenfrequency, illustrated in Figure 3.15 where raw data is shown for one real blade but from two different measurements. It can be seen that the peaks are shifted and during the system identification process this created problems. The slight shifts in frequency were introduced by reattaching the accelerometers, changing the input and also changing the testsetup, e.g. see Figure 3.8. Generally for accelerance data, this was not an issue as the statistical evaluation could obtain better models but for receptance data it caused occasional problems.

3.3.2 Blade

Remember from section 2.10, that co-located and co-oriented force excitation and response must be had at the same position to be able to build a full $\mathbf{B}$ matrix. For this to work an approximation was introduced during the blade measurements. Only 26 accelerometers were available during the vibration tests and in order to acquire good spatial resolution of the blade models most of them were equally distributed over the blade and only the minimal set needed focused at the coupling positions. The error from the assumed co-located and co-oriented force excitations and responses introduced is visualised in Figure 3.16 and 3.17 for input in the x and y directions, respectively. The reference accelerometer for input in x was placed under the load cell, seen in Figure 3.10c, in a separate test. Accelerometer 1 was located on the opposite side and it was assumed that these two outputs would produce the same, but shifted, signals. Because the surface was not flat, the accelerometer was tilted relative to accelerometer 1. The results in Figure 3.16 are considered adequate. For input y, the difference is larger as the distance between the two direct output accelerometers is also greater. See Figure 3.8b and especially Figure 3.2b where input y is marked with number 28. It is easy to see that there should in fact exist a difference. This difference was neglected. It should be noted that for input in z, accelerometer 7 served as the direct accelerance, seen in Figure 3.1.

Further, in the system identification procedure it was of interest to obtain experimental models without the effect of the rigid body modes in the frequency area of interest as the N4SID method works best on data without rigid body contribution, in order to estimate the antiresonances satisfactory. Thus rigid body modes from the FE model of the blade were substracted from the experimental FRD. The same rigid body modes were later added to the identified system. In Figure 3.18 the raw receptance data is shown in cyan with the contribution from the FE rigid body modes in black and in red a model without the impact of the rigid body

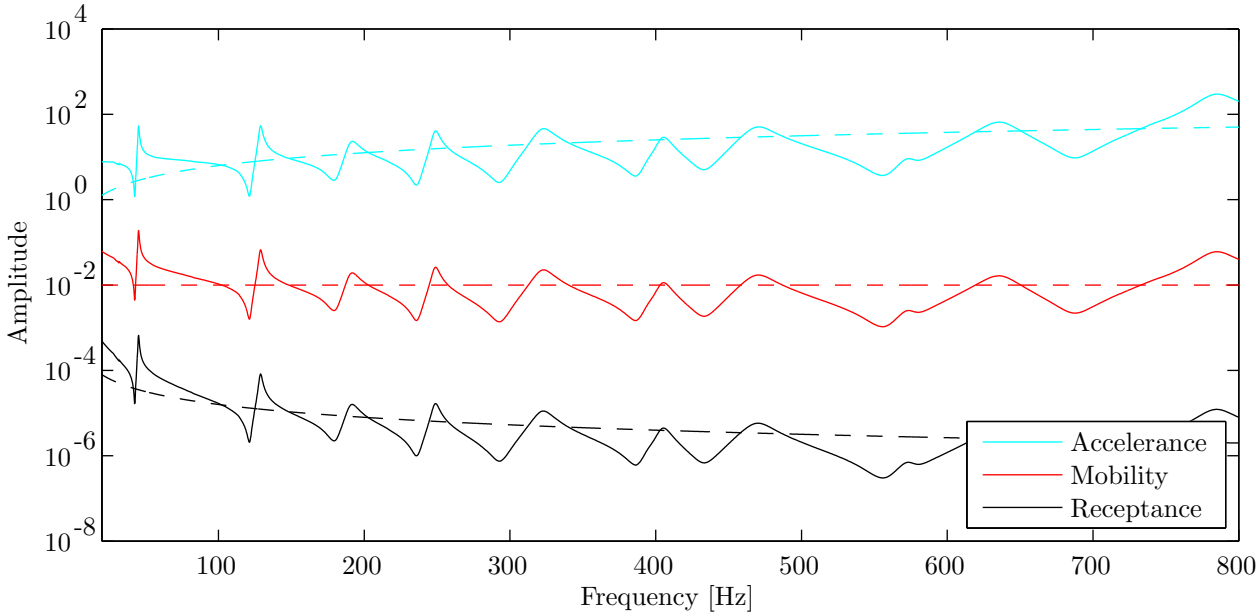

Figure 3.14: *Difference between accelerance (cyan), mobility (red) and receptance (black) data. Notice also the relative trends of each data set.*

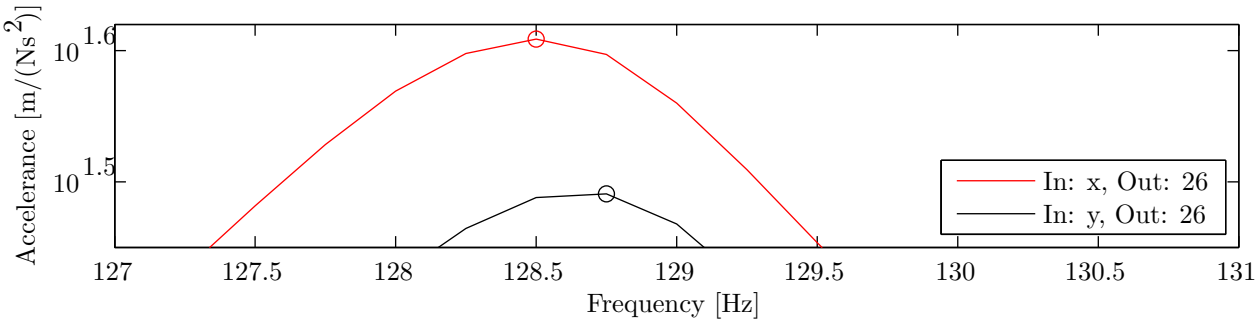

Figure 3.15: *Second eigenfrequency for two measurements of blade 841. The red curve has a resonance frequency at 128.5 Hz while the black curve has a resonance frequency at 128.75 Hz. The frequency step is 0.25 Hz which means that they differ by one frequency line.*

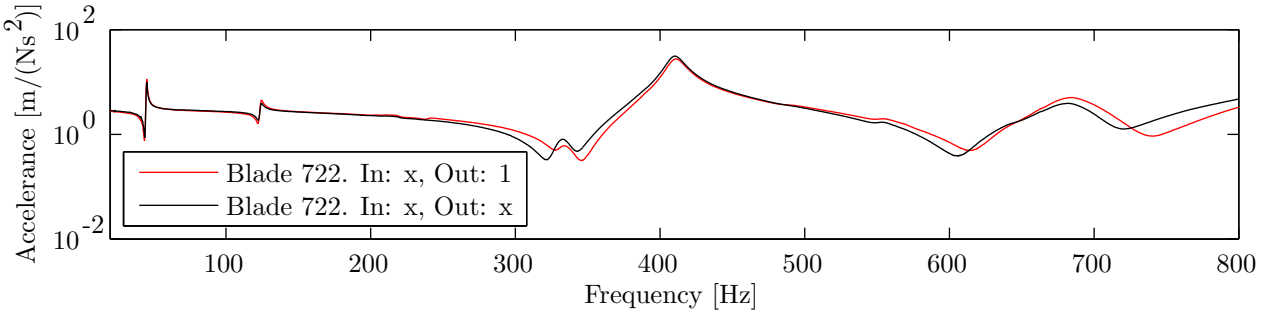

Figure 3.16: *Difference between the transfer function for input in x and output 1 and the direct accelerance, i.e. the output was located under the input as shown in Figure 3.10c.*

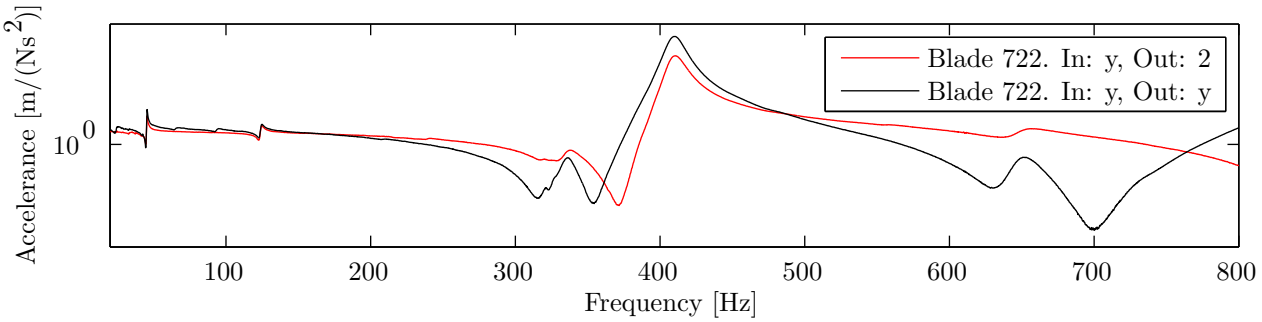

Figure 3.17: *Difference between the transfer function for input in y and output 2 and the direct accelerance.*

modes. Thus it is seen that the rigid body contribution to the flexible modes mainly affects the antiresonances. Instead of measuring the rigid body modes, which is known to be very hard and produce inaccurate results, it was assumed that the FE rigid body modes were an adequate estimate. Furthermore, mixing rigid body modes from these two models did not affect the results where analytical and experimental models were compared.

3.3.3 Blade Bracket

The same procedure used for identification of the blades was performed for data of the blades with mounted brackets, but the system identification of the data was more troublesome, even with the automated order estimation. The system identification missed obvious modes in the middle of the frequency range. One assembly in particular was hard to identify; blade 841 coupled with bracket 03 around 400 Hz. Thus, the data was split in three frequency regions, in each of which system identification was performed whereafter the models were merged together.

Rigid body modes were again removed from the experimental data in the same manner as before. It was

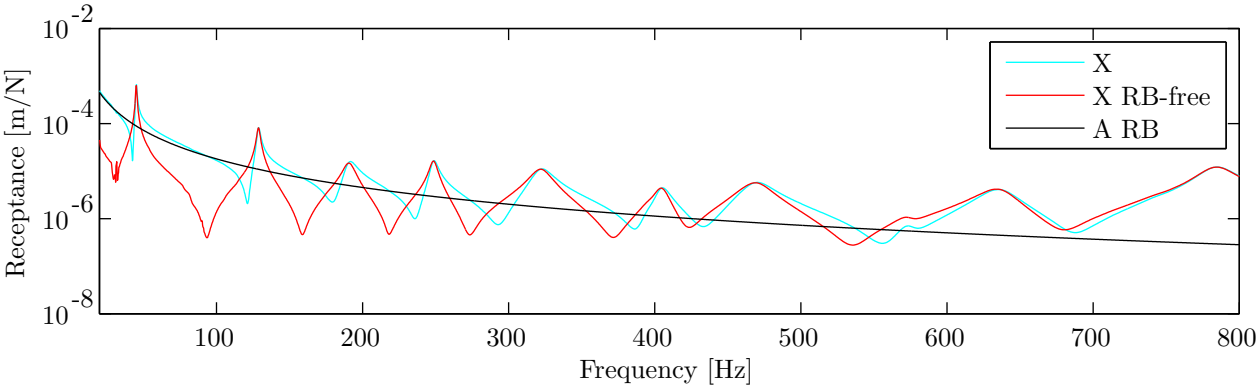

Figure 3.18: *Rigid body free data of blade 841 with input in z and output 7. The X stands for experimental data, A for analytical data and RB for rigid body.*

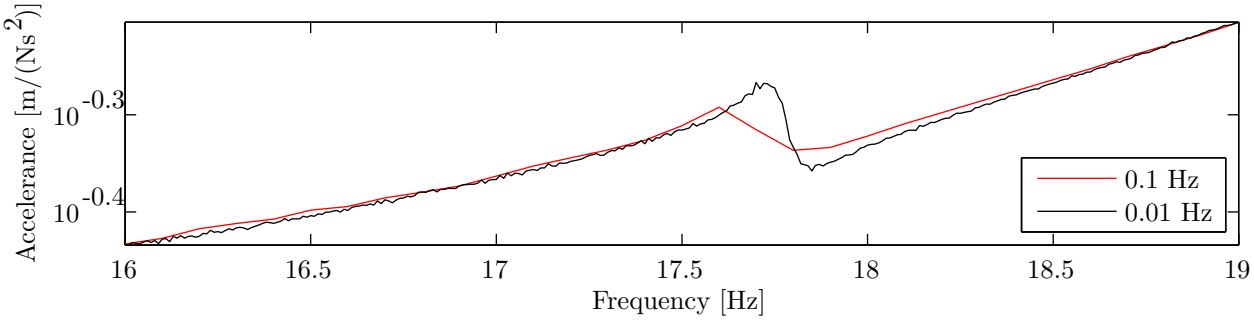

Figure 3.19: *The zigzag pattern formed from the very fine frequency step size, which was used for some frequency intervals in the final assembly, compared to the coarse step size.*

assumed that the coupling configuration did not matter as the same centre of mass and the mass of the total system was the same in all configurations. Also, the FE rigid body modes were a crude estimate and choosing rightly between these estimates was impossible, thus isostatic coupling was used.

3.3.4 Blade Bracket Hub

For the final assembly - hub assembled to brackets and blades - only one measurement was performed. The acquired data was transformed to mobility data with the rigid body modes removed by using approximate FE model rigid body modes as before. The automatic system identification procedure used to identify the blade and blade bracket models was not used in this identification as it could not separate between modes very close in frequency, discussed in chapter 5. It was known from FE analysis that mode clusters would be present due to the symmetry of the structure. Thus, the step size had to be reduced in order to capture all modes with only one input. A step size of 0.1 Hz, reduced at some selected frequency intervals to 0.01 Hz, was used. The measurements were performed from 10 Hz to 300 Hz as it was assumed that only the first few modes would have a good correlation. Further, it must also be noted that the acquisition system did not produce smooth data at the lower step size of 0.01 Hz, as shown in Figure 3.19. Notice how the curve is forming a zigzag pattern, which could potentially be a problem in the system identification phase.

The system identification of the obtained data was performed by estimation of a very large model and removing states manually with the procedure described earlier.

3.3.5 Physical Models

The system identification procedure did not produce physically consistent models, which are required for the state-space synthesis method, [SA07]. In other words $\mathbf{CB} \neq \mathbf{0}$. This was enforced by introducing highly damped auxiliary states with corresponding eigenfrequencies of two orders higher than the highest from the identified system. The effect from these states on the frequency function was minimal as can be seen in Figure 3.20.

Also, the passivity criterion, stated in section 2.1.3, was not satisfied for the measured data. In reality, the components measured were passive but due to the large amount of electronic measurement equipment and the large approximations in the direct accelerances, see section 3.3.2, the acquired data could be non-passive. For direct mobility FRFs the phase must lie between [-90°, 90°], [SA07]. This is shown in Figure 3.21 and 3.22 for two channels from two different inputs of the raw measurements. If FRF data from measurements with input in x were used the identified system was non-passive, removing this input from the identification procedure generally produce better models but some channels were still not passive, that is, the system identification procedure does not consider passivity. Removing too much information would in it self produce poor models and thus other methods must be employed to enforce passivity, as outlined in section 2.11. It should be noted that using this method will also produce systems that satisfy Newton's second law. In this thesis the non-passive system will be used but an evaluation of the differences between the non-passive systems with added axillary modes and the physical systems will be performed as there is interest in creating another methodology to enforce passivity. The evaluation is presented in section 4.6 and discussed in chapter 5.

In Figure 3.23 the direct mobility is seen for the identified model with enforced reciprocity. It can be seen that in particular blade 841 at around 400 Hz is not passive, this is further discussed in chapter 5. Investigating the figure closer shows that the models are almost not passive in the entire domain of interest.

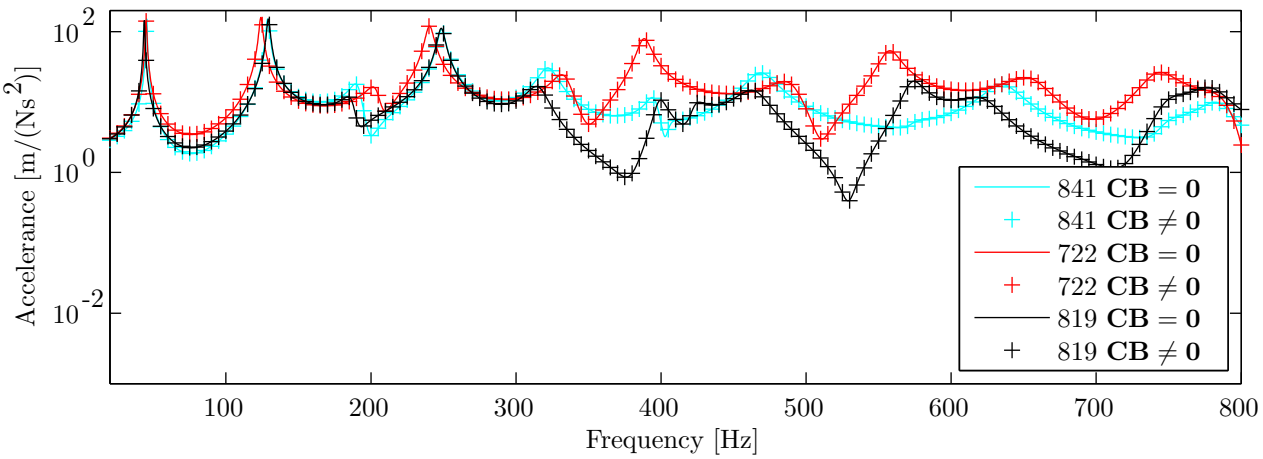

Figure 3.20: *The impact of the high auxiliary modes on the blade systems.*

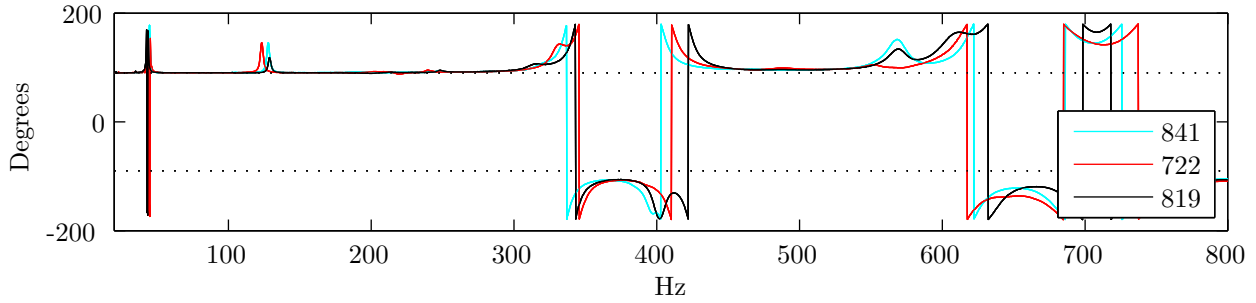

Figure 3.21: *Direct mobility for raw FRF data with input in x and output from channel 1, the dotted lines mark the limits at 90° and -90°.*

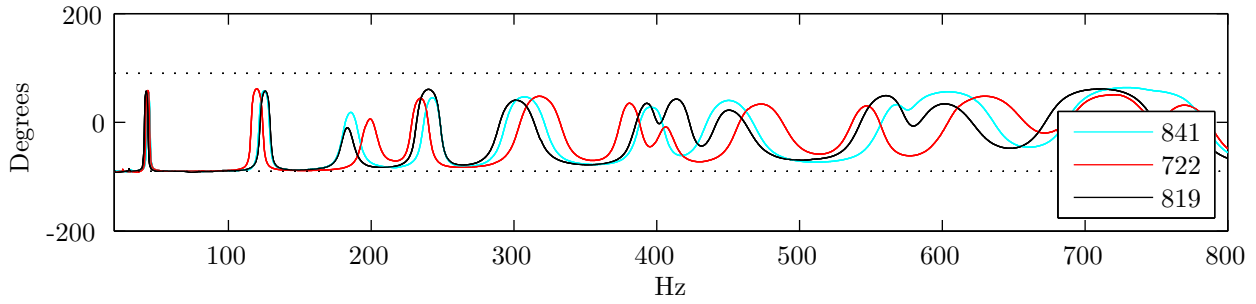

Figure 3.22: *Direct mobility for raw FRF data with input in z and output from channel 3, the dotted lines mark the limits at 90° and -90°.*

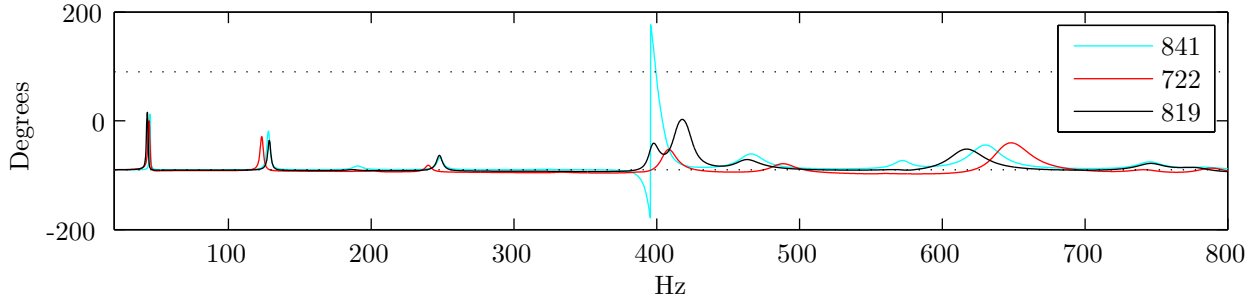

Figure 3.23: *Direct mobility for identified models with input in x and output from channel 1, the dotted lines mark the limits at 90° and -90°.*

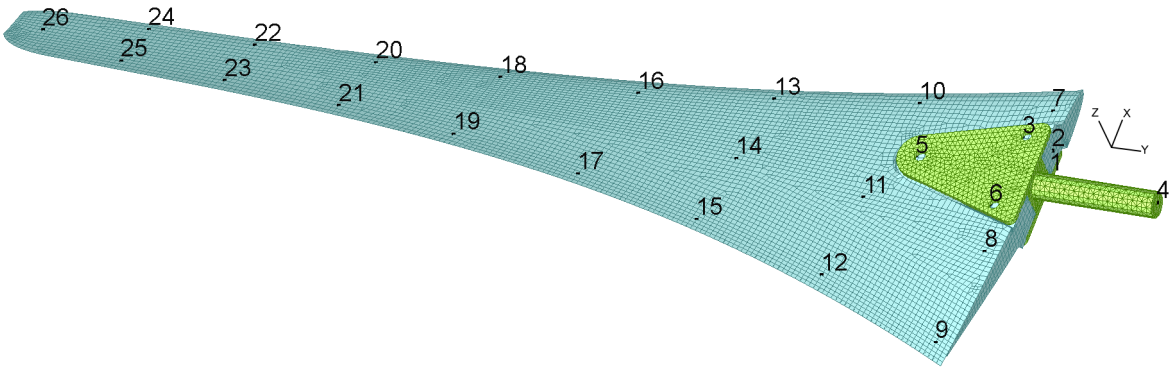

Figure 3.24: *The FE model of the blade mounted to the FE model of the bracket with measurement locations.*

3.4 Coupling

The response and force excitation must be known at all the interface locations to be able to couple a structure, but positioning an input at every interface location was very difficult and performing more measurements on the same model without changing the system too much was very complicated. To solve this problem, if the components are assumed linear, the reciprocity theorem can be used, described in section 2.10. Thus, it was only necessary to measure the structures at one point, with co-located and co-oriented force excitation and responses. In this thesis three co-located and co-oriented force excitations and responses were used for the experimental models used for coupling. This was due in part to controllability issues, i.e. it was hard to find an input position for which all modes in the frequency range of interest were well excited.

The CMS coupling, with a Craig-Bampton reduction, was used for the analytical coupling. The FBS and state-space methods were used for experimental-analytical coupling. Comparisons between all three methods are presented. To obtain models from the FBS method, comparable to the state-space and CMS methods, the synthesised FRD was identified again after coupling.

A FE coupling in FEMAP was also considered with a glued connection property. For this method only the eigenvalues were compared with the other methods.

3.4.1 Blade Bracket

The blade and bracket coupling combinations considered consisted of an analytical blade coupled to an analytical bracket and an experimental blade with an analytical bracket. The couplings were compared to the measurements of the coupled components. A FE blade and bracket couple is shown in Figure 3.24 with the numbering used.

3.4.2 Bracket Hub

The hub and bracket was built as one FE model which was coupled either to FE blades or experimental blades. The coupled systems were compared to measurements of the assembled structure. The numbering used in the analytical models and the experimental measurements can be seen in Figure 3.25.

4 Results

The correlation between the blade models and the blade bracket models are presented. Then, analytical coupling between the components is presented followed by the experimental-analytical coupling. A comparison between the state-space and FBS methods is also presented for experimental-analytical coupling along with an evaluation of the numerical problems encountered for the state-space coupling method. Some problems regarding physicality in the used models is also presented in section 4.6.

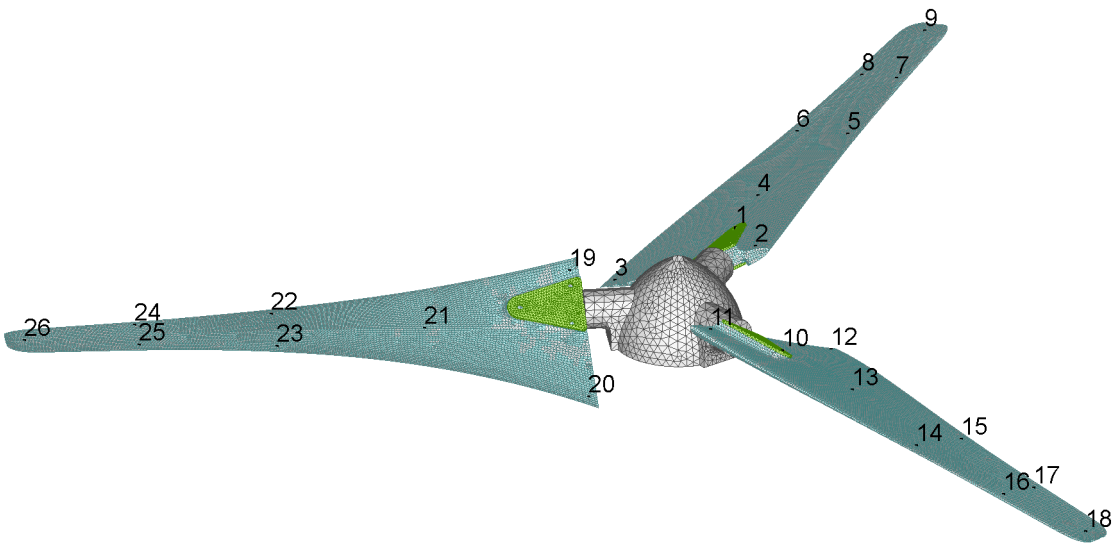

Figure 3.25: *FE model of the hub mounted to three blades and brackets.*

It should be noted that for analytical models a model order of 40 gave good results compared to the original, unreduced model. Model order here means the number of generalised DOFs in the reduced models, i.e. the total number of generalised DOFs of the models were larger as 26 physical coordinates were kept for the blade models for example. A relative error, between the reduced and original models, below 0.001 % for the first mode to below 0.01 % for the tenth mode of the blade model is had. The bracket and hub models had an relative error for all ten first modes under 0.001 %. This was considered adequate and without any impact of the results.

When talking about modes it is usually implied to mean the flexible modes if not stated otherwise.

4.1 Blade Models

The MAC correlation between the first 11 modes for the three experimental blades and the FE blade model is shown in Figure 4.1. The MAC matrix is block symmetric, thus only the upper half is shown. Red borders represent a correlation between 1 and 0.95, cyan borders a correlation between 0.9 and 0.85, green borders a correlation between 0.9 and 0.85 and finally yellow borders represent a correlation between 0.85 and 0.8. A correlation of 1 means that the eigenvectors match perfectly and a correlation as low as 0.9 is considered good while everything under 0.8 is considered bad.

The first thing to notice is that in general a very good correlation for the first six modes is achieved and that there is almost no cross-correlation. The seventh mode correlates poorly in general but between blade 841 and 819 and between blade 722 and the FE blade there is a correlation between 0.95 and 0.9 and 0.85 and 0.8, respectively. Correlations for modes 8 to 10 also gave good correlations between the models. Mode seven is an edgewise bending mode which is hard to measure and which was not modelled in the FE model, cf. [Joh+13].

The 11 first eigenfrequencies for the three experimental blade models and the FE blade are shown in Table 4.1 along with the mean (μ, Hz), the standard deviation (σ, Hz) and the coefficient of variance (COV, %) for the three experimental blades. Also, the relative error (%) between the measured mean relative to the FE blade is given. It can be seen that the spread between the blades is considerable and that the errors for modes 8 and 10 are considerably larger compared to the other modes. The mass (gramme) is also given in the table for the three blades and the FE blade along with the mean (gramme) of the three blades, the standard deviation (gramme), the coefficient of variance and the relative error with respect to the FE model. The spread of the mass is very small.

The spread between the three blades can also be seen in Figure 4.2, where the FRFs of the three blades for input in z and output 7 is shown. From this figure it can also be seen that there is a considerable spread, especially around mode six and seven.

In Appendix C the modeshapes for the first nine flexible modes are shown both for the experimental and FE models.

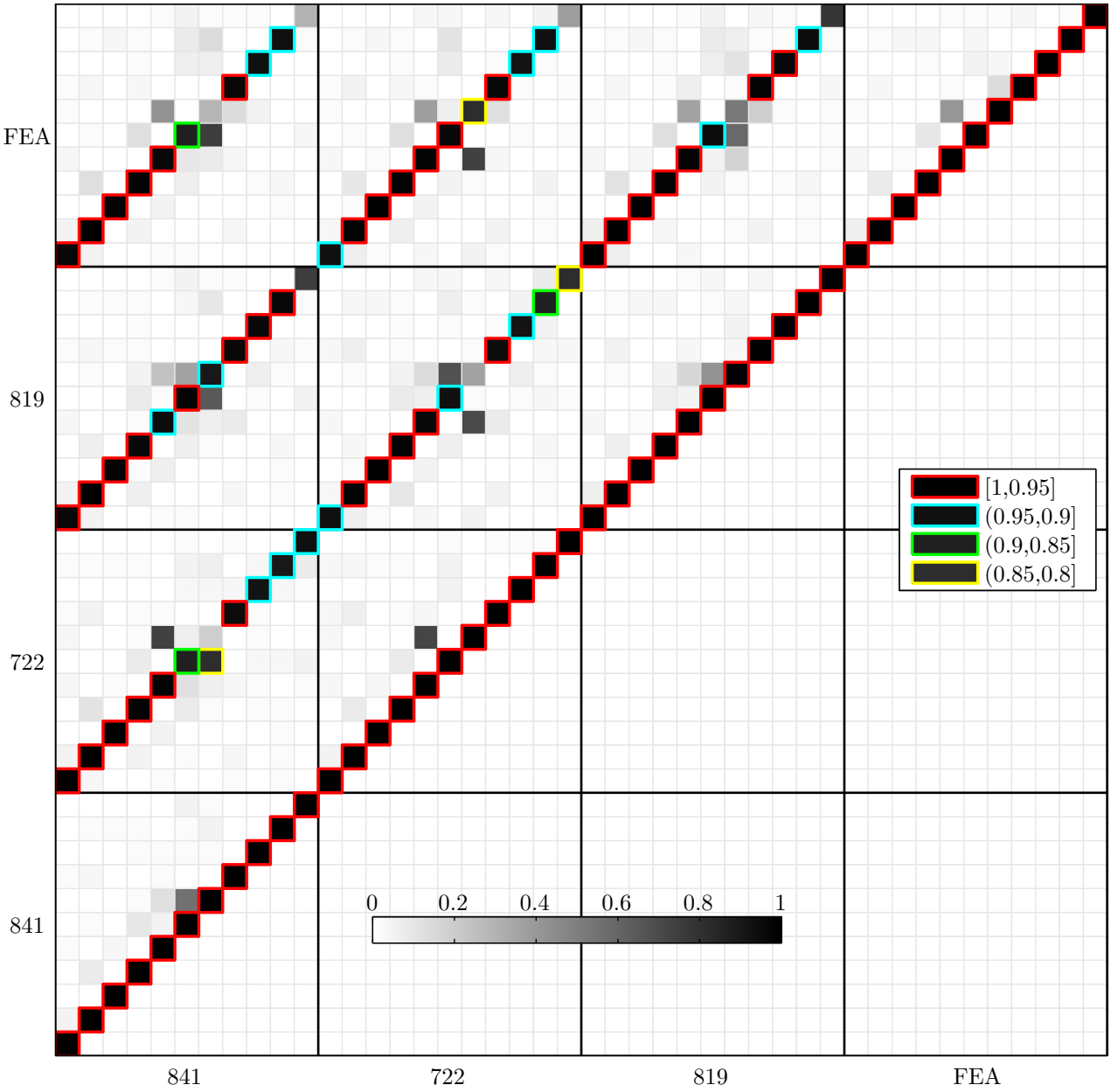

Figure 4.1: *MAC matrix for the 11 first modes between 3 experimental blades and the FE blade. 4 colour codes are given where red marks a correlation between 0.95 and 1, cyan a correlation between 0.9 and 0.95, green a correlation between 0.85 and 0.9 and yellow a correlation between 0.8 and 0.85.*

Table 4.1: Eigenfrequencies (Hz) and mass (gramme) for all the blades along with mean (μ, Hz and gramme), standard deviation (σ, Hz and gramme) and coefficient of variation (COV, %) of all the experimental blades. The FE model eigenfrequencies (Hz) and mass (gramme) are also shown along with the relative error (%) between the measured mean and the FE element blade.

Set	Blades				Statistics			
Component	841	722	819	FEA	μ	σ	COV	Error
Mode 1	45.37	45.00	43.72	45.82	44.70	0.86	1.93	2.51
Mode 2	128.76	124.08	129.24	130.67	127.36	2.85	2.24	2.60
Mode 3	190.79	203.49	186.66	197.65	193.65	8.77	4.53	2.06
Mode 4	248.64	240.32	248.44	254.21	245.80	4.75	1.93	3.42
Mode 5	322.12	333.15	315.29	339.93	323.52	9.01	2.79	5.07
Mode 6	395.36	388.16	398.94	412.58	394.16	5.49	1.39	4.67
Mode 7	404.56	410.33	423.24	453.22	412.71	9.56	2.32	9.82
Mode 8	468.74	489.54	463.86	495.47	474.05	13.64	2.88	4.52
Mode 9	572.88	557.26	573.00	598.12	567.71	9.05	1.59	5.36
Mode 10	635.25	654.52	621.72	660.11	637.16	16.49	2.59	3.60
Mode 11	746.52	742.21	747.93	758.33	745.55	2.98	0.40	1.71
Mass	830.50	829.70	830.10	797.11	830.10	0.40	4.89e-04	-3.97

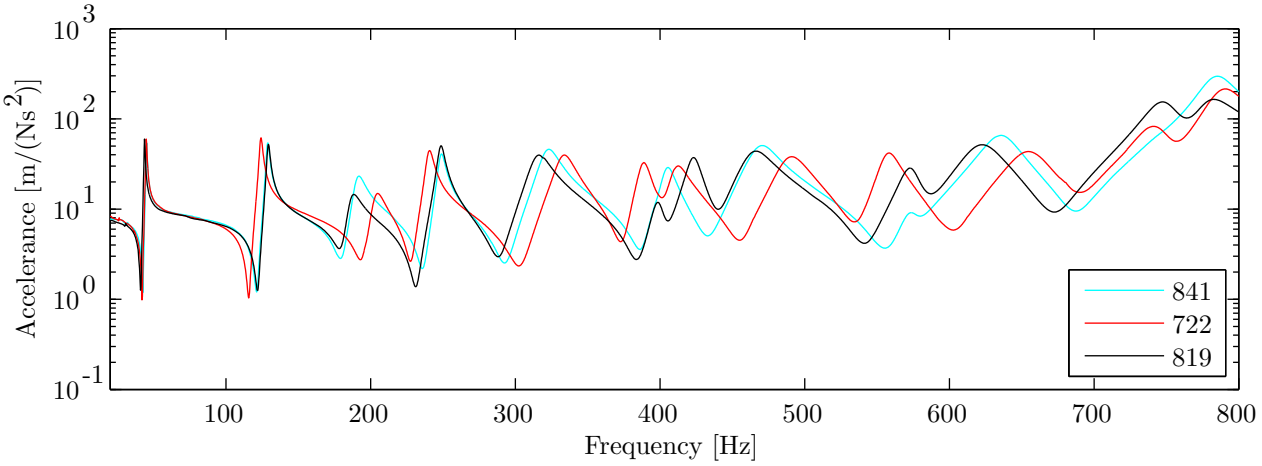

Figure 4.2: *Spread between the raw FRFs of the blades with input in z and output from channel 7 as shown in Figures 3.8 and 3.1.*

4.2 Blade Bracket Models

The MAC matrix between the three experimental models of the blade and bracket assemblies is seen in Figure 4.3, which shows that blade models 841/01 and 722/02 correlate well. The correlation between 841/01 and 819/03 is not as good; mode six and seven show no correlation. The correlation between models 722/02 and 819/03 is also not very good; the first five modes correlate well while the sixth mode is on the limit and everything above is without correlation. There is also a larger off-diagonal correlation compared to the blade models.

In Table 4.2, the 11 first modes are presented along with the mean (μ, Hz), the standard deviation (σ, Hz) and the coefficient of variance (COV, %). The mass is also shown for the components along with the mean (μ, gramme), the standard deviation (σ, gramme) and the coefficient of variance (COV, %). The standard deviation is largest for mode 10, then 8, 11 and 5. It can also be concluded from these results that the spread is large. In Figure 4.4, the FRFs for the three models, again with input in z and output 7, are shown. First notice that the first two eigenfrequencies are much lower in amplitude compared to the blades alone, caused by the increase in damping. Further it is easy to see that over 350 Hz there exist a large spread which is consistent with the MAC results. It should also be noted that the spread does not necessarily mean that the models are poor but rather that the attached brackets have a large impact on the dynamics of the coupled systems, which show a larger variation.

Mode 10 for component 722/02 should in fact be mode 11. From the FRF of this component, in Figure 4.4, it can be seen that around 620 Hz the curve is smooth. Thus, in the system identification process, the tenth mode is not considered. This is not a problem as the data is only used as validation data and the correlation is not found to exceed 10 modes anyhow. Though, it should be considered if coupling will be performed with this data.

As noted before, the first mode between blade 722 and 819 correlates between 0.9 and 0.85, this is due the effect the Dytran accelerometer has on the first mode, cf. Figure C.2a in Appendix C.

Table 4.2: Eigenfrequencies (Hz) and mass (gramme) for all the blades mounted with brackets along with mean (μ, Hz and gramme), standard deviation (σ, Hz and gramme) and coefficient of variation (COV, %) of all the experimental bracket mounted blades.

Set	Blades/Brackets			Statistics		
Component	841/01	722/02	819/03	μ	σ	COV
Mode 1	40.81	40.21	39.54	40.19	0.63	1.58
Mode 2	117.14	111.89	118.15	115.73	3.36	2.90
Mode 3	189.45	204.01	187.90	193.79	8.89	4.59
Mode 4	225.76	218.90	223.45	222.70	3.49	1.57
Mode 5	318.93	332.56	311.59	321.03	10.64	3.31
Mode 6	367.96	357.02	370.09	365.02	7.01	1.92
Mode 7	374.90	387.89	387.96	383.58	7.52	1.96
Mode 8	474.94	508.01	475.52	486.16	18.93	3.89
Mode 9	545.73	528.64	534.41	536.26	8.69	1.62
Mode 10	634.03	700.06	626.78	653.62	40.38	6.18
Mode 11	743.11	730.43	707.09	726.88	18.27	2.51
Mass	1343.20	1343.90	1343.80	1343.60	0.38	2.82e-04

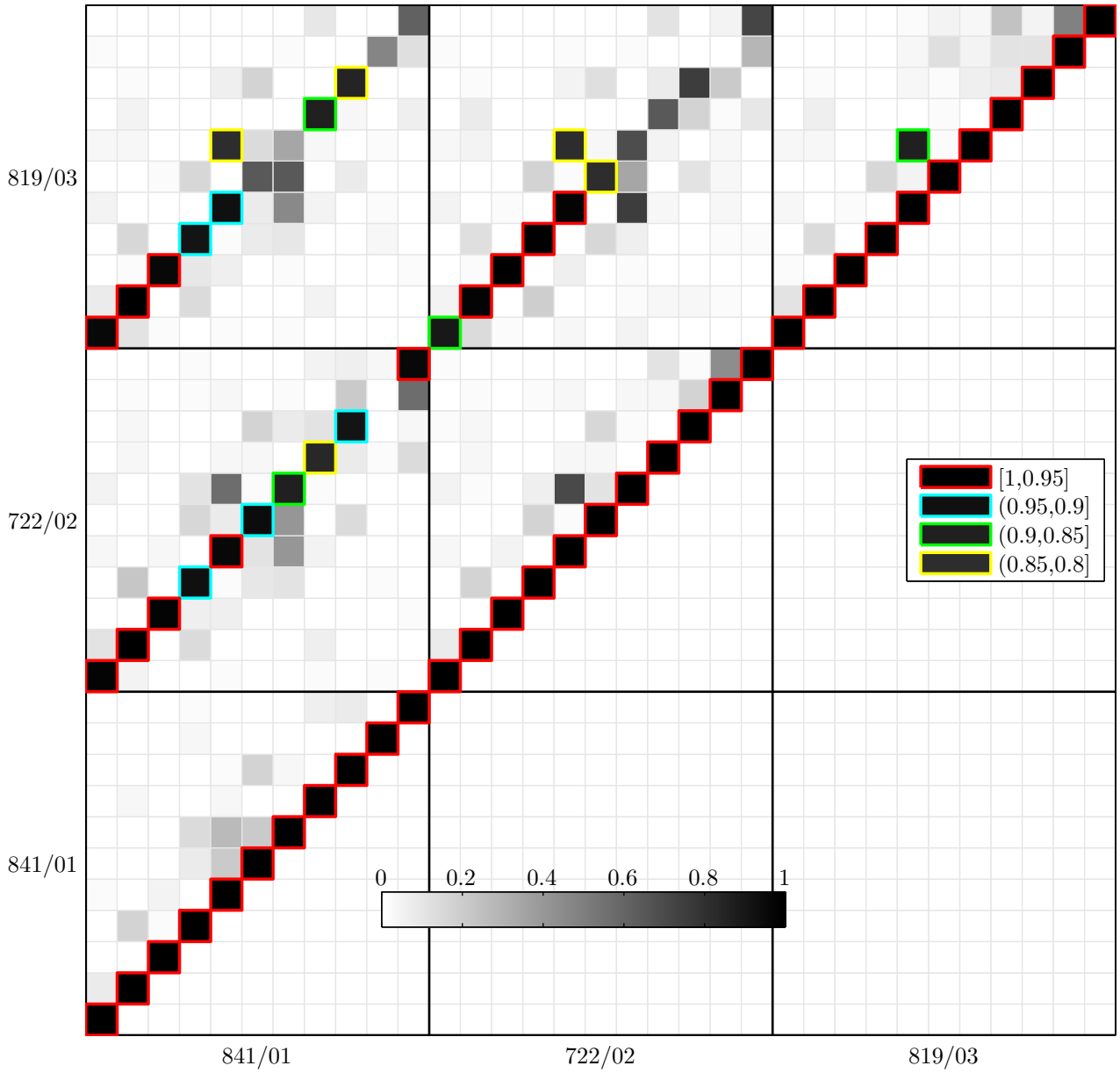

Figure 4.3: *MAC matrix for the 11 first modes between 3 experimental blades mounted with brackets. 4 colour codes are given where red marks a correlation between 0.95 and 1, cyan a correlation between 0.9 and 0.95, green a correlation between 0.85 and 0.9 and yellow a correlation between 0.8 and 0.85.*

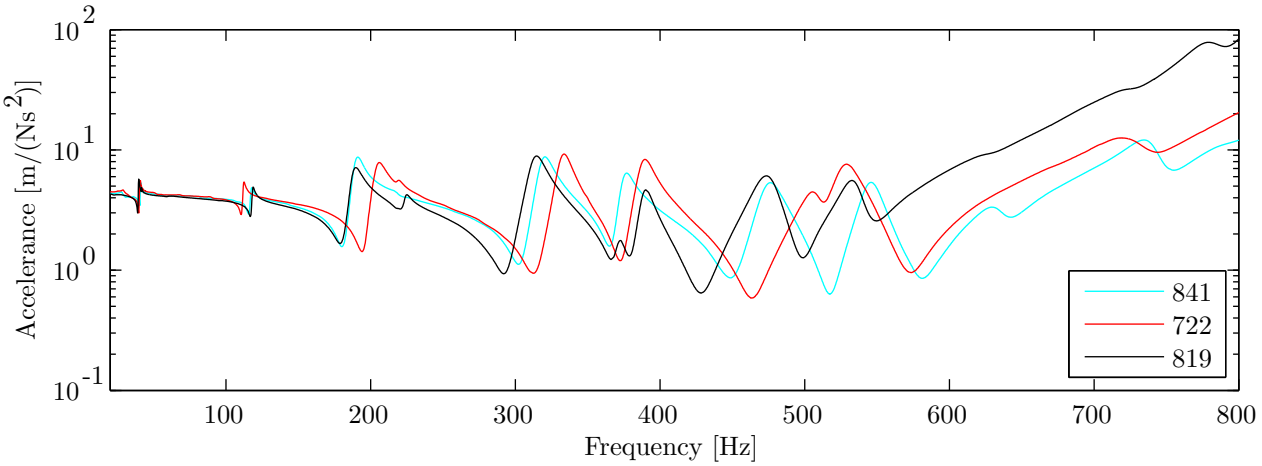

Figure 4.4: *Spread between the raw FRFs of the bracket mounted blades with input in z and output 7 as shown in Figures 3.8 and 3.24.*

4.3 Analytical Coupling

The results from the analytical coupling between the bracket mounted blades and hub assembly are presented here. The analytical models are only coupled with the CMS method as extensive comparisons between the CMS, FBS and state-space methods are performed in section 4.5.

4.3.1 Blade Bracket

In Figure 4.5, the three considered configurations of the analytical couplings are compared to the measured components. It can be seen that the isostatic coupling and the *low* coupling configurations give similar correlation relative to the measured data but are not equal as can be seen in the MAC matrix. Thus, the dynamics of the coupling is not modelled good with an isostatic configuration nor a stiffer version of the same coupling. Much better results are found for the *high* coupling configuration. This configuration is also much stiffer compared to the the two other configurations and suggests that the real coupling is stiffer compared to the isostatic coupling. The best correlation is had with model 722/02 where the seven first modes correlated well. Model 841/01 missed modes 6, 7 and 9 but gave good correlations for the other modes, up to mode 11. Model 819/03 correlated good up to mode six and for mode seven and eight the correlation was on the limit of what was considered a good correlation.

In Table 4.3, the eigenfrequencies for the 11 first modes are shown for the analytical models along with the mean (μ, Hz) of the measured models. Also the masses (gramme) for the different models is presented. The relative errors (%) are given for these quantities between the analytical couplings relative to the measured mean and it can be seen that the mass difference is negligible. The dynamics on the other hand differ quite a lot for the isostatic (error 1) and low coupling (error 2) configurations, especially above mode 4 and 7 for both configurations. Here it is easier to see that the low configuration gives better correlation with respect to the eigenfrequencies compared to the isostatic configuration. Thus, a stiffer coupling it seems is desirable, but not as stiff as the *high* configuration (error 3). The FEMAP connection is close to the *high* configuration (error 4).

It should be noted that the three sets of bolts have a mass of 65.90 gramme each and that the three brackets have a uniform mass of 447.2 gramme. For the FE model of the bracket, the bolts are modelled so that they were included in a total mass of the model, thus a density of 5000 kg/m^3 was used, which results in a mass of 517.74 gramme. The geometry of the bracket was not verified but only chosen so that it fit the FE blade. Also, the FE model of the bracket had the first eigenfrequency around 2432.70 Hz, the second at 2444.60 Hz and the third at 3033.30 Hz. Thus, the bracket could be considered as a rigid body in the frequency range of interest. In other words, the geometry is not as critical as for the blade although it is important to have the centre of mass coincide with that of the real bracket. The bracket is not experimentally verified with vibration tests as the accelerometer attachment method would not produce satisfactory results for frequencies over 1000 Hz and the dynamics of this component alone was not of interest as the coupling depended mostly on the added mass to the system and the joint dynamics.

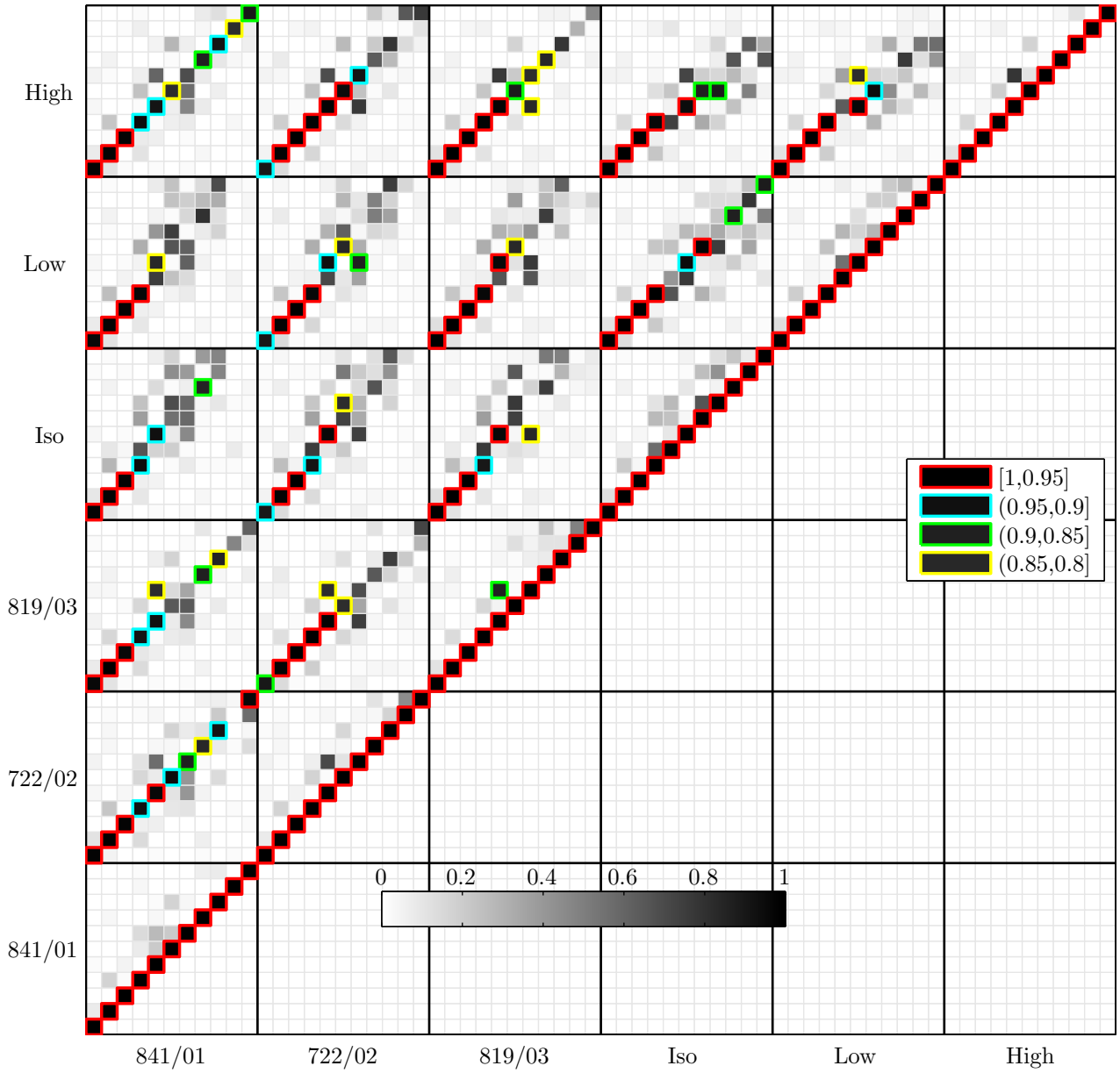

Figure 4.5: *MAC matrix for the 11 first modes between the experimental (measured) models and the three different coupling configurations of the analytical bracket mounted blade. 4 colour codes are given where red marks a correlation between 0.95 and 1, cyan a correlation between 0.9 and 0.95, green a correlation between 0.85 and 0.9 and yellow a correlation between 0.8 and 0.85.*

Table 4.3: Eigenfrequencies (Hz) for the different analytical coupling configurations of the blade bracket system, and the measured mean (μ, Hz) from Table 4.2. Also, the relative error E (%) between the measured mean and the analytically coupled models is shown, where E 1 stand for the relative error between Iso coupling and measured mean, E 2 between *Low* and measured mean, E 3 between *High* and measured mean and E 4 between FEMAP and measured mean. The mass (gramme) is also shown for the models with their relative error.

Set	Blades/Brackets					Error			
Component	μ	Iso	Low	High	FEMAP	E 1	E 2	E 3	E 4
Mode 1	40.19	41.21	41.39	41.3	41.32	2.54	2.98	2.77	2.81
Mode 2	115.73	117.39	118.1	118.78	118.73	1.44	2.05	2.64	2.6
Mode 3	193.79	195.5	195.68	198.18	197.94	0.88	0.98	2.27	2.14
Mode 4	222.7	221.2	226.68	232.92	232.53	-0.67	1.78	4.59	4.41
Mode 5	321.03	251.99	305.81	346.78	345.24	-21.51	-4.74	8.02	7.54
Mode 6	365.02	329.54	338.99	386.99	385.85	-9.72	-7.13	6.02	5.71
Mode 7	383.58	356.14	368.33	422.3	421.56	-7.15	-3.98	10.09	9.9
Mode 8	486.16	378.71	429.41	529.31	524.92	-22.1	-11.67	8.88	7.97
Mode 9	536.26	470.13	483.25	575.64	572.84	-12.33	-9.88	7.34	6.82
Mode 10	653.62	504.57	531.7	713.85	703.96	-22.8	-18.65	9.21	7.7
Mode 11	726.88	545.59	568.61	795.78	789.91	-24.94	-21.77	9.48	8.67
Mass	1343.63	1314.90	1314.90	1314.90	1314.90	-2.14	-2.14	-2.14	-2.14

4.3.2 Blade Bracket Hub

The difference in the FRFs between the measured and analytically coupled systems are shown in Figure 4.6. A relatively high damping is introduced in the analytically systems, after coupling, for the sake of comparison. From Table 4.4, it can be seen that the eigenfrequencies at some frequencies come in pairs. This is hard to see in the FRFs in Figure 4.6 but it is easy to see that there are resonance frequencies for the measured model around 110 Hz which is not present in any of the analytically coupled models. The mass difference is very small, shown in Table 4.4. The bracket mounted hub, including bolts and epoxy, has a mass of 3907 gramme, the FE model has a mass of 3900 kg and a density of 3530 kg/m^3.

The geometry of the FE hub model was verified with the real hub. The measurements are found in Appendix A. The first three eigenfrequencies for the FE model of the bracket mounted hub model as one are 1691.30 Hz, 1691.50 Hz and 1777.20 Hz. It should be noted that the bearing and the rubberised cylinder, described in Appendix A, are modelled as part of the hub, thus it is simplified. The geometry of the real hub corresponded well with the FE geometry, with a deviation around 0.005 m.

4.4 Experimental-Analytical Coupling

The experimental-analytical couplings was performed with the state-space and the FBS methods, a comparison between these two methods is also presented. Note that the components synthesised with the state-space method are unstable, which is addressed in section 4.6.

4.4.1 Blade Bracket

In Figure 4.7, the eigenvector correlation is presented as a MAC matrix for components coupled with the state-space and the FBS methods, compared the the measured system. It can be seen that the first 5 modes for system 841/01 is had with the state-space coupling and that up to six modes are correlated well for the other two components. Further, it is enough to compare the FBS method to the state-space method to realise that they produce identical results. The spread between the components is not as large as expected, usually the first five to six modes correlate well.

From Table 4.5 it can be seen that a relatively large spread is obtained for mode 7, 8, 10 and 11. Also, the first eigenfrequency has a large error for all models. The comparison between the state-space and FBS methods is of interest as they should produce the same results, for models satisfying Newton's second law. Results are found in Table 4.6 where it is seen that there is no difference between the methods.

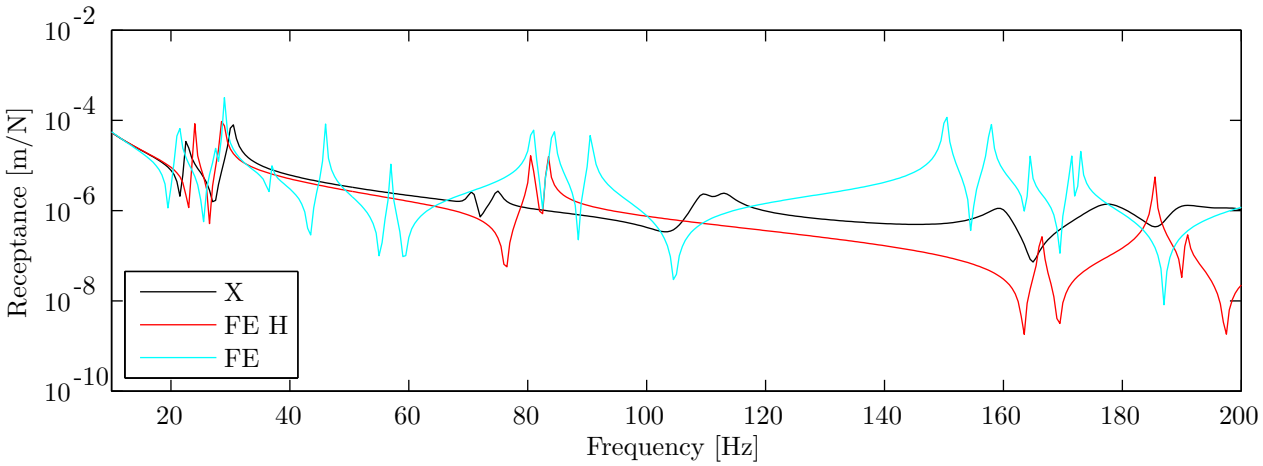

Figure 4.6: *Receptance FRFs with input at position 19 and output at position 9, as seen in Figure 3.25, for the experimentally measured hub assembly model denoted X, the analytically synthesised model with high coupling configuration denoted FE H and the analytically synthesised model with isostatic coupling configuration denote FE.*

Table 4.4: Eigenfrequencies (Hz) and mass (gramme) for the experimentally measured and the analytically coupled hub assembly. Also, the error (%) between the measured mean and the analytically synthesised models is shown. Error 1 stand for the relative error between Iso coupling and measured mean, Error 2 between High coupling and measured mean and Error 3 between FEMAP coupling and measured mean.

Set	Blades/Brackets				Error		
Component	Experiment	Iso	High	FEMAP	Error 1	Error 2	Error 3
Mode 1	22.6	21.28	23.98	22.75	-5.84	6.11	0.66
Mode 2	30.26	27.83	28.7	30.29	-8.03	-5.16	0.10
Mode 3	31.04	28.98	29.49	30.29	-6.64	-4.99	-2.5
Mode 4	70.61	36.71	80.65	78.48	-48.01	14.22	10.00
Mode 5	71.21	45.97	81.74	82.3	-35.44	14.79	13.00
Mode 6	74.83	56.97	83.33	82.3	-23.87	11.36	9.1
Mode 7	109.3	80.81	166.31	130.97	-26.07	52.16	17.00
Mode 8	112.82	84.28	166.53	130.99	-25.3	47.61	14.00
Mode 9	159.78	90.64	185.4	174.91	-43.27	16.03	8.7
Mode 10	177.39	149.88	189.83	188.71	-15.51	7.01	6.00
Mode 11	189.22	150.3	190.72	189.41	-20.57	0.79	0.1
Mass	6398.2	6291	6291	6291	-0.02	-0.02	-0.02

In Figures 4.8 and 4.9 the FRFs for the difference between the coupled models are shown for models satisfying Newton's second law and models violating it, respectively. As it has been pointed out before, the state-space method relies on the physical law explicitly but nothing has be asserted for the FBS method. Thus, in Figure 4.10, two coupled systems, one with the state-space method and one with the FBS method are shown, both violating Newton's second law compared to a physical system. It can be seen that the FBS method works perfect in this scenario while the state-space method shows deviations from the correct FRF.

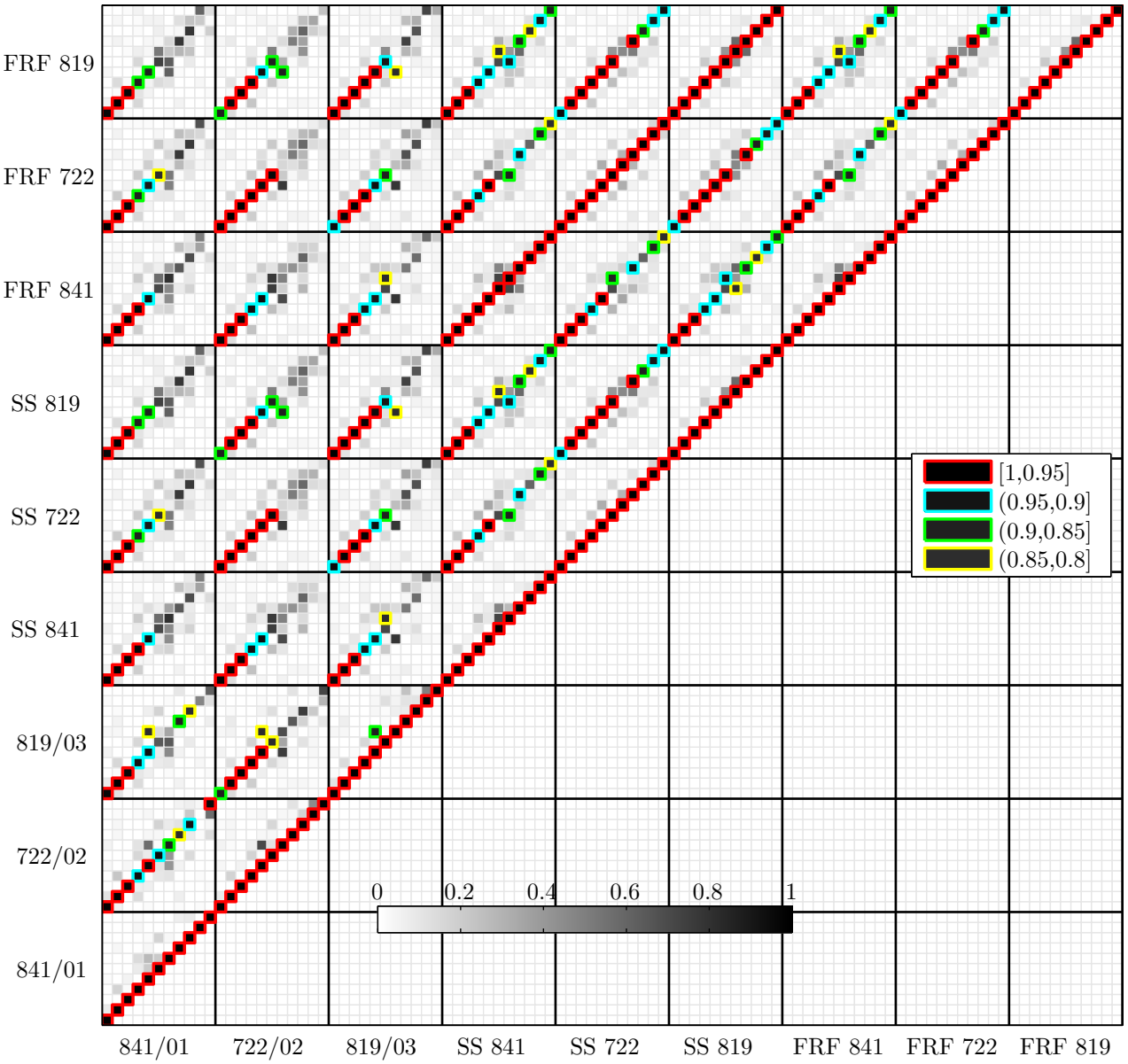

Figure 4.7: *MAC matrix for the 11 first modes between the experimental models of the bracket mounted blades and experimental-analytical state-space and FBS coupled components. 4 colour codes are given where red marks a correlation between 0.95 and 1, cyan a correlation between 0.9 and 0.95, green a correlation between 0.85 and 0.9 and yellow a correlation between 0.8 and 0.85.*

Table 4.5: Eigenfrequencies (Hz) for all the experimental-analytical bracket mounted blades along with the error (%) between the experimental-analytical synthesised components, with the state-space method, and the experimentally measured systems. Error 1 stand for the relative error between SS 841/FEA and SS 841/01, Error 2 between SS 722/FEA and SS 722/02 and Error 3 between SS 819/FEA and SS 819/03.

Set	Blades/Brackets			Error		
Component	SS 841/FEA	SS 722/FEA	SS 819/FEA	Error 1	Error 2	Error 3
Mode 1	43.01	41.92	41.08	5.39	4.24	3.89
Mode 2	119.52	114.17	120.55	2.04	2.04	2.03
Mode 3	187.35	201.35	184.91	-1.11	-1.3	-1.59
Mode 4	229.24	220.29	229.33	1.54	0.64	2.63
Mode 5	308.69	322.83	304.88	-3.21	-2.92	-2.15
Mode 6	391.92	355.8	391.27	6.51	-0.34	5.72
Mode 7	410.04	405.19	408.84	9.37	4.46	5.38
Mode 8	437.3	466.13	442.78	-7.93	-8.24	-6.89
Mode 9	548.52	518.58	537.05	0.51	-1.9	0.49
Mode 10	584.9	606.98	582.37	-7.75	-13.3	-7.09
Mode 11	634.01	645.84	617.42	-14.68	-11.58	-12.68

Table 4.6: The relative error (%), for the experimental-analytical coupled blade bracket system, between the state-space and frequency based coupling for the 11 first flexible modes.

Set	Blades/Brackets										
Mode	M 1	M 2	M 3	M 4	M 5	M 6	M 7	M 8	M 9	M 10	M 11
Error 1	0	0	0	0	0	0	0	0	0	0	0
Error 2	0	0	0	0	0	0	0	0	0	0	0
Error 3	0	0	0	0	0	0	0	0	0	0	0

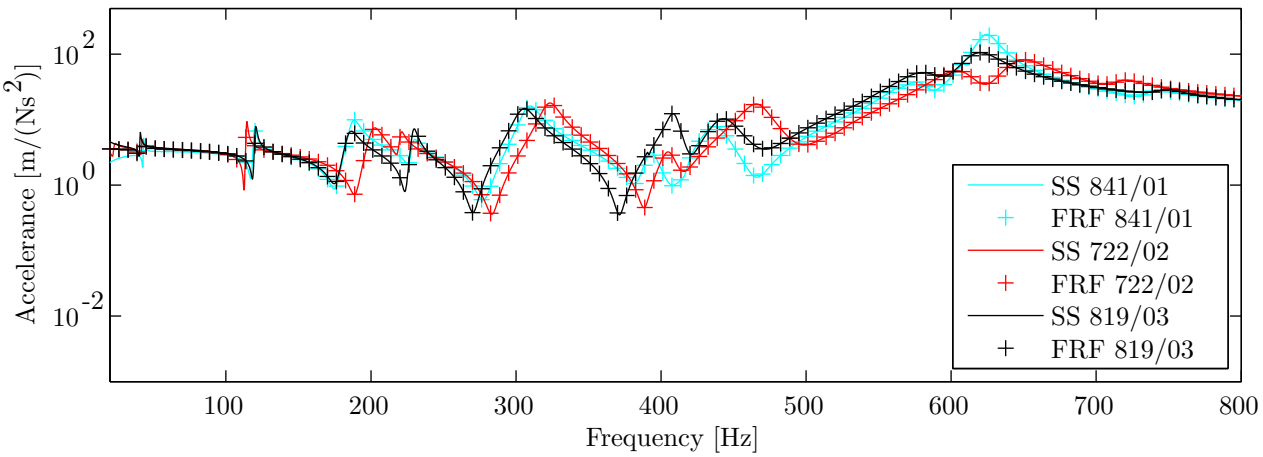

Figure 4.8: *Difference between FBS and state-space based substructuring methods when* $\mathbf{CB} = \mathbf{0}$*, for experimental-analytical coupling of the blade bracket system.*

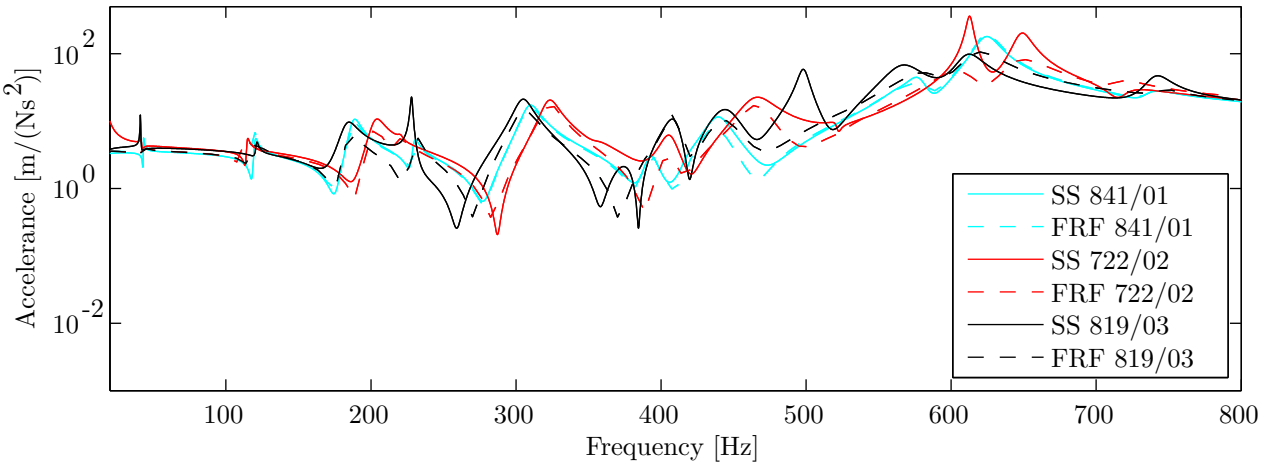

Figure 4.9: *Difference between FBS and state-space based substructuring methods when* $\mathbf{CB} \neq \mathbf{0}$*, for experimental-analytical coupling of the blade bracket system.*

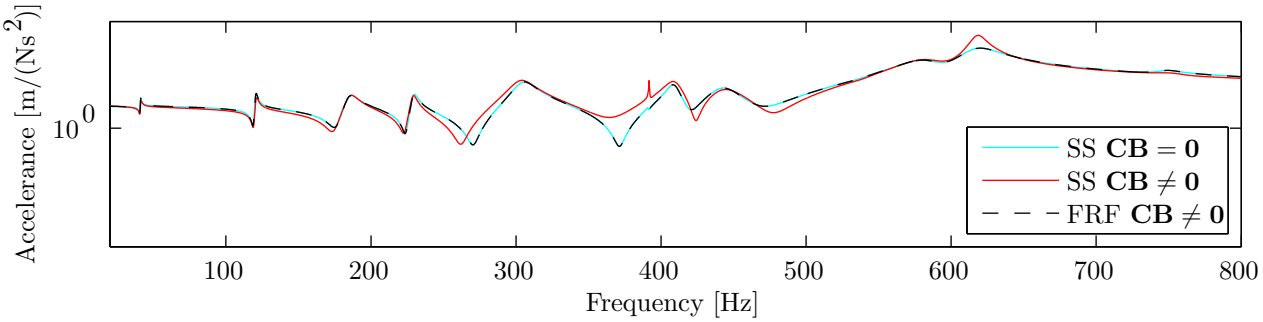

Figure 4.10: *Difference between non-physical coupled models with the FBS and state-space based substructuring methods compared to a physically coupled model, for experimental-analytical coupling of the blade bracket system.*

4.4.2 Blade Bracket Hub

The FRF of the experimental-analytically synthesised model of the hub assembly structure can be seen in Figure 4.11 for the models satisfying Newtons's second law. Arguably, slightly worse correlation is had compared to the analytical models. From Table 4.7 it can be seen that the state-space synthesised model and the frequency synthesised model differ while their FRFs were equal, this is because the table presents data for a FBS model that is identified with a coarse frequency step size, they are considered equal. In the figure it is also seen that the mode multiples have switched place relative the measured data and also that a relatively high error is had for the first eigenfrequency. The synthesised models again does not model the area around 110 Hz. The spread in discrepancy is in general relatively high after 80 Hz.

4.5 Numerical Problems

The state-space method was found to be numerically unstable. The choice of the arbitrary subspace of the nullspace of $\mathbf{B}_c$ for transformation to coupling form was in fact only arbitrary in theory; the choice of this matrix greatly affected the results. A case study made with only FE models where the CMS method is used to verify the results between the FBS and state-space coupling, which should be exactly the same in theory, is presented in this section. The FBS method is dropped as it gives exactly the same results as the CMS method for noise-free data synthesised from the analytical models used and since a system identification procedure must be introduced. FE models with orders 20 and 80, obtained by the Craig-Bampton reduction, described in section 2.7.2, of the full FE models, are used in order to outline the effect higher model orders have. Three methods are employed, denoted M1, M2 and M3. M1 is the method that works best and it is based on a state-space system transformed to real diagonal form before it is transformed to coupling form, where the

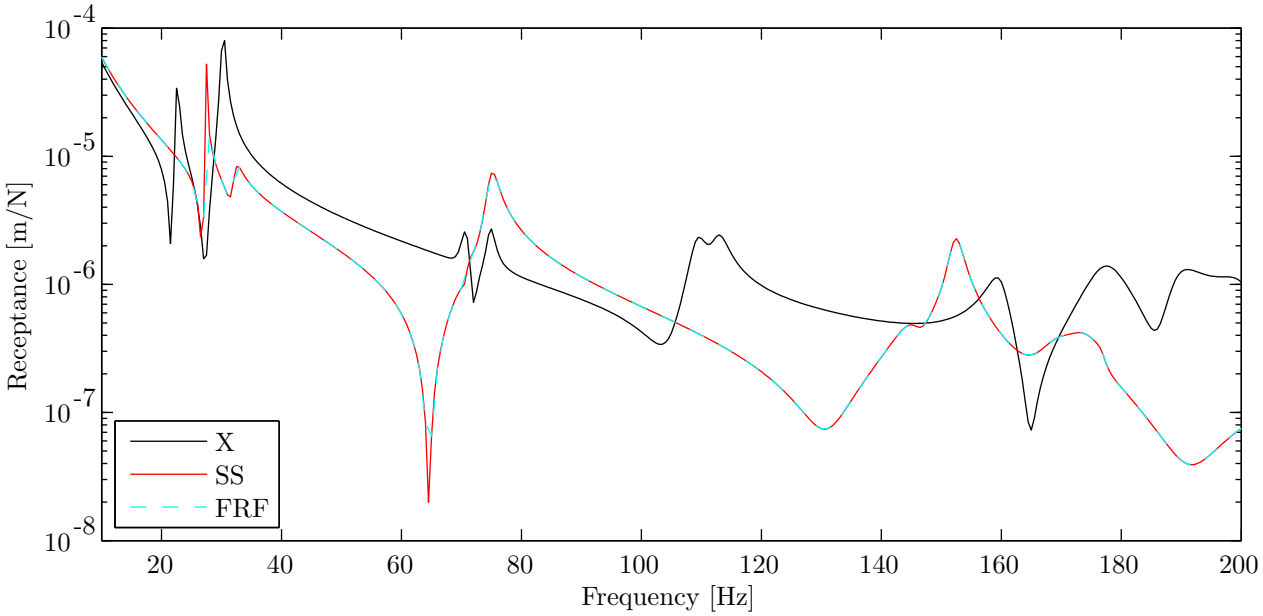

Figure 4.11: *Receptance FRFs for the experimentally measured model denoted X, the experimental-analytical synthesised model with the state-space method denoted SS and with the FBS method denoted FRF.*

Table 4.7: Eigenfrequencies (Hz) for the measured hub assembled system and the experimental-analytical systems coupled with the state-space method (denoted SS) and the FBS method (denoted FRF). Relative error between the SS (Error 1) and FRF (Error 2) methods relative the measured data is also shown.

Set	Blades/Brackets			Error	
Component	Experiment	SS	FRF	Error 1	Error 2
Mode 1	22.6	26.87	27.41	18.89	21.28
Mode 2	30.26	27.16	27.74	-10.24	-8.33
Mode 3	31.04	31.38	32.22	1.1	3.8
Mode 4	70.61	69.7	70.88	-1.29	0.38
Mode 5	71.21	70.36	73.31	-1.19	2.95
Mode 6	74.83	72.54	75	-3.06	0.23
Mode 7	109.3	140.83	145.93	28.85	33.51
Mode 8	112.82	147.6	152.29	30.83	34.98
Mode 9	159.78	148.54	154.7	-7.03	-3.18
Mode 10	177.39	166.41	173.84	-6.19	-2
Mode 11	189.22	170.05	176.94	-10.13	-6.49

arbitrary subspace of $\mathbf{B}_c$ needed for the transformation is chosen so that it creates a full rank transformation matrix consisting of ones and zeros. M2 uses an unaltered initial state-space system, transformed to coupling form by a subspace matrix created by choosing pseudorandom values from the standard uniform distribution. The method M3 uses the same subspace as M1 but without the diagonal transformation of the initial state-space matrices. It should be pointed out that method M2 can produce greatly different results on exactly the same data with higher order models depending on the outcome of the random process.

The FRFs of the blade, bracket and coupled system for the two systems of different order are shown in Figures 4.12 to 4.17. The original state-space system is denoted SS and produces exactly the same results as the second order form systems, thus only one is shown. The state-space system on coupling form, or synthesised state-space systems from these coupling form models, where appropriate, are denoted SSC.

The eigenvalues for the first four modes and the condition number of the respective $\mathbf{A}$ matrices and for the transformation matrices $\mathbf{T}$ are shown in Table 4.8 for models of order 20, in Table 4.9 the same is shown for models of order 80.

The results in the figures show that method M1 gives identical results for coupling form for both the blade and bracket models for both model orders. This can also be seen in the tables where the eigenfrequencies match perfectly to the reference data. Method M3 on the other hand looks quite good the for blades with model order 20 but not as well for a blade of model order 80. It can be seen that the resonance amplitudes are much lower than for the reference data. Also, for the bracket, method M3 produces poor results for both models of order 20 and 80 which can be seen in the enlarged region of the first eigenfrequency. On the other hand, for the coupled system the method seems to produce reasonable results although from the tables it can be seen that there is a difference in the second decimal for the first mode for models of order 20 and even larger errors for models of order 80.

Method M2 is easily the worst, producing unacceptable results for very low model orders as can be seen in the FRF figures. Especially the bracket model is badly described, for which the eigenfrequencies miss by a fair margin. The antiresonances are also not captured well and the coupled system shows a large spread. From the tables, the exact difference in eigenfrequencies is seen but the synthesised system with models of order 20 is seen to be forgiving. This is something that should be noticed as it is very easy to miss the large difference in the FRFs and individual components if only the eigenfrequencies of the coupled systems are verified. The coupled system with models of order 80 on the other hand shows an extreme case where the two first flexible modes correspond to something resembling rigid body modes. As mentioned, this is an extreme case and widely different results are held by executing the same script on the same data.

The condition numbers shown in the tables are of little guidance as to what is going on. For example, the condition number of the transformation matrix $\mathbf{T}$ used in method M1 for both the smaller and larger systems show a very high value. On the other hand, method M2, which was shown to produce very poor results, has a condition number smaller by a factor of 7 to 8. The same pattern is seen for the state matrix of the coupling form; i.e. smaller condition number for the method that produces poor results.

It should be noted that the density of the bracket used in these evaluations is $\rho = 7800\ kg/m^3$, thus lower eigenfrequencies are had for the coupled system compared to the models presented above. Also, only six inputs and outputs were considered in the models, the necessary amount for coupling.

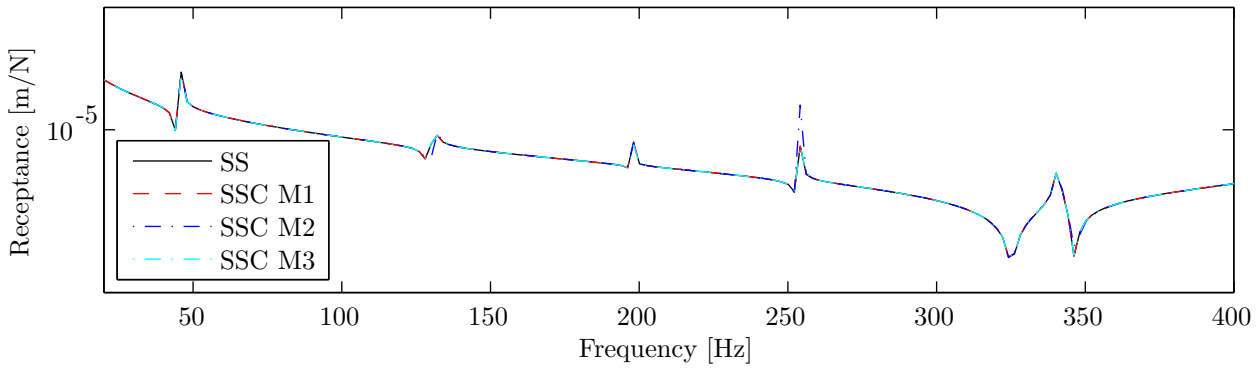

Figure 4.12: *FRFs of the blade (model order 20) with input at position 7 and output at position 7 as shown in Figure 3.1. The original state-space system (SS) and the state-space system on coupled form denoted (SSC) for the three different methods are shown.*

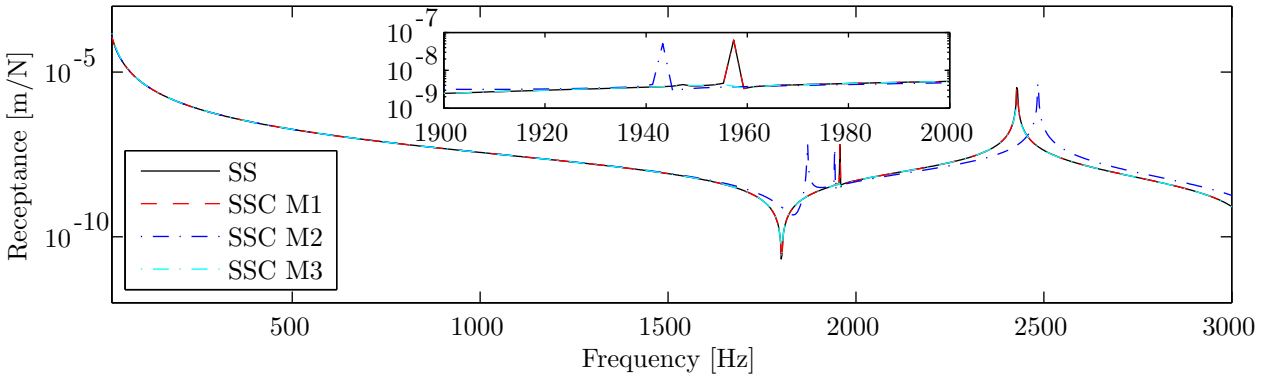

Figure 4.13: *FRFs of the bracket (model order 20) with input at position 7 and output at position 7 as shown in Figure 3.4. The original state-space system (SS) and the state-space system on coupled form denoted (SSC) for the three different methods are shown.*

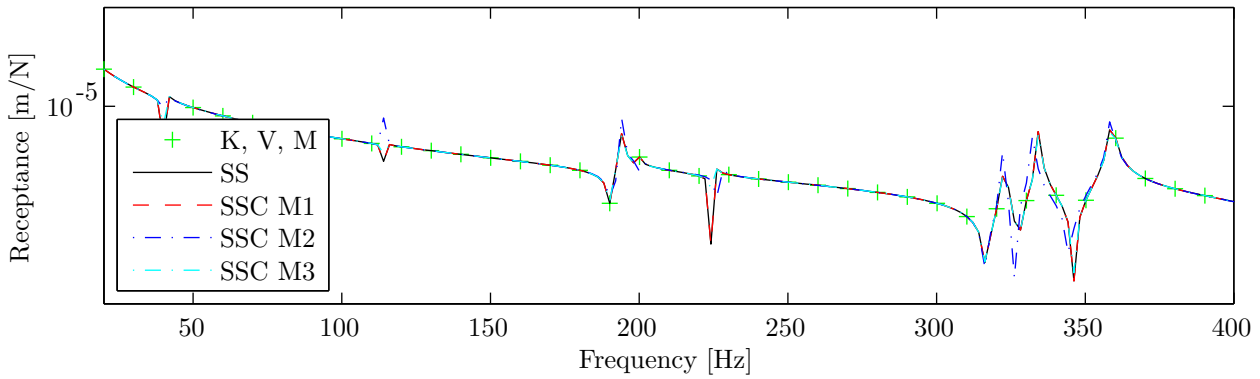

Figure 4.14: *FRFs of the coupled models (component model order 20) of the blade and bracket with input at position 7 and output at position 7 as shown in Figure 3.24. The CMS method (denoted K, V, M) is marked with green plus signs and the state-space (SS) representation of the same system with a red dashed line. The three couplings produced by the state-space method (SSC) are also shown.*

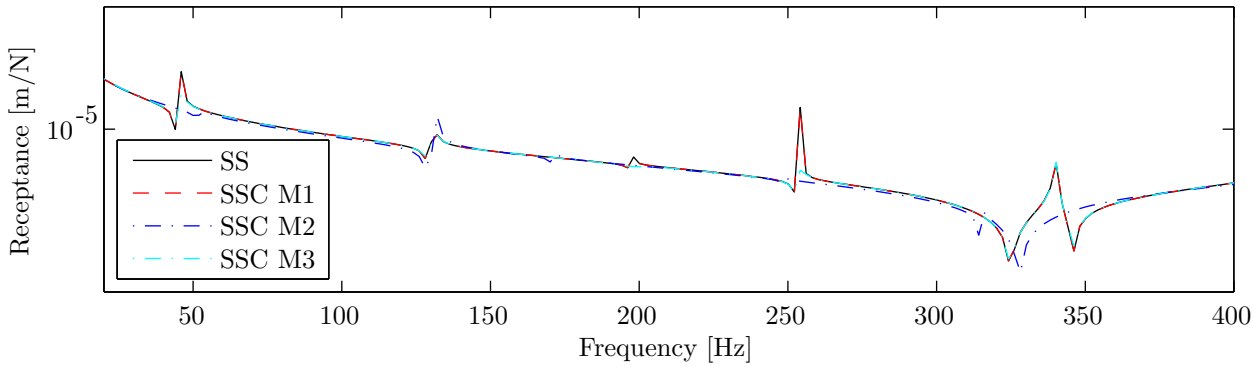

Figure 4.15: *FRFs of the blade (model order 80) with input at position 7 and output at position 7 as shown in Figure 3.1. The original state-space system (SS) and the state-space system on coupled form denoted (SSC) for the three different methods are shown.*

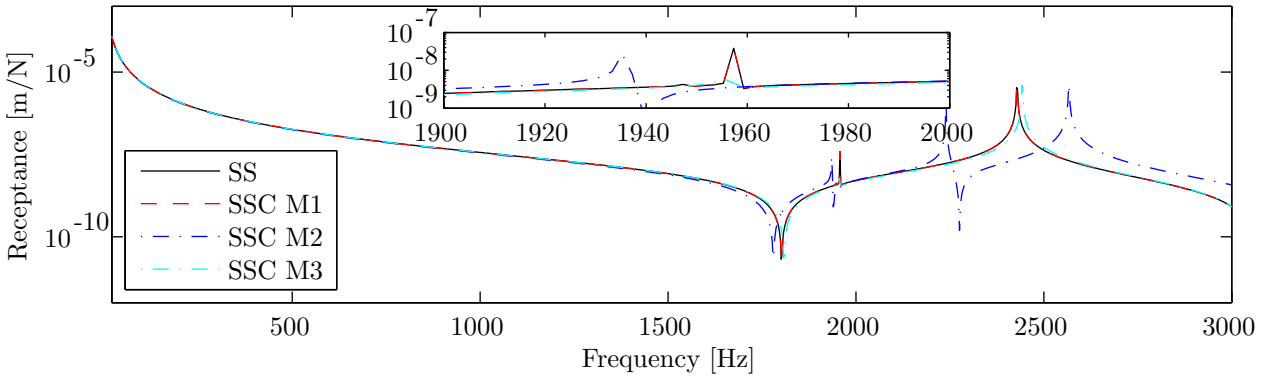

Figure 4.16: *FRFs of the bracket (model order 80) with input at position 7 and output at position 7 as shown in Figure 3.4. The original state-space system (SS) and the state-space system on coupled form denoted (SSC) for the three different methods are shown.*

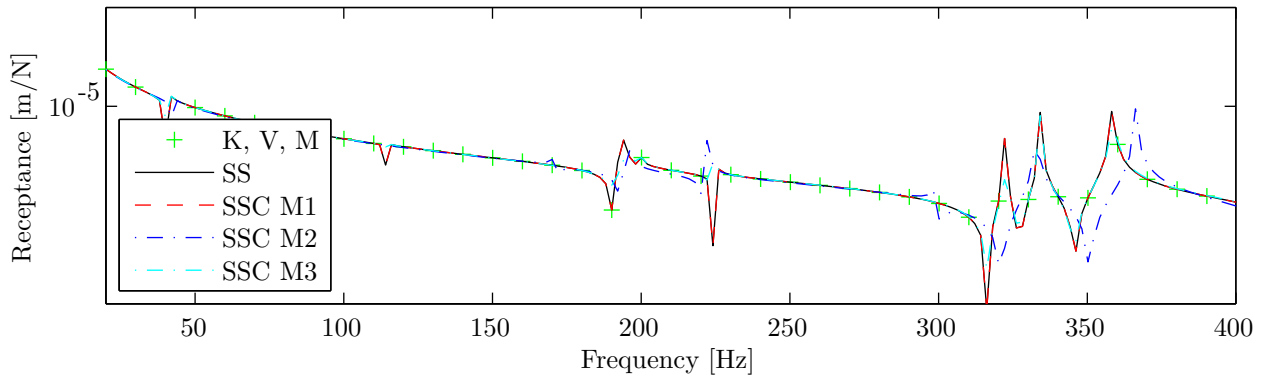

Figure 4.17: *FRFs of the coupled models (component model order 80) of the blade and bracket with input at position 7 and output at position 7 as shown in Figure 3.24. The CMS method (denoted K, V, M) is marked with green plus signs and the state-space (SS) representation of the same system with a red dashed line. The three couplings produced by the state-space method (SSC) are also shown.*

4.6 Unstable Systems

It was noted that the synthesis procedure for experimental-analytical models produced unstable systems. In this section, an investigation of these problems is performed.

4.6.1 Violation of Newton's Second Law for Analytical Models

For experimental-analytical coupling the instability is caused by non-physical models where both Newton's second law and passivity can be unfulfilled. Since the state-space synthesis (SSS) method is based on the assumption that $\mathbf{CB} = \mathbf{0}$, this can be altered for an analytical model that is otherwise valid.

By adding Gaussian noise, $\mathbb{N}(0, 1)$, of order 10^{-9} to the $\mathbf{B}$ and $\mathbf{C}$ matrices for the FE blade model only, the state-space method produces unstable coupled systems. The relatively high noise is chosen so that the unstable modes come down in frequency. A smaller noise addition would produce high frequency unstable modes. Interestingly, it is found that this very small noise addition does not produce an unstable coupling form systems of the single components but rather for the synthesised systems. In Table 4.10 the first five eigenvalues are shown for two systems, one with $\mathbf{CB} = \mathbf{0}$ and the other with $\mathbf{CB} \neq \mathbf{0}$, for the blade and bracket models, coupling form models and synthesised system.

By increasing the difference between the input and output matrix product, the instability is increased in the sense that many more poles were unstable after the synthesis of components while decreasing it lowered the

Table 4.8: Eigenfrequencies (Hz) for FE models of the blade and bracket, with model order **20**, and condition numbers (Cond) for the state-space **A** matrices and the transformation matrices **T** of these models.

Method 1	Blade		Bracket		Coupled System		
System	SS	SSC	SS	SSC	K, M	SS	SSC
Mode 1	45.82	45.82	1947.73	1947.73	40.32	40.32	40.32
Mode 2	130.69	130.69	1957.28	1957.28	114.21	114.21	114.21
Mode 3	198.01	198.01	2428.55	2428.55	193.50	193.50	193.50
Mode 4	254.28	254.28	3143.08	3143.08	199.66	199.66	199.66
Cond(**A**)	6.7e+16	5.9e+20	5.9e+16	1.1e+21		4.8e+18	6.4e+20
Cond(**T**)		1.3e+11		1e+12			
Method 2	Blade		Bracket		Coupled System		
System	SS	SSC	SS	SSC	K, M	SS	SSC
Mode 1	45.82	45.75	1947.73	1908.74	40.32	40.32	40.25
Mode 2	130.69	130.49	1957.28	1944.52	114.21	114.21	114.06
Mode 3	198.01	198.20	2428.55	2456.84	193.50	193.50	193.74
Mode 4	254.28	254.51	3143.08	3206.51	199.66	199.66	199.86
Cond(**A**)	6.7e+16	2e+18	5.9e+16	5.1e+17		4.8e+18	4.5e+18
Cond(**T**)		7e+03		5.5e+03			
Method 3	Blade		Bracket		Coupled System		
System	SS	SSC	SS	SSC	K, M	SS	SSC
Mode 1	45.82	45.84	1947.73	1947.80	40.32	40.32	40.38
Mode 2	130.69	130.70	1957.28	1957.34	114.21	114.21	114.20
Mode 3	198.01	198.01	2428.55	2428.33	193.50	193.50	193.53
Mode 4	254.28	254.28	3143.08	3143.09	199.66	199.66	199.67
Cond(**A**)	6.7e+16	2.7e+17	5.9e+16	2.2e+17		4.8e+18	1.6e+19
Cond(**T**)		1.4e+02		26			

Table 4.9: Eigenfrequencies (Hz) for FE models of the blade and bracket, with model order **80**, and condition numbers (Cond) for the state-space **A** matrices and the transformation matrices **T** of these models.

Method 1	Blade		Bracket		Coupled System		
System	SS	SSC	SS	SSC	K, M	SS	SSC
Mode 1	45.82	45.82	1947.71	1947.71	40.32	40.32	40.32
Mode 2	130.67	130.67	1957.27	1957.27	114.19	114.19	114.19
Mode 3	197.64	197.64	2428.55	2428.55	193.24	193.24	193.24
Mode 4	254.17	254.17	3142.97	3142.97	199.56	199.56	199.56
Cond(**A**)	4.1e+16	1.9e+19	4e+18	6.2e+22		1.5e+17	2.6e+20
Cond(**T**)		1.5e+11		1.4e+13			
Method 2	Blade		Bracket		Coupled System		
System	SS	SSC	SS	SSC	K, M	SS	SSC
Mode 1	45.82	0.06	1947.71	1937.18	40.32	40.32	0.23
Mode 2	130.67	0.10	1957.27	2237.15	114.19	114.19	0.80
Mode 3	197.64	49.90	2428.55	2562.04	193.24	193.24	44.76
Mode 4	254.17	128.36	3142.97	3146.71	199.56	199.56	113.77
Cond(**A**)	4.1e+16	3.3e+18	4e+18	1.6e+18		1.5e+17	9e+17
Cond(**T**)		1.2e+04		2.2e+04			
Method 3	Blade		Bracket		Coupled System		
System	SS	SSC	SS	SSC	K, M	SS	SSC
Mode 1	45.82	45.68	1947.71	1956.27	40.32	40.32	40.50
Mode 2	130.67	130.68	1957.27	1956.27	114.19	114.19	114.20
Mode 3	197.64	197.86	2428.55	2442.42	193.24	193.24	193.81
Mode 4	254.17	254.11	3142.97	3144.53	199.56	199.56	199.47
Cond(**A**)	4.1e+16	3.7e+17	4e+18	6.2e+20		1.5e+17	5.2e+18
Cond(**T**)		4.1e+02		1.4e+02			

number of unstable poles. In Table 4.10 it can be seen that the physical system produce completely different damping compared to the non-physical system. With perturbations larger than 10^{-14} stable and unstable systems were produced but never asymptotically stable. Smaller differences produced asymptotically stable synthesised systems for the analytical models.

The results were obtained with Method 1, as described in section 4.5. Any other method would produce both coupling form systems and unstable synthesised systems. Interestingly, the synthesised systems satisfy Newton's second law in both cases. It was verified that the perturbed systems were passive.

Table 4.10: First few poles, where the real part describes damping and the complex part the eigenfrequencies (Hz), for original system, coupling form system and synthesised system for two different cases, with $\mathbf{CB} = \mathbf{0}$ and $\mathbf{CB} \neq \mathbf{0}$.

$\mathbf{CB} \approx 10^{-9}$	Blade		Bracket	
System	$\mathbf{CB} \approx 10^{-9}$, SS	$\mathbf{CB} \approx 10^{-9}$, SSC	$\mathbf{CB} = \mathbf{0}$, SS	$\mathbf{CB} = 10^{-10}$, SSC
Mode 10	-0.0005 + 725.81i	-0.00049 + 725.81i	-0.0005 + 42075.25i	-0.0005 + 42075.25i
Mode 11	-0.0005 + 834.32i	-0.0005 + 834.32i	-0.0005 + 42384.84i	-0.0005 + 42384.84i
Mode 12	-0.0005 + 915.97i	-0.0005 + 915.97i	-0.0005 + 46665.46i	-0.0005 + 46665.46i
Mode 13	-0.0005 + 1030.76i	-0.00051 + 1030.76i	-0.0005 + 52383.55i	-0.0005 + 52383.55i
Mode 14	-0.0005 + 1091.94i	-0.0005 + 1091.94i	-0.0005 + 55460.53i	-0.0005 + 55460.53i

	Coupled System
System	$\mathbf{CB} = \mathbf{0}$, SSC
Mode 10	-0.00053 + 713.85i
Mode 11	-0.00049 + 795.78i
Mode 12	-0.00012 + 885.66i
Mode 13	-0.00106 + 991.94i
Mode 14	0.00126 + 1019.73i

$\mathbf{CB} = \mathbf{0}$	Blade		Bracket	
System	$\mathbf{CB} = \mathbf{0}$, SS	$\mathbf{CB} = 10^{-10}$, SSC	$\mathbf{CB} = \mathbf{0}$, SS	$\mathbf{CB} = 10^{-10}$, SSC
Mode 10	-0.0005 + 725.81i	-0.0005 + 725.81i	-0.0005 + 42075.25i	-0.0005 + 42075.25i
Mode 11	-0.0005 + 834.32i	-0.0005 + 834.32i	-0.0005 + 42384.84i	-0.0005 + 42384.84i
Mode 12	-0.0005 + 915.97i	-0.0005 + 915.97i	-0.0005 + 46665.46i	-0.0005 + 46665.46i
Mode 13	-0.0005 + 1030.76i	-0.0005 + 1030.76i	-0.0005 + 52383.55i	-0.0005 + 52383.55i
Mode 14	-0.0005 + 1091.94i	-0.0005 + 1091.94i	-0.0005 + 55460.53i	-0.0005 + 55460.53i

	Coupled System
System	$\mathbf{CB} = \mathbf{0}$, SSC
Mode 10	-0.0005 + 713.85i
Mode 11	-0.0005 + 795.78i
Mode 12	-0.0005 + 885.66i
Mode 13	-0.00049 + 991.94i
Mode 14	-0.0005 + 1019.73i

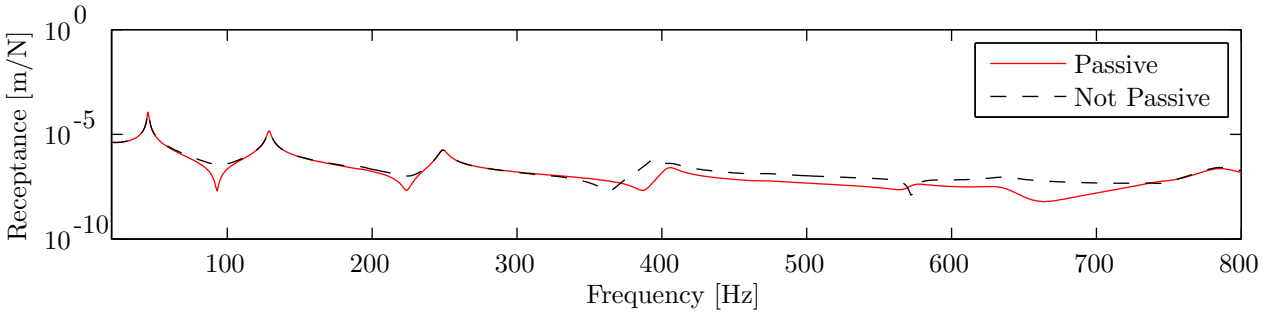

Figure 4.18: *The difference between the passive and non-passive models for blade 841 with input at location 6 and output at location 1.*

4.6.2 Passivity

From Table 4.11 it can be seen that the the eigenvalues between the passive and non-passive systems match perfectly. For the synthesised systems there is a spread in eigenfrequencies starting at mode three. The non-passive system is seen to be unstable, positive real part for eigenvalue 7 and 11, while the passive system is stable. Notice that the real part differs for all modes, this was also seen in the previous section. Thus the damping from the experimental-analytical coupling with the state-space method can not be trusted.

In Figure 4.18 and 4.19, the reason for not using the passive system is shown. It can be seen in the second figure that the FRF is completely wrong for the passive system. This is probably due to the very coarse frequency vector used in the optimisation, described in section 2.11. For a fine frequency resolution the algorithm never converged.

Table 4.11: First 11 modes on complex form with damping ratio and eigenfrequency (Hz) for passive and non-passive blade models of blade 841 and synthesised systems.

	Blade		Coupled	
System	Not Passive	Passive	Not Passive	Passive
Mode 1	-1.71+45.31i	-1.71+45.31i	-4.83-42.95i	-1.53-42.99i
Mode 2	-6.84+128.76i	-6.84+128.76i	-0.49-119.14i	-5.84-119.29i
Mode 3	-25.42+190.8i	-25.42+190.8i	-25.47+187.28i	-24.34+187.6i
Mode 4	-15.81+248.64i	-15.81+248.64i	-4.79-228.14i	-13.57-228.2i
Mode 5	-42.47+322.12i	-42.47+322.12i	-37.08+308i	-38.25+308.77i
Mode 6	-28.63+395.18i	-28.63+395.18i	-18.29-390.45i	-30.4-391.41i
Mode 7	-31.87+404.55i	-31.87+404.55i	44.83-412.34i	-28.63-395.13i
Mode 8	-66.43+468.74i	-66.43+468.74i	-59.98-434.13i	-53.4-437.32i
Mode 9	-44.58+572.87i	-44.58+572.87i	-147.61+530.07i	-37.03+536.96i
Mode 10	-79.4+635.25i	-79.4+635.25i	-86.9+583.35i	-59.07-583.91i
Mode 11	-67.7+746.51i	-67.7+746.51i	42.86+621.47i	-43.25+620.55i

5 Discussion

This section starts out considering the blade models, followed by the synthesised blade and bracket assembly and the fully assembled system. Then, the numerical properties of the state-space algorithm are discussed followed by a discussion of the physical properties of the obtained models. The chapter ends with a discussion of the theoretical developments.

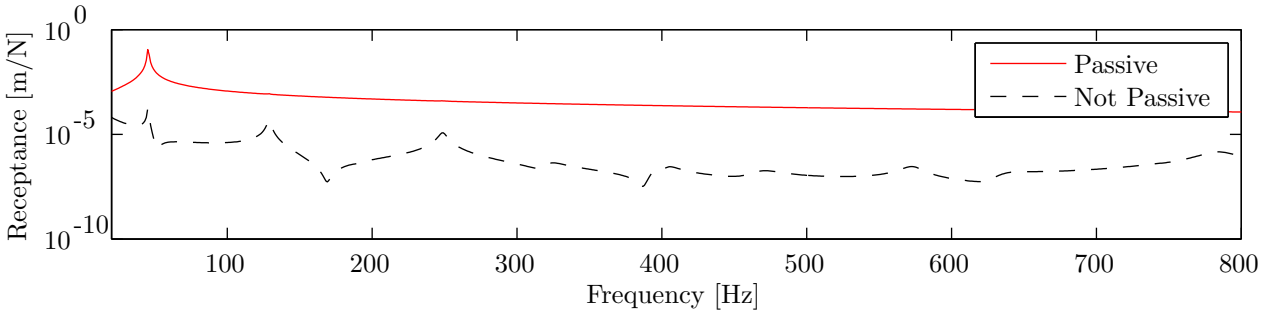

Figure 4.19: *The difference between the passive and non-passive models for blade 841 with input at location 6 and output at location 13.*

5.1 Models

The level of correlation between the blades, and hence by deduction also the bracket mounted blades, was expected from earlier work [Gib+13]. In that work however, the seventh mode was identified as a spurious mode whereas it in fact is an edge-wise mode which is very hard to capture with the current experimental arrangement. The accelerometers only measure in the normal direction and thus no matter the input, the seventh mode will produce mostly noise in the majority of the accelerometers as these are mounted perpendicular to its principal direction of motion, cf. chapter 3. Measuring with tri-axial accelerometers would probably solve this problem. Further, the FE model is not validated with respect to the seventh mode, see [Joh+13].

The measurements of the bracket mounted blades show an even larger spread. It has been shown that the interface area between the blade and the bracket is not fully linear, [Ste+13; Reu+13]. Further, the torque applied to the bolts was not considered and this is possibly a source of error. Thus, the assumption that the bracket mounted blades are fully linear is probably inaccurate, especially around the contact area.

For the hub assembly measurement it is also possible that the testsetup was not adequate in the sense that the number of inputs was not large enough to resolve the modal multiplicity of the structure and that the dynamics of the supporting structure was triggered; this was a problem during the early tests of the blade bracket systems. Due to time limitations the hub assembly system was not fully evaluated, only one measurement was performed whereas at least two inputs should have been used. The reader is referred to [Rah12; Roh12] where a more thorough study has been performed on these systems.

Compared to other researchers, [Rah12; Roh12; RM13; NM13; MNM13; Bru+13; RKR13], smaller variations in the eigenfrequencies are found for the blade and blade bracket systems. It is probable that there exist different versions of the blades and other researcher have used different mass-loading techniques and brackets.

A minor parametric study considering stiffness properties of the FE model of the bracket showed that an increase in the bracket stiffness did not significantly affect the results. Lowering the stiffness highly impacted the results, however. This lead to the conclusion that the analytical brackets and hub models, used in the synthesis procedure, are not the main source of error. The stiffness of the original bracket is already stiff enough for it to be regarded almost as a rigid body which is why the increase in stiffness does not affect the results. Changing the mass of the bracket coupled to the blade did not affect the results considerably as the mass-loading is at a relatively stiff location of the blade and the flexible part of the blade is still free.

For future work it is advised that more care is taken during the measurements of the coupled components.

5.2 Synthesis

The relatively large difference between the identified data and the data where reciprocity is enforced, see Appendix D, suggests that either measurement errors were made or the components are not fully linear in the higher frequency region, something which has been identified for the contact region, [Ste+13; Reu+13]. The difference is relatively large between the absolute value of some of the resonance frequencies, seen in Appendix D, which will also result in a badly coupled system. Further it can be seen in Appendix B that around 400 Hz the blades show diverging behaviour, either from measurement errors or non-linearity, meaning that the reciprocal theorem might not be valid. It should be noted that mode seven is around 400 Hz and it is very sensitive to small angle variations for the system input. Further, this could explain the better obtained

correlation for the *high* analytical coupling, where all DOFs in contact between the blade and bracket model are constrained with rigid links to centre nodes with six DOFs, further described in section 3.1.1. It can be argued that it is a more realistic coupling configuration relative to the isostatic coupling, but the FE blade is also fully linear and thus no assumptions have to be made and approximations introduced. But it should be stated that with the same coupling configuration the experimental-analytical coupling produced better results compared to the analytical coupling, probably because of the relatively large spread in modal properties between the blades. This further implies that it is of interest to use experimental models of the blades for coupling.

Further work should investigate the joint dynamics where more advanced methods for the coupling are proposed, such as the transmissions simulator [May12b]. As mentioned before, there is probably non-linearity present at the interface locations [Ste+13; Reu+13] which must be modelled correctly. The interface DOFs should be chosen more carefully and the experimental models measured with input output relation for all the interface DOFs to as large an extent as possible. There has been research of the optimal placement of interface DOFs which could be used [Bru+13]. An FE model of the blade which includes the seventh mode in the validation would be of interest as well. It would also be interesting to couple the *high* coupling configuration of the bracket to the experimental blade model as the results obtained for the analytical models coupled with the *high* coupling configuration were good.

5.3 Numerical Instability

The state-space coupling method proposed by Sjövall and Abrahamsson has been used by Sjövall [Sjö07] and Liljerehn [Lil12] on smaller systems. Liljerehn has achieved good correlations compared to FE data [Lil12]. The blade considered in this thesis is more complex in its geometry and material properties compared to previously used components. No mention of numerical problems has been found in previous research.

From the results in section 4.5 it is seen that in general the bracket is transformed to coupled form poorer. Thus it is believed that systems with a high first eigenfrequency or a large spread between eigenfrequencies will produce poorer coupling form systems. It is also showed that higher model orders produce more unstable systems, which is to be expected. Thus for other researchers using this method it is advised that both the eigenfrequencies but also the input and output matrices are monitored as the numerical instability is shown to affect the FRFs while the eigenfrequencies can be almost correct. It might be possible to numerically find some deviations in the transformed state, input and output matrices for equal systems but with different subspace of the nullspace matrices.

Further work must be performed on this algorithm as these numerical problems seriously cripple the algorithm for industrial use. A theoretical investigation where the inverted transformation matrix is explicitly formed would be a possibility. As found in section 4.5 the best way to mitigate the numerical problems is to transform the original state-space system to real diagonal form.

5.4 Physical Laws

The passivity criterion has been discussed by Sjövall [Sjö07], where a solution to the problem is presented by estimating a second order form by optimisation, which is described in section 2.11. It is shown in section 4.6.2 that this method produced stable systems but some channels were estimated poorly which affected the coupled system negatively in that the eigenfrequencies of the coupled systems were somewhat estimated but eigenvectors were completely wrong. A very coarse frequency vector had to be used for the frequency response data for the optimisation routine to converge. This is one explanation why the estimated systems are not correct, but increasing the resolution made the convergence very slow and a solution was never obtained, even though the damping was assumed to be of Caughey type for which Sjövall argues that the optimisation problem becomes simpler. It was of interest to obtain 26 outputs for full correlation between experimental reference systems. The same optimisation procedure was tried with only six outputs where the same eigenvalues were obtained but no eigenvector correlation could be performed. Further, it is possible that the author has introduced errors. There exist other methods of going from a second order system to first order form [FGP98; JP85] but these have not been employed.

It is of interest to keep the post processing to a minimum and therefore of interest to fulfil the passivity criterion in the system identification procedure. The algorithm developed by Yaghoubi and Abrahamsson [YA12; YA13] could potentially be extended to include this. It could also be extended to include the enforcement of Newton's second law with axillary states, as used in this thesis. No good method is proposed in this thesis

to achieve a passive system in the system identification procedure but there exist efforts in literature, e.g. McKelvey [MM05].

It has also been shown that small levels of numerical noise in either the $\mathbf{C}$ or $\mathbf{B}$ matrices, making their product nonzero, produced unstable systems for otherwise physical systems in every sense while the eigenfrequencies were not altered. From section 4.5 it was found that using anything else than method M1, where the original state-space system is transformed to real diagonal form and a specific subspace of the nullspace of $\mathbf{B}_c$ is used further described in section 4.5, also produced highly unstable systems. Thus, the passivity criterion is not solely responsible for this behaviour.

In any case, it should be avoided to rewrite the first order system to second order form only to get a physical system and then convert back to first order form, if the simplicity of the method is to be kept. Although the coupling is still performed with real DOFs whereas the component mode synthesis (CMS) method uses generalised coordinates, it is hard to motivate the use of the state-space method in such a setting, as the numerical problems are still present and a modal second order form is obtained. Then it might be simpler to use the CMS with the coupling procedure proposed by Allen and Mayes [AM07].

5.5 Theoretical Development

The state space method has been placed among the three other methods proposed by de Klerk et al. [KRV08] by translating the synthesis procedure to the general framework.

For analytical models a new transformation is proposed, which circumvents the use of the nullspace and thus also the numerical instabilities. For further work on the proposed comparison and a more general comparison between the state-space synthesis (SSS) and the CMS methods the transformation presented by Friswell [FGP98] can be used. This holds some problems as both the generalised states and the physical coordinates become coupled in the equations. If successful it would be possible to write the original state space-system on coupling form without the use of nullspaces.

For future work on this method it would be of interest to include the possibility to easily subtract models from coupled systems. This has been adressed by Sjövall [Sjö07] but includes an optimisation procedure. If this is solved the transmission simulator method [May12b] could be translated to the state-space synthesis method. It has been shown to hold great promise for modelling the joints implicitly, as shown by Rohe [RM13; Roh12], which is believed to be a large source of error in this work.

6 Conclusion

This work has been performed as part of the Society for Experimental Mechanics (SEM) Substructuring Focous group research project to increase the knowledge in experimental substructuring. A testbed, the Ampair 600W wind turbine, proposed by the research group has been used in conjuncture with a first order state-space synthesis method. The experimental models have been identified with system identification techniques. Problems exist with this procedure when the physicality of the identified models are of importance, these problems are discussed within this thesis.

The problems with the state-space method are highlighted. Numerical instability in the transformation to coupling form for fully physical systems is of main concern. The transformation is extremely sensitive even for small systems and almost unusable for large systems if the wrong procedure is used. A workaround is presented that mitigate the numerical instabilities but does not solve them fully.

The amount of violation of Newton's second law is also quantified and a solution is proposed where axillary states are added to the system enforcing a physically consistent system with minimal effect on the dynamics in the region of interest.

No solution for the enforcement of the passivity criterion is found but it has been shown that, even though the synthesised systems are unstable, the eigenfrequencies and modeshapes are correctly estimated. The results are further equivalent to those obtained when coupling the same models using a frequency-based substructuring approach. It is proposed that the enforcement of physically consistent models be performed in the system identification procedure.

A theoretical comparison for an altered state-space synthesis is performed with the CMS method. It has been shown that the produced systems are equal and it is proposed that this altered form is used for analytical

systems as the numerical instabilities are circumvented. The state-space method is also translated into the general framework.

The blades of the testbed have been coupled to their brackets with a state-space and an FBS method for experimental-analytical models and with the CMS method for analytical models, with three coupling configurations. It is found that the analytical model correlates better with verification data for a stiff coupling configuration, up to the seven first modes. For isostatic coupling the experimental-analytical coupling is found to produce the best results. The blade bracket models assembled to the hub is found to produce significantly different results compared to the experimentally measured system and the results are inconclusive.

In conclusion, this work adds to the field of substructuring as an experimental study of the testbed is performed and the state-space coupling approach is used with larger data sets. It is shown that if the numerical and passivity problems can be solved, the method is very promising. More advanced modelling of the coupling must be employed for better results. Also, it is possible that the measurements of the blades were contaminated with errors, visible for frequencies over 400 Hz in the reciprocal properties, which would explain the abrupt change in the MAC results above mode six. It is also possible that the blades are not truly linear in the higher frequency region which would render the reciprocal assumption used invalid.

Hopefully the problems found can be solved to enable users a simple yet powerful method for substructuring on first order form.

References

[Abr00] T. Abrahamsson. *Linear System Theory in Vibration Engineering*. Chalmers, 2000.

[Abr90] T. Abrahamsson. "Modal Analysis and Synthesis in Transient Vibration and Structural Optimization Problems". PhD Thesis. Chalmers University of Technology, 1990.

[All02] R. J. Allemang. The Modal Assurance Criterion (MAC): Twenty Years of Use and Abuse. *Conference Proceedings of the Society for Experimental Mechanics Series. 20th IMAC, A Conference on Structural Dynamics* (2002), 397–405.

[AM07] M. S. Allen and R. L. Mayes. Comparison of FRF and Modal Methods for Combining Experimental and Analytical Substructures. *Conference Proceedings of the Society for Experimental Mechanics Series. 25th IMAC, A Conference on Structural Dynamics* (2007).

[BJ60] R. E. D. Bishop and D. C. Johnson. *The Mechanics of Vibration*. Cambridge University Press, 1960. ISBN: 1-107-40245-X.

[Bru+13] J. Brunetti et al. Selection of Interface DoFs in Hub-Blade(s) Coupling of Ampair Wind Turbine Test Bed. *Conference Proceedings of the Society for Experimental Mechanics Series. 31th IMAC, A Conference on Structural Dynamics* (2013).

[CK06] R. R. Craig and A. J. Kurdila. *Fundamentals of Structural Dynamics, Second Edition*. Wiley, 2006. ISBN: 0-471-43044-7.

[Cra00] R. R. Craig. A Brief Tutorial on Substructure Analysis and Testing. *Conference Proceedings of the Society for Experimental Mechanics Series. 18th IMAC, A Conference on Structural Dynamics* (2000), 899–908.

[Ewi00] D. J. Ewins. *Modal Testing: Theory and Practice, Second Edition*. Research Studies Press, 2000. ISBN: 0-863-80218-4.

[FGP98] M. I. Friswell, S. D. Garvey, and J. E. T. Penny. Extracting Second-Order Systems from State-Space Representations. *AIAA Journal* **37**.1 (1998), 132–135. DOI: 10.2514/2.679.

[Fol09] G. B. Folland. *Fourier Analysis and Its Applications*. American Mathematical Society, 2009. ISBN: 0-821-84790-2.

[Gib+13] M. Gibanica et al. Spread in modal data obtained from wind turbine blade testing. *Conference Proceedings of the Society for Experimental Mechanics Series. 31th IMAC, A Conference on Structural Dynamics* (2013).

[GL96] G. H. Golub and C. F. V. Loan. *Matrix Computations, Third Edition*. The Johns Hopkins University Press, 1996. ISBN: 0-801-85414-8.

[HA12] J. Harvie and P. Avitabile. Comparison of Some Wind Turbine Blade Tests in Various Configurations. *Conference Proceedings of the Society for Experimental Mechanics Series. 30th IMAC, A Conference on Structural Dynamics* (2012), 73–79. DOI: 10.1007/978-1-4614-2422-2_9.

[HK71] K. Hoffman and R. Kunze. *Linear Algebra, Second Edition*. Prentice-Hall, 1971. ISBN: 0-135-36797-2.

[JBF88] B. Jetmundsen, R. L. Bielawa, and W. G. Flannelly. Generalized Frequency Domain Substructure Synthesis. *Journal of the American Helicopter Society* **33**.1 (1988), 55–54. DOI: 10.4050/JAHS.33.55.

[Joh+13] A. T. Johansson et al. Modeling and Calibration of Small-scale Wind Turbine Blade. *Conference Proceedings of the Society for Experimental Mechanics Series. 31th IMAC, A Conference on Structural Dynamics* (2013).

[JP85] J.-N. Juang and R. S. Pappa. An eigensystem realization algorithm for modal parameter identification and model reduction. *Journal of Guidance, Control, and Dynamics* **8**.5 (1985), 620–627. DOI: 10.2514/3.20031.

[Kai80] T. Kailath. *Linear Systems*. Prentice-Hall, 1980. ISBN: 0-135-36961-4.

[KRV08] D. de Klerk, D. J. Rixen, and S. N. Voormeeren. General Framework for Dynamic Substructuring: History, Review and Classification of Techniques. *AIAA Journal* **46**.5 (2008), 1169–1181. DOI: 10.2514/1.33274.

[LE02] W. Liu and D. J. Ewins. Substructure Synthesis Via Elastic Media. *Journal of Sound and Vibration* **257**.2 (2002), 361–379. DOI: 10.1006/jsvi.2002.5044.

[Lil12] A. Liljerehn. "Component Synthesis of Machine Tool and Cutter for Process Optimisation". Licentiate Thesis. Chalmers University of Technology, 2012.

[Lin13] A. Linderholt. Model Calibration of an A600 Wind Turbine Blade. *Conference Proceedings of the Society for Experimental Mechanics Series. 31th IMAC, A Conference on Structural Dynamics* (2013).

[Lju99] L. Ljung. *System Identification: Theory for the Use, Second Edition*. Prentice Hall, 1999. ISBN: 0-136-56695-2.

[MAL96] T. McKelvey, H. AkCay, and L. Ljung. Subspace-based Multivariable System Identification From Frequency Response data. *IEEE Transactions on Automatic Control* **41**.7 (1996), 960–979. DOI: 10.1109/9.508900.

[Mana] *MATLAB 2013a Documentation*. Version 2011.1. Mathworks, 2013. URL: http://www.mathworks.se/help/matlab/.

[Manb] *MD Nastran & MSC Nastran 2011 Dynamic Analysis User's Guide*. Version 2011.1. MSC, 2011. URL: http://simcompanion.mscsoftware.com/infocenter/index?page=content&id=DOC9847&cat=MSC_MD_NASTRAN_DOCUMENTATION_2011&actp=LIST.

[May12a] R. L. Mayes. An Introduction to the SEM Substructures Focus Group Test Bed - The Ampair 600 Wind Turbine. *Conference Proceedings of the Society for Experimental Mechanics Series. 30th IMAC, A Conference on Structural Dynamics* (2012), 61–71. DOI: 10.1007/978-1-4614-2422-2_7.

[May12b] R. L. Mayes. Tutorial on Experimental Dynamic Substructuring Using the Transmission Simulator Method. *Conference Proceedings of the Society for Experimental Mechanics Series. 30th IMAC, A Conference on Structural Dynamics* (2012), 1–9. DOI: 10.1007/978-1-4614-2422-2_1.

[Mei96] L. Meirovitch. *Principles and Techniques of Vibrations*. Prentice Hall, 1996. ISBN: 0-023-80141-7.

[MM05] T. McKelvey and S. O. R. Moheimani. Estimation of Phase Constrained MIMO Transfer Functions With Application to Flexible Structures With Mixed Collocated and Non-collocated Actuators and Sensors. *Proceedings of the 16th IFAC World Congress* (2005).

[MNM13] D. Macknelly, M. Nurbhai, and N. Monk. Additional Modal Testing of Turbine Blades and the Application of Transmission Simulator Substructuring Methodology for Coupling. *Conference Proceedings of the Society for Experimental Mechanics Series. 31th IMAC, A Conference on Structural Dynamics* (2013).

[NM12] M. Nurbhai and D. Macknelly. Modal Assessment of Wind Turbine Blade in Preparation of Experimental Substructuring. *Conference Proceedings of the Society for Experimental Mechanics Series. 30th IMAC, A Conference on Structural Dynamics* (2012), 71–72. DOI: 10.1007/978-1-4614-2422-2_8.

[NM13] M. Nurbhai and D. Macknelly. Dynamic Substructuring Wind Turbine Blade Finite Element Model Update and Correlation with Test. *Conference Proceedings of the Society for Experimental Mechanics Series. 31th IMAC, A Conference on Structural Dynamics* (2013).

[OM94] P. V. Overschee and B. D. Moor. N4SID: Subspace Algorithms for the Identification of Combined Deterministic-Stochastic Systems. *Automatica* **30**.1 (1994), 75–93. DOI: 10.1016/0005-1098(94)90230-5.

[Onl] *SEM Substructuring Wiki*. June 2013. URL: http://substructure.engr.wisc.edu/substwiki/.

[Rah12] S. Rahimi. "Experimental Dynamic Substructuring". Master's Thesis. TU Delft, 2012.

[Red08] J. N. Reddy. *An Introduction to Continuum Mechanics*. Cambridge University Press, 2008. ISBN: 0-521-87044-5.

[Reu+13] P. Reuss et al. Identification of Nonlinear Joint Characteristic in Dynamic Substructuring. *Conference Proceedings of the Society for Experimental Mechanics Series. 31th IMAC, A Conference on Structural Dynamics* (2013).

[RKR13] S. Rahimi, D. de Klerk, and D. J. Rixen. The Ampair 600 Wind Turbine Benchmark: Results From the Frequency Based Substructuring Applied to the Rotor Assembly. *Conference Proceedings of the Society for Experimental Mechanics Series. 31th IMAC, A Conference on Structural Dynamics* (2013).

[RM13] D. P. Rohe and R. L. Mayes. Coupling of a Bladed Hub to the Tower of the Ampair 600 Wind Turbine using the Transmission Simulator Method. *Conference Proceedings of the Society for Experimental Mechanics Series. 31th IMAC, A Conference on Structural Dynamics* (2013).

[Roh12] D. P. Rohe. "Validation of Experimental-Analytical Substructuring Using the Transmission Simulator Method". Master's Thesis. University of Wisconsin-Madison, 2012.

[SA07] P. Sjövall and T. Abrahamsson. Component system identification and state-space model synthesis. *Mechanical Systems and Signal Processing* **21**.7 (2007), 2697–2714. DOI: 10.1016/j.ymssp.2007.03.002.

[SJ94] T.-J. Su and J.-N. Juang. Substructure system identification and synthesis. *Journal of Guidance, Control and Dynamics* **17**.5 (1994), 1087–1095. DOI: 10.2514/3.21314.

[Sjö04] P. Sjövall. "Component Synthesis and Identification in Structural Dynamics". Licentiate Thesis. Chalmers University of Technology, 2004.

[Sjö07] P. Sjövall. "Identification and Synthesis of Components for Vibration Transfer Path Analysis". PhD Thesis. Chalmers University of Technology, 2007.

[Ste+13] D. Steinepreis et al. Interface Damping of the Ampair Wind Turbine Test Bed (Presentation only). *Conference Proceedings of the Society for Experimental Mechanics Series. 31th IMAC, A Conference on Structural Dynamics* (2013).

[YA12] V. Yaghoubi and T. Abrahamsson. Automated Modal Analysis Based on Frequency Response Function Estimates. *Conference Proceedings of the Society for Experimental Mechanics Series. 30th IMAC, A Conference on Structural Dynamics* (2012), 9–18. DOI: 10.1007/978-1-4614-2425-3_2.

[YA13] V. Yaghoubi and T. Abrahamsson. The Modal Observability Correlation as a Modal Correlation Metric. *Conference Proceedings of the Society for Experimental Mechanics Series. 31th IMAC, A Conference on Structural Dynamics* (2013).

A Experiments

All the parts used in this thesis are shown in Figure A.1 and A.2. By looking at Figure A.2a it can be seen that the holes on the hub where the brackets were mounted are equipped with a cylinder, embedded with a rubberised material cylinder. In Figure A.2b the bearing is shown which allowed the blades to rotate smoothly and finally in Figure A.2c the bolts used to mount the brackets to the blades are shown. All other parts are shown in Figure A.1 where the cylinder (1) and the spring (3) were attached to the shaft (4) and then inserted into the hub (7). The brackets were then inserted into the hub holes and the parts marked with (2) were attached to the cylinder (1) and the brackets (6). Finally the back plate was mounted and the blades mounted to the brackets.

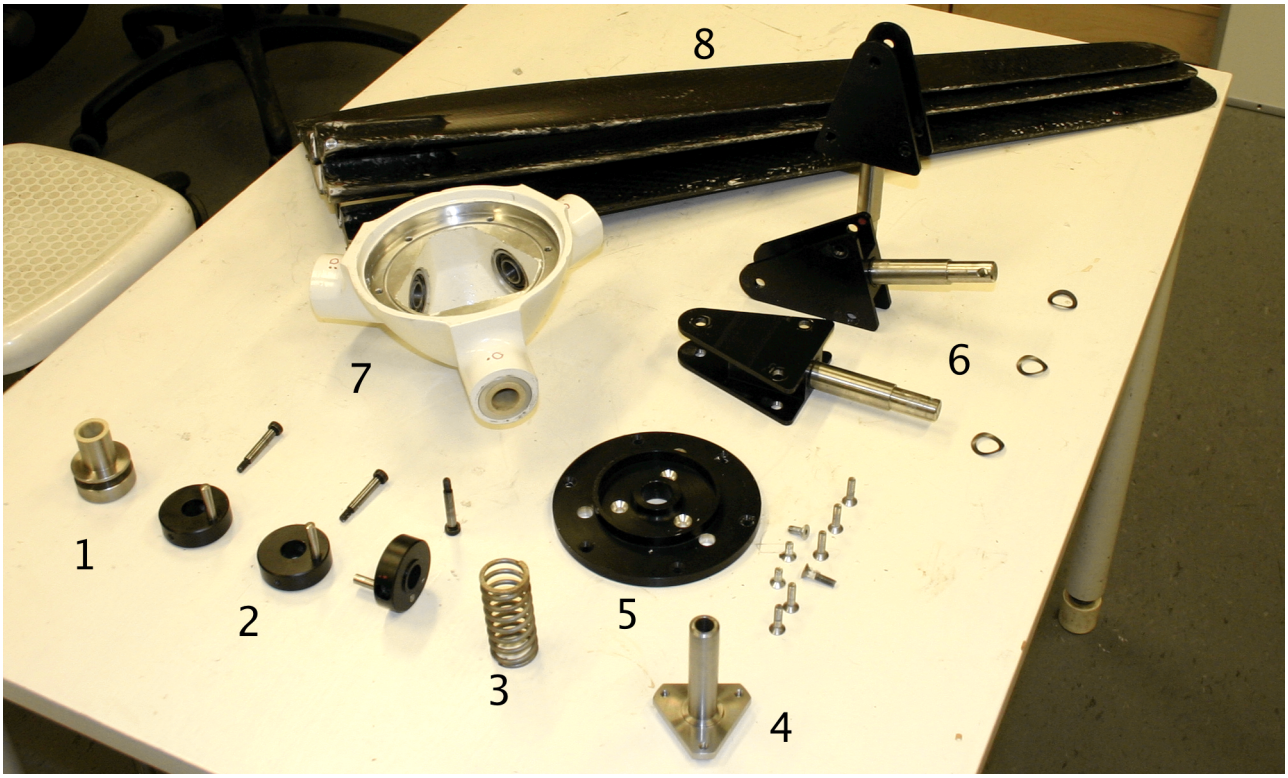

Figure A.1: *All the parts used except for the bolts that coupled the brackets to the blades, shown instead in Figure A.2c. (1) Cylinder mounted on the spring mounted shaft. (2) These parts were attached to the brackets and the cylinder. (3) Spring that was mounted onto the shaft. (4) Shaft that went into the middle of the hub. (5) Back plate and screws. (6) Three brackets. (7) Hub. (8) Three blades.*

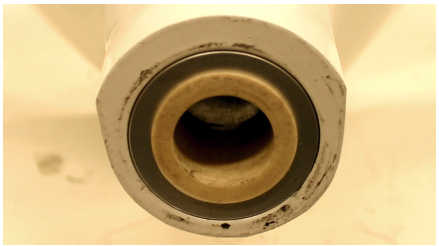

(a) *Hole for bracket in hub.*

(b) *Bearing.*

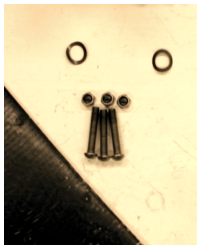

(c) *Mounts.*

Figure A.2: *The three parts not seen in Figure A.1. (a) Cylinder with a rubber material inserted into the hub so that the bracket would fit well. (b) Bearing mounted in the hub. (c) Screws used to coupled the brackets to the blades.*

The assembled bracket mounted with part (2), the bearing and the rubberised cylinder can be seen in Figure A.3a. The back of the hub mounted with brackets without the backplate can be seen in Figure A.3b. The hub was filled with epoxy to mitigate the dynamics of the internal parts. The contact between the blade and the bracket can be seen in Figure A.3c. It is seen that the interface does not fit perfect and that the bracket is bent when bolted. These effects are further discussed in chapter 5.

(a) *Bracket.* (b) *Backside of the hub.* (c) *Blade bracket interface.*

Figure A.3: *(a) The parts attached to the bracket shaft inside the hub. (b) Backside of the hub without the backplate, showing the assembled structure. (c) The contact between the bracket and the blade.*

B Reciprocity

It is assumed that the measured systems fulfil the reciprocity theorem and here a few FRFs are shown for a quantitative validation of the reciprocity of the systems. In Figure B.1 the measured blades are shown with a comparison of the data used in [Gib+13] which should yeild close to identical results. In Figure B.2, the input in z (7) and output 1 is verified with input in x and output 7 as Figure 3.16 shows that the output from position 1 is the direct accelerance for input in x. This is the reason why no data is compared with force input in the y direction as the direct accelerance differs considerably.

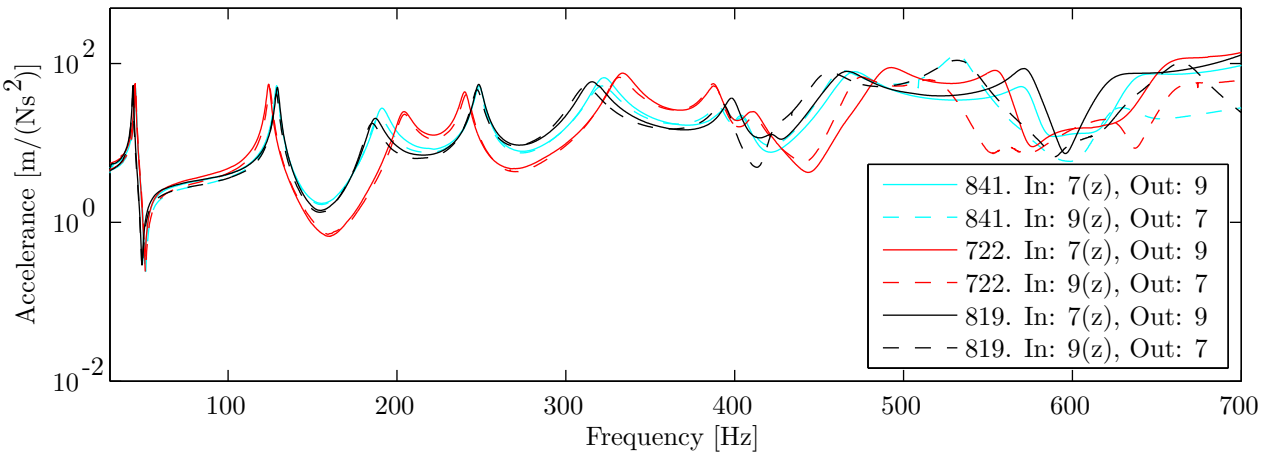

Figure B.1: *FRFs of the three blades with solid lines representing input at position 7 and output at position 9 and dashed lines representing input at position 9 and output at position 7 with positions numbered as shown in Figure 3.1. Data for FRF with input at position 9 and output at position 7 is from [Gib+13].*

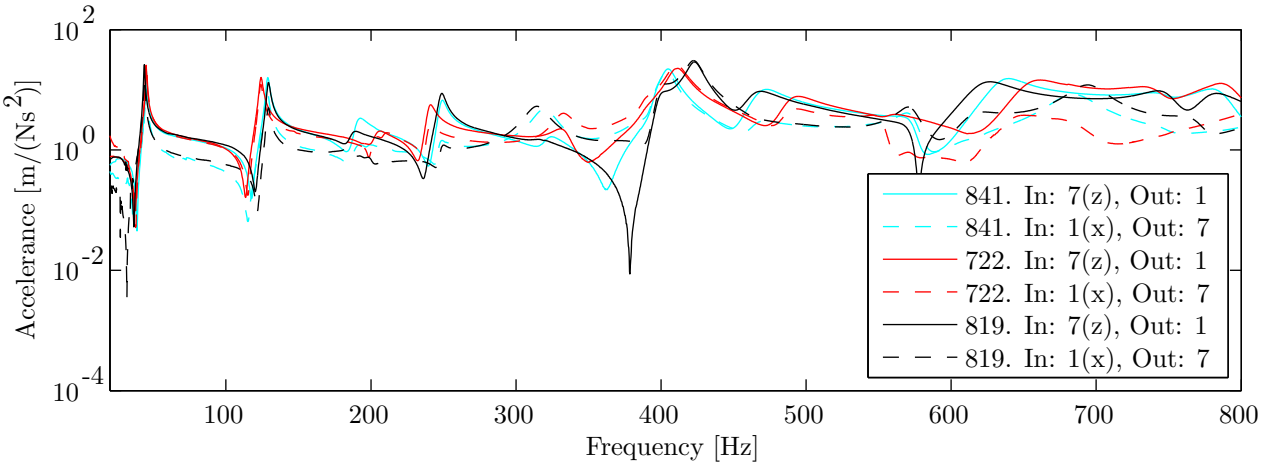

Figure B.2: *FRFs of the three blades with solid lines representing input at position 7 and output at position 1 and dashed lines representing input at position 1 and output at position 7 with positions numbered as shown in Figure 3.1.*

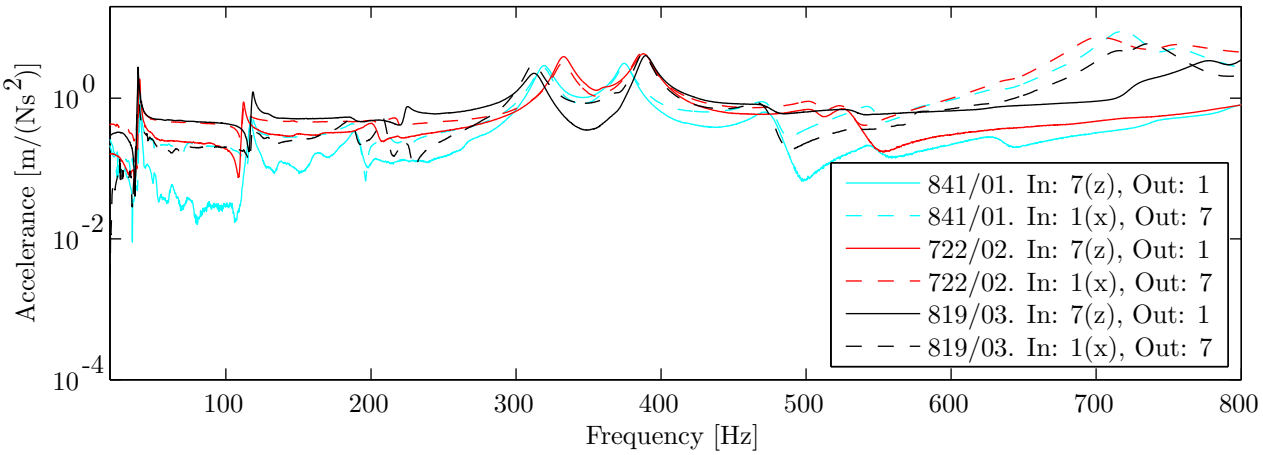

Figure B.3: *FRFs of the three bracket mounted blades with solid lines representing input at position 7 and output at position 1 and dashed lines representing input at position 1 and output at position 7 with positions numbered as shown in Figure 3.24.*

C Modeshapes

In Figure C.1 modes one to six and eight to nine can be seen to give a good estimate of the modeshapes and all four models resemble each other. Mode seven on the other hand produce different results between the four models. It is the first edgewise mode and as the accelerometers only measure in their normal direction, the results are greatly influenced by noise. The FE blade is not validated with respect to this mode and thus it can not be considered to give a real representation either. Note that the correlation for the first mode between blade 722 and 819 and 722 and the FE blade is only between 0.95 and 0.9, see Figure 4.1. This is due to the effect of the Dytran accelerometer which can be seen to affect mode 1 in Figure C.1a. If that particular channel is removed from the correlation analysis these correlations becomes consistent with the other first mode correlations.

The blade bracket system is similar to the blade system and shown in Figure C.2. In Figure C.3 the three first modes of the hub bracket blade system are shown.

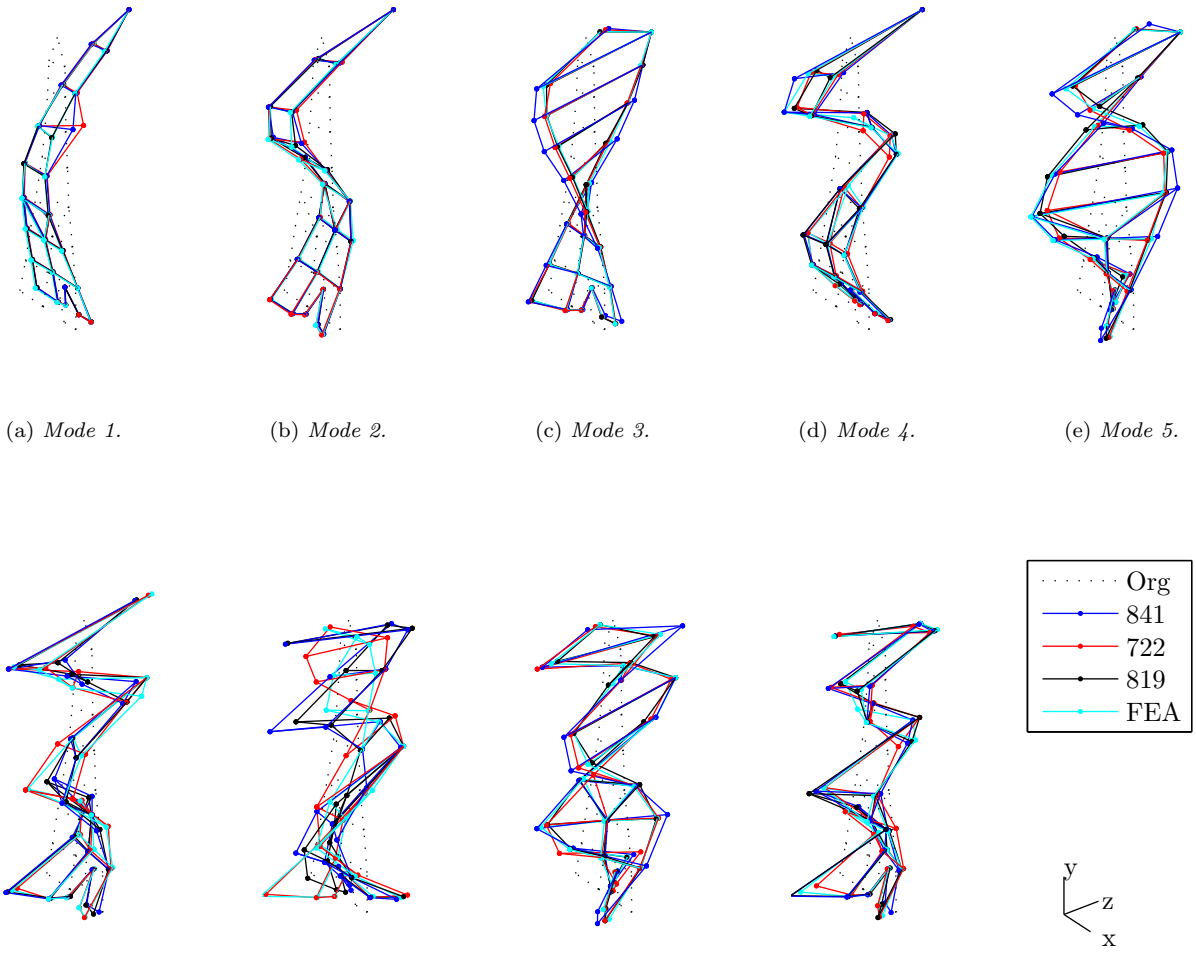

(a) *Mode 1.* (b) *Mode 2.* (c) *Mode 3.* (d) *Mode 4.* (e) *Mode 5.*

(f) *Mode 6.* (g) *Mode 7.* (h) *Mode 8.* (i) *Mode 9.* (j) *Legend.*

Figure C.1: *The first 9 flexible modes of the blade system showing the three measured systems and the FE model.*

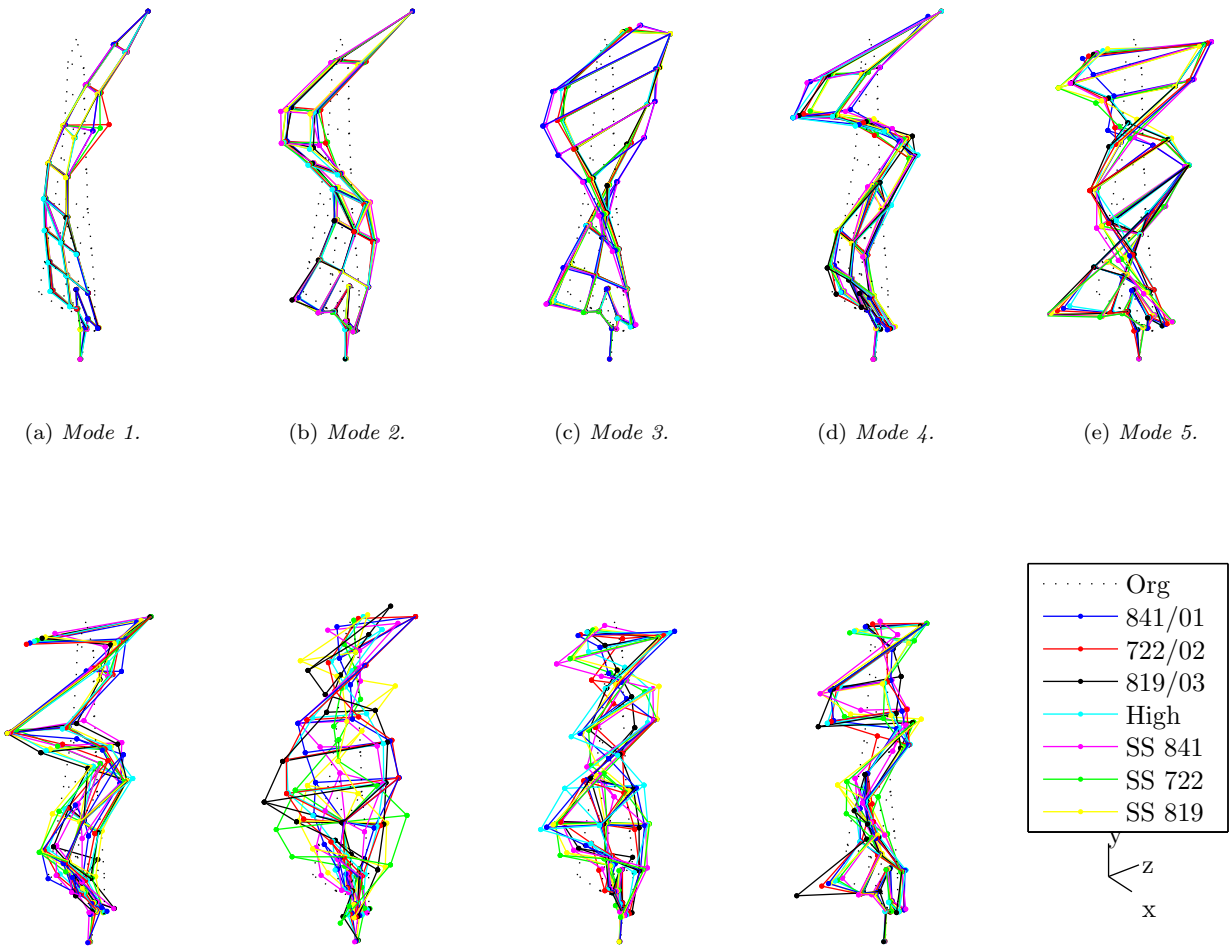

(a) *Mode 1.* (b) *Mode 2.* (c) *Mode 3.* (d) *Mode 4.* (e) *Mode 5.*

(f) *Mode 6.* (g) *Mode 7.* (h) *Mode 8.* (i) *Mode 9.* (j) *Legend.*

Figure C.2: *The first 9 flexible modes of the blade bracket system showing the three measured systems and the three experimental-analytical coupled systems as well as a purely analytical system denoted High.*

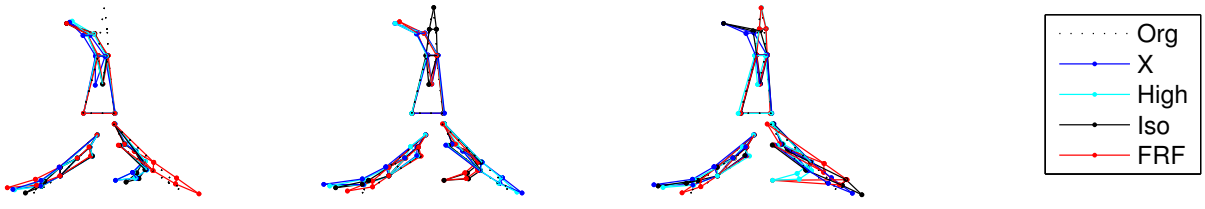

(a) *Mode 1.* (b) *Mode 2.* (c) *Mode 3.* (d) *Legend.*

Figure C.3: *The first 3 flexible modes of the hub bracket blade system showing the measured system and the experimental-analytical coupled systems, denoted FRF, as well as a purely analytical systems denoted High and Iso.*

D Frequency Response Functions

Presenting all the FRFs is not feasible as 234 functions are had only from the blade measurements. A selected few FRFs are shown which outline some interesting features not shown before. It can be seen that that the identified data (blue) fits good for most channels. The blue model is not used in the coupling as the input must be known at all interface locations and thus reciprocity is enforced and the red model shows what is actually used. The figures only show the FRFs at the interface locations with different inputs. It should also be noted that the FE FRFs are here shown with a proportional damping where the proportional constant is set to $\alpha = 10$, such that the amplitudes between the FE models and experimental models resemble more, for visual purposes. It can be seen that the FE model, as the MAC matrix also shows, correspond well with the measured data, mode seven is easy to find for the FE FRFs but harder for the measured FRFs.

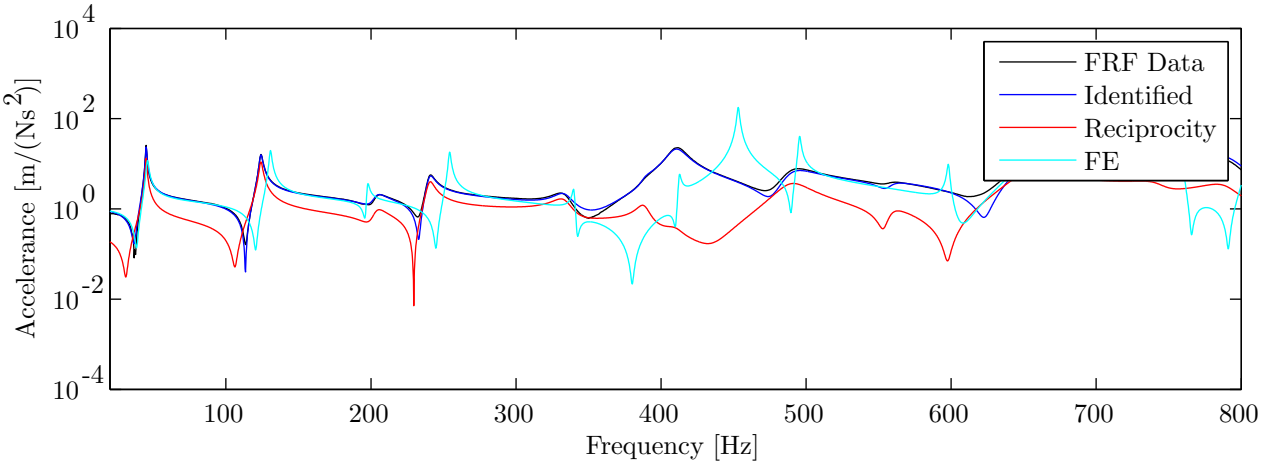

Figure D.1: *FRFs of blade 722 (black), model (blue), reciprocity enforced (red) and of the FE model of the blade (cyan) for input in z and output 1.*

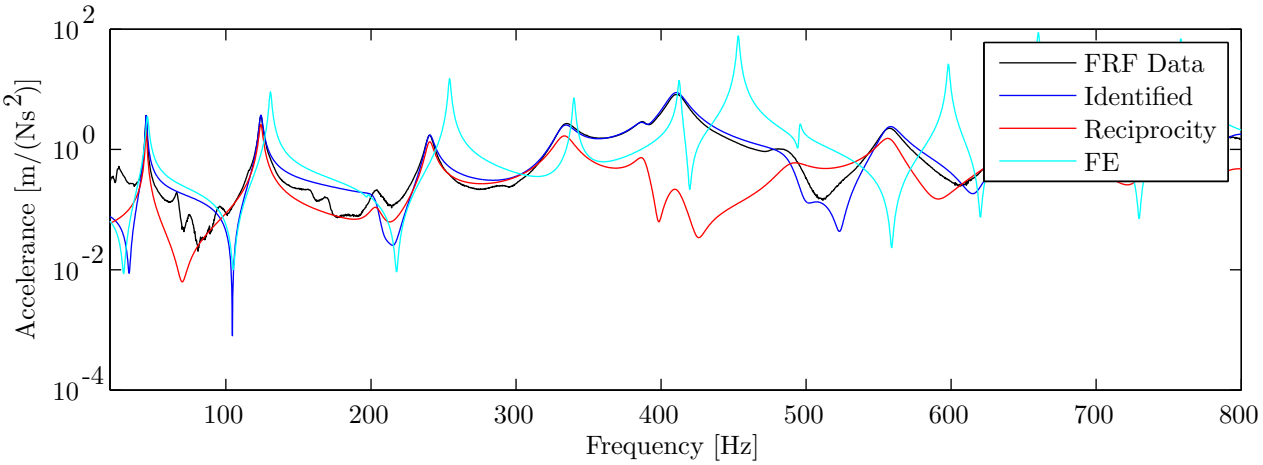

Figure D.2: *FRFs of blade 722 (black), model (blue), reciprocity enforced (red) and of the FE model of the blade (cyan) for input in z and output 2.*

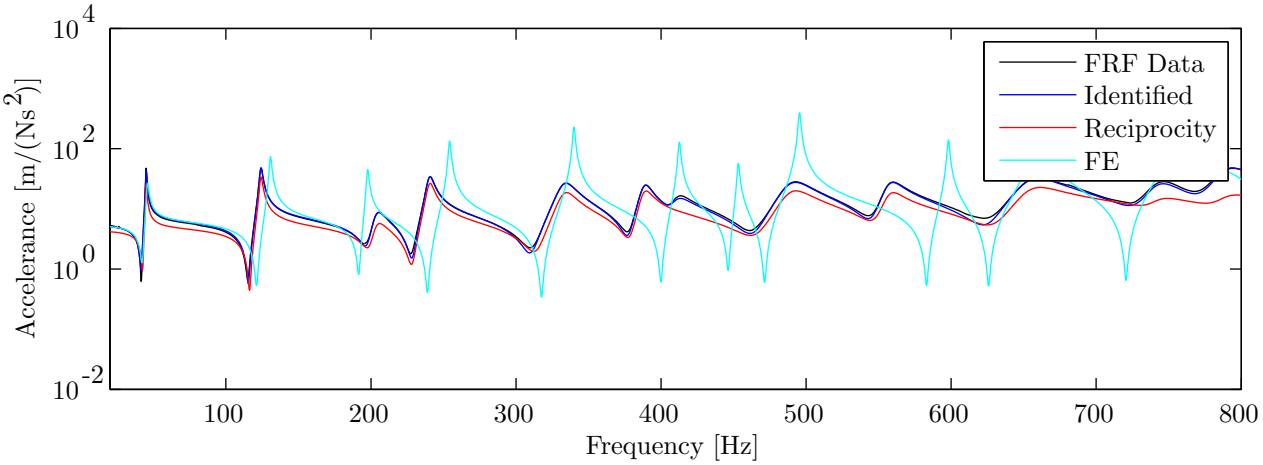

Figure D.3: *FRFs of blade 722 (black), model (blue), reciprocity enforced (red) and of the FE model of the blade (cyan) for input in z and output 3.*

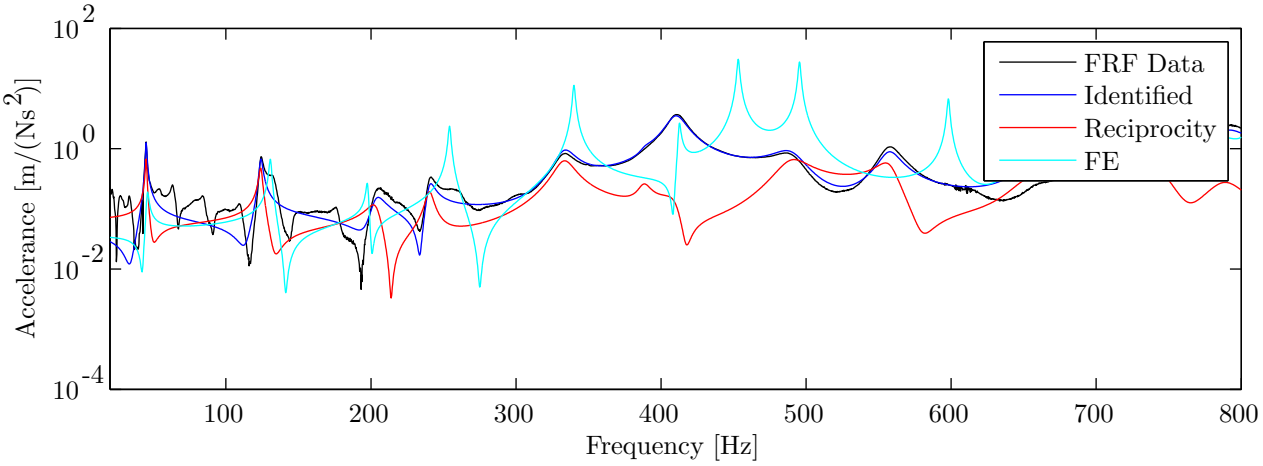

Figure D.4: *FRFs of blade 722 (black), model (blue), reciprocity enforced (red) and of the FE model of the blade (cyan) for input in z and output 4.*

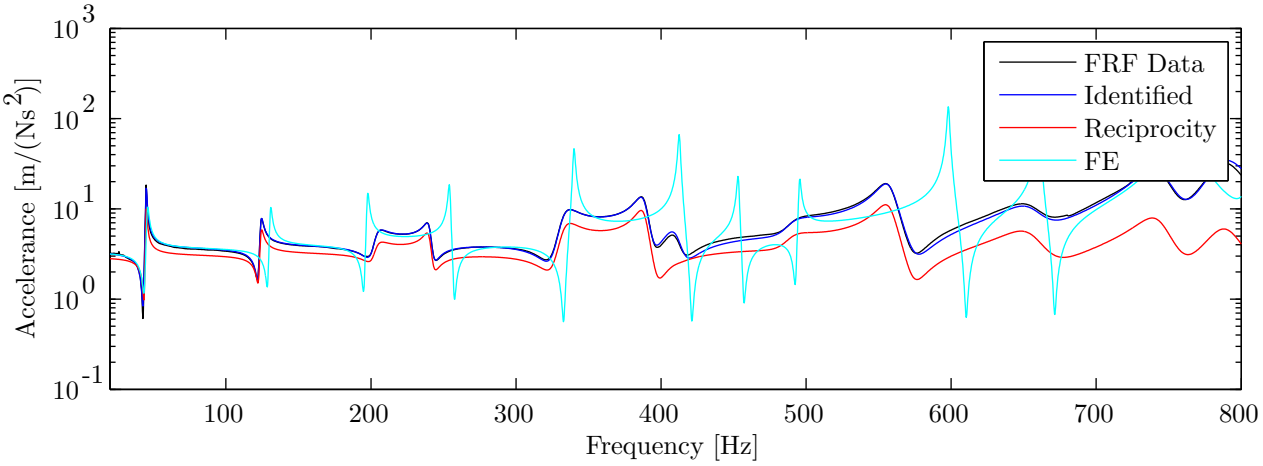

Figure D.5: *FRFs of blade 722 (black), model (blue), reciprocity enforced (red) and of the FE model of the blade (cyan) for input in z and output 5.*

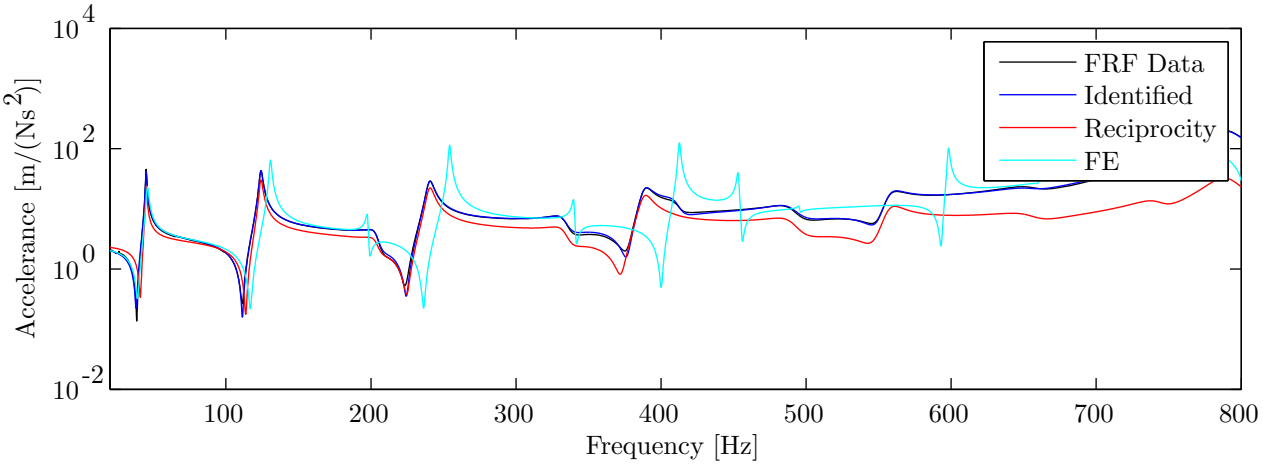

Figure D.6: *FRFs of blade 722 (black), model (blue), reciprocity enforced (red) and of the FE model of the blade (cyan) for input in z and output 6.*

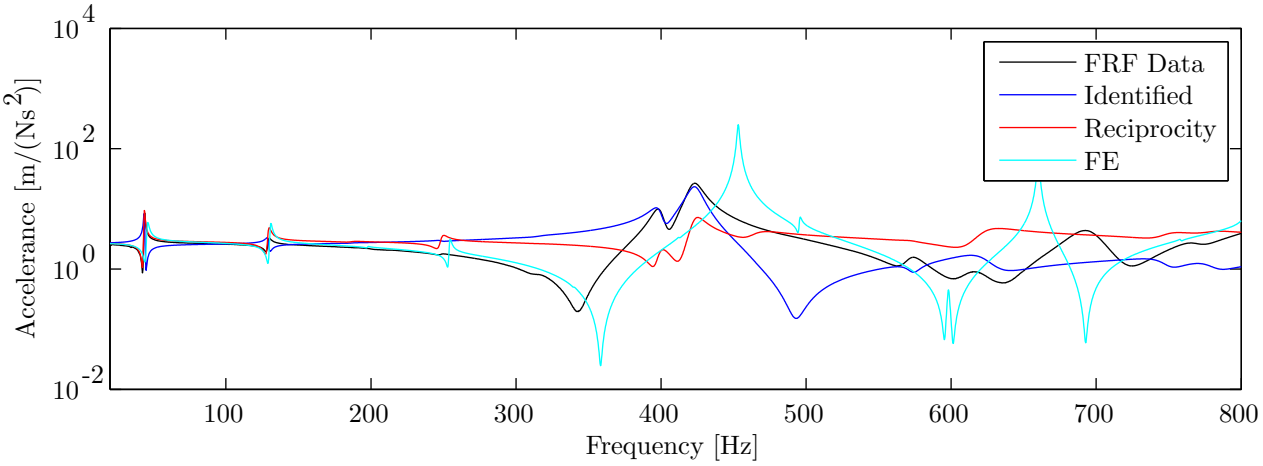

Figure D.7: *FRFs of blade 819 (black), model (blue), reciprocity enforced (red) and of the FE model of the blade (cyan) for input in x and output 1.*

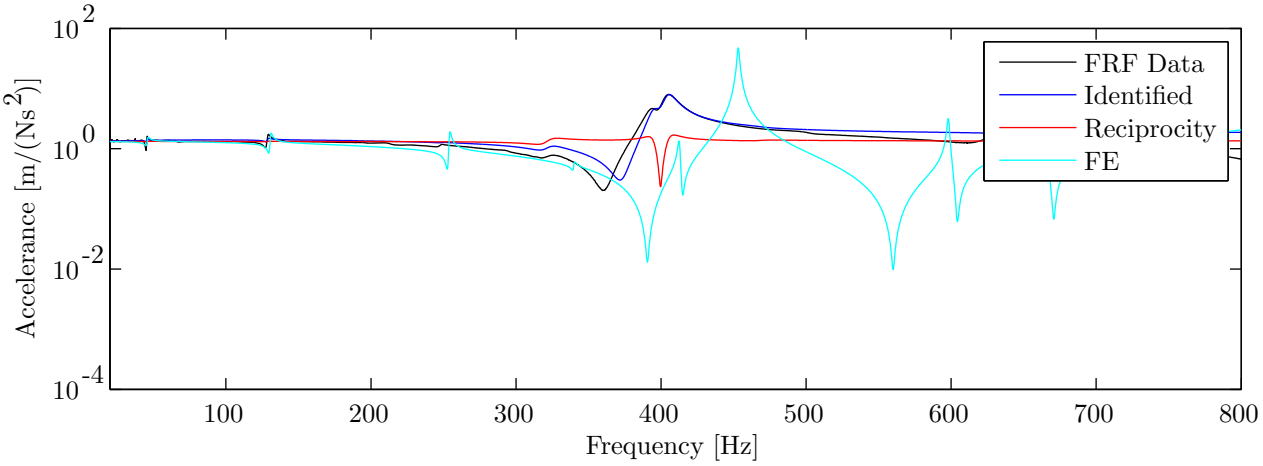

Figure D.8: *FRFs of blade 841 (black), model (blue), reciprocity enforced (red) and of the FE model of the blade (cyan) for input in y and output 2.*